REPORT DOCUMENTATION PAGE

Form Approved
OMB NO. 0704-0188

1. AGENCY USE ONLY (Leave Blank)	2. REPORT DATE (resubmission date)	3. REPORT TYPE AND DATES COVERED
	June 24, 2006	Final Progress; June 1 2001-Jan. 31 2005

4. TITLE AND SUBTITLE :
Dynamic Multi-axial Loading Response and Constitutive/Damage Modeling of Titanium and Titanium Alloys

5. FUNDING NUMBERS
DAAD19-01-1-0635

6. AUTHOR(S)
Akhtar S. Khan

7. PERFORMING ORGANIZATION NAME(S) AND ADDRESS(ES)
Dept. of Mechanical Engineering, ECS 234, The University of Maryland Baltimore County, 1000 Hilltop Circle, Baltimore, MD 21250

8. PERFORMING ORGANIZATION REPORT NUMBER

9. SPONSORING / MONITORING AGENCY NAME(S) AND ADDRESS(ES)
U. S. Army Research Office
P.O. Box 12211
Research Triangle Park, NC 27709-2211

10. SPONSORING / MONITORING AGENCY REPORT NUMBER
42435.1-EG

11. SUPPLEMENTARY NOTES
The views, opinions and/or findings contained in this report are those of the author(s) and should not be construed as an official Department of the Army position, policy or decision, unless so designated by other documentation.

12 a. DISTRIBUTION / AVAILABILITY STATEMENT
Approved for public release; distribution unlimited.

12 b. DISTRIBUTION CODE

13. ABSTRACT (Maximum 200 words)

Specific aims of the project were to determine response of several economical Ti-6Al-4V alloys under quasi-static and dynamic compression and torsion loading over a wide range of strain-rates and temperatures, and constitutive/damage modeling of the measured response for implementation in computer codes for penetration simulation.

During the three funding periods, response of several of these alloys (material provided by Army Research Lab., Aberdeen) were determined under compression and torsion loading over a wide range of strain-rates (10^-6 to 10^3 per sec.) and temperatures (755-200 K). Material constants were determined for the Johnson-Cook (JC) and Khan-Huang-Liang (KHL) models. Multi-axial experiments were then performed and observations were compared to predictions from JC and KHL models. It has been clearly demonstrated that KHL model predicts the observed response of the material far superior than JC model. These findings are significant and KHL model is ready for incorporation in computer codes of the US Army for penetration simulations regarding light-weight tank design. Microstructures and anisotropy in the material were also studied.

Results achieved are presented in three executive summaries, while details of these results are provided in three appendices which are actually three papers, either already published or are in print in a leading journal.

14. SUBJECT TERMS
High strain-rate, constitutive models, Johnson-Cook Model, Khan-Huang-Liang Model, microstructure, anisotropy, Ti-6Al-4V

15. NUMBER OF PAGES
91

16. PRICE CODE

17. SECURITY CLASSIFICATION OR REPORT	18. SECURITY CLASSIFICATION ON THIS PAGE	19. SECURITY CLASSIFICATION OF ABSTRACT	20. LIMITATION OF ABSTRACT
UNCLASSIFIED	UNCLASSIFIED	UNCLASSIFIED	UL

Final Progress Report
Proposal No.: 42435-EG

TABLE OF CONTENTS

Final Progress Report
Proposal No.: 42435-EG

Dynamic Multi-axial Loading Response and Constitutive/Damage Modeling of Titanium and Titanium Alloys

Principal Investigator: Akhtar S. Khan
Department of Mechanical Engineering
University of Maryland, Baltimore County

Research Objectives

Titanium alloys, and ceramics encapsulated in titanium alloys are considered for next generation of lightweight tanks. The objectives of this research project are to obtain responses of newly developed economical, but with much higher Oxygen content, Ti-6Al-4V alloys, determine the suitability of existing constitutive relations to model these responses, and to determine material constants for these models (e.g., JC and KHL models) for incorporation in computer codes for penetration simulation.

These objectives are being achieved through uniaxial loading experiments over a wide range of strain rates and temperatures in the first year of funding, and through multi-axial loading experiments over a wide strain rate range and a wide temperature range in the second and third year of funding, respectively.

Approach

Uniaxial compressive experiments, over a wide range of strain rates and temperatures, are used to determine material constants for two constitutive models (Johnson-Cook and Khan-Huang-Liang); experiments are performed on several titanium (Ti-6Al-4V) alloys. The results from these models are correlated to these experimental data to demonstrate the flexibility in each model. Most other investigators who have performed similar studies, stopped at this stage. The approach taken by other scientists is not right because if correlations are done with the same experiments from which the material constants are determined, then correlations should be always good for any constitutive model. We have gone one step further, which is very desirable, if not required, to validate a constitutive model. In the phase of the current year of funding, multi-axial loading experiments (e.g. dynamic torsion followed by dynamic compression using Kolsky or split Hopkinson bar technique, uniaxial compression followed by biaxial compression, etc) have been

performed and compared to predictions from these two constitutive models to establish validity of these two models over a wide ranges of strain rates and temperatures.

Background

Since the introduction of titanium and titanium alloys around 1950, they have become important materials for aerospace, energy, and chemical industries. They are used chiefly for parts that require good corrosion resistance, moderate strength up to 588 K, and lightweight. Titanium alloys, especially Ti-6Al-4V, an $\alpha+\beta$ type titanium alloy is largely used alloy in many industries because of its extremely attractive properties like high specific strength, good deformability, reasonable ductility and ability to withstand high temperatures and resistance to corrosion. It is primarily used in aero-engine, gas turbines and other applications. The development of a relatively economical Ti-6Al-4V alloy, with a low interstitial content has prompted a lot of interest in its possible use in armor tanks because of improved ductility, whereas the conventional more expensive Ti-6Al-4V alloy has been used primarily in aerospace components chiefly because of its high strength to weight ratio. This advantage has also been contemplated in various applications like armor, including ceramic tiles encapsulated in these titanium alloys.

However, applications of this material especially in defense structures require a thorough understanding of the mechanical properties and deformation responses under different loading conditions. Of all the kinds of deformations, dynamic deformation is of prime importance when it comes to use for military applications and it should be studied in detail. Also, the dynamic deformation investigation need to be multiaxial in nature so as to simulate the real life applications. Although multiaxial dynamic deformation is most essential, one needs a complete set of experimental observations to make essential judgments regarding the applicability. Also, one needs to model the constitutive response for dynamic rate of loadings as well. The constitutive model which is required for finite element and hydro-code simulations has to be simple, with lesser number of material constants to reduce calculation times and should also depend on experiments which can be performed with ease to reduce experimentation time and thus be cost effective. The present investigation emanates from these requirements.

Different constitutive models have been proposed over the last few decades describing the material behavior for high strain rate applications in the plastic regime. These can be classified into two categories; the purely phenomenological ones, e.g., Johnson–Cook (JC) and Khan–Huang–Liang (KHL) models, and the physically based models e.g., the ones by Zerilli and Armstrong, Mechanical Threshold Stress and the one proposed by Nemat Nasser et al. The phenomenological models usually are very simple in nature and have lesser number of material constants involved than the so called physically based models. Also, the experiments required for the determination of the material constants in the phenomenological models are easily performed than those required by the physically based models. The two phenomenological models are

compared and their capabilities to model complex material behavior are understood in the first phase of this investigation.

Also, it is a well known fact that the mechanical properties of this titanium alloy are heavily influenced by its impurities and heat treatment, so it is imperative that this alloy be understood in terms of the microstructure, constituents, and the processing history. The unalloyed titanium exists in mainly two forms, α-titanium (hcp structure) at room temperature, and at high temperatures it exists as β-titanium (bcc structure). Alloying of this material is performed by adding aluminum and vanadium, whereas oxygen, nitrogen, and carbon are the interstitial impurities. Aluminum, oxygen, nitrogen, and carbon are the α stabilizers, while vanadium, iron and manganese are the β stabilizers. The α phase (primary and secondary) is more dominant in the temperature ranging from 300 K to 800 K, while the amount of β phase starts to increase thereon and is almost totally β-phase at about 1270 K, which is called the β transus temperature. The α phase is much harder than the β phase, so the drop in stress levels upon increase of temperatures can be noticed with increasing β content. However, formability increases as the phase changes from α to β. The uniaxial behavior of three different alloys with different alloying and interstitial content are experimentally studied, modeled and understood in terms of the chemical composition, microstructure, etc., in the second phase of this investigation.

In the last phase of this investigation, the multiaxial response of one of the alloys which was manufactured using single electron beam melting process was studied and modeled. Dynamic torsion, dynamic torsion followed by dynamic compression experiments, and non-proportional uni-axial to biaxial experiments were performed to understand the multi-axial response of the alloy. Because of the HCP crystal structure of the alloy at low to moderate temperatures and production in a plate geometry, this alloy has been known to exhibit anisotropy. Also, there is a significant difference in the flow stress in tension and compression. An anisotropic model was chosen with capability to model the anisotropic response and also the strength differential along with the proposed constitutive model to simulate the response under complex dynamic multiaxial loadings.

Executive Summary of Achievements I

Dynamic deformation has been of interest not only in impact and penetration related problems but also in high speed machining. Titanium alloys have been studied by several investigators because of their use in aero-engine, gas turbines and other applications due to their high strength to weight ratio, ductility, and ability to withstand high temperatures and resist corrosion. The development of relatively economical Ti–6Al–4V alloy, with resulting high oxygen content, has sparked interest in its possible use in lightweight tanks; the conventional, more expensive Ti–6Al–4V alloy has been used primarily in aerospace components. The potential applications in armor, including ceramic tiles encapsulated in titanium alloys, have motivated several studies (Gray III,

1997; Follansbee and Gray, 1989; Lesuer, 2000; Nemat-Nasser et al., 2001; Majorell et al., 2002).

However, most of these studies have been insufficient and not comprehensive (Follansbee and Gray, 1989) to ascertain the material response under different loading conditions, or the range of strain rates in the investigations has been insufficient (Nemat-Nasser, 2001). Also, some inadequacies and contradictions are found in the published modeling efforts. The constitutive models used for high strain rate applications can be classified in two categories; the purely phenomenological ones, e.g., Johnson–Cook (JC) (Johnson and Cook, 1983) and Khan–Huang–Liang (KHL) models (Khan and Huang, 1992; Khan and Liang, 1999; Khan and Zhang, 2000, 2001) and so-called, ‘‘physically based models’’ e.g., the ones by Zerilli and Armstrong (1987), Mecking and Kocks (1981), etc., that were used frequently by Follansbee and Gray (1989), and in a modified form by Nemat-Nasser et al. (2001). The latter group discusses the mechanisms of plastic deformation, mainly dislocations. However, the material constants are determined by not measuring any deformation mechanism related quantity, but by choosing constants to ‘‘fit’’ the uniaxial stress–strain curves at different strain rates and temperatures, just like the purely phenomenological models. Mecking and Kocks model, as used by Follansbee and Gray (1989) has 23 constants, while these constants range from 12 to 8 in case of Cheng and Nemat-Nasser (2000) and Nemat-Nasser et al. (2001), respectively, depending on whether they include modeling of dynamic strain aging or not. Johnson–Cook and Khan–Huang–Liang models have 5 and 6 constants, respectively. Johnson–Cook and Khan–Huang–Liang models are used in this investigation due to their advantage of fewer constants and their ability to model the observed material response as closely as with models with many more constants.

Modeling approach

The material constants for both, the modified KHL and JC models were determined. Using these material constants, correlations were obtained and compared to experimental results. The modified KHL model is as follows:

$$\sigma = \left[A + B\left(1 - \frac{ln\,\dot{\varepsilon}}{ln\,D_0^p} \right)^{n_1} \varepsilon_p{}^{n_0} \right] \left(\frac{\varepsilon}{\dot{\varepsilon}^*} \right)^c \left(\frac{T_m - T}{T_m - T_{ref}} \right)^m \tag{1}$$

where, σ is the true (Cauchy) stress and ε^p is the true plastic strain. T_m, T, T_{ref} are melting, current, and reference temperatures, respectively. $D_0^p = 10^6\ s^{-1}$ (arbitrarily chosen

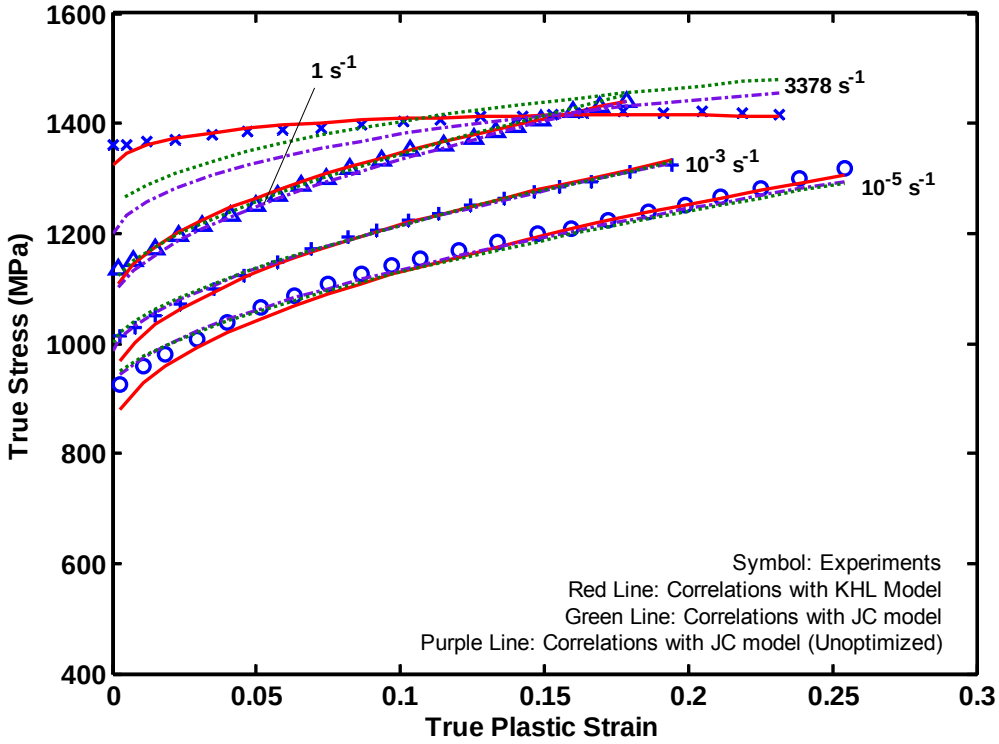

Fig. 1. Comparisons between KHL model and JC model correlations for alloy 3 studied in the investigation at room temperature and different strain rates.

upper bound strain rate) and $\dot{\varepsilon}^*$=1 s^{-1}(reference strain rate, at a reference temperature of T_{ref}, usually room temperature, at which material constants A, B and n_0 are determined). $\dot{\varepsilon}$ is the current strain rate. n_1, C and m are additional material constants. For Ti-6Al-4V alloys, the melting temperature was taken to be 1933 K (ASM handbook, 1994). The reference temperature was the constant room temperature for experiments at 296K.
The JC model which has been used previously is given as follows:

$$\sigma = \left[A + B\left(\varepsilon^{p}\right)^{n_0}\right]\left(1 + C\ln\frac{\dot{\varepsilon}}{\dot{\varepsilon}^*}\right)\left(1 - \left(\frac{T - T_r}{T_m - T_r}\right)^{m}\right) \tag{2}$$

The KHL model has two distinct advantages over the JC model. These are the addition of another material constant, n_1, which is able to simulate the decreasing work hardening behavior of certain materials with increase in strain rate. The second advantage is the modified temperature term which enables to simulate the material behavior below the reference temperature T_{ref}. In the JC model the temperature term cannot accommodate the case when the current temperature is lower than the reference temperature as then the above term within parenthesis becomes a negative number raised to the power m. The model material constants are determined through systematic procedure and further refined using least square optimization technique. An illustrative example of the modeling using JC and KHL is shown in Fig. 1 for one of the alloys studied during the

current investigation. The figure clearly shows the capability of the KHL model against the JC model in predicting the material behavior under different loading conditions. Also, the JC model and KHL model comparisons are shown for a similar alloy data published in the literature in Fig. 2.

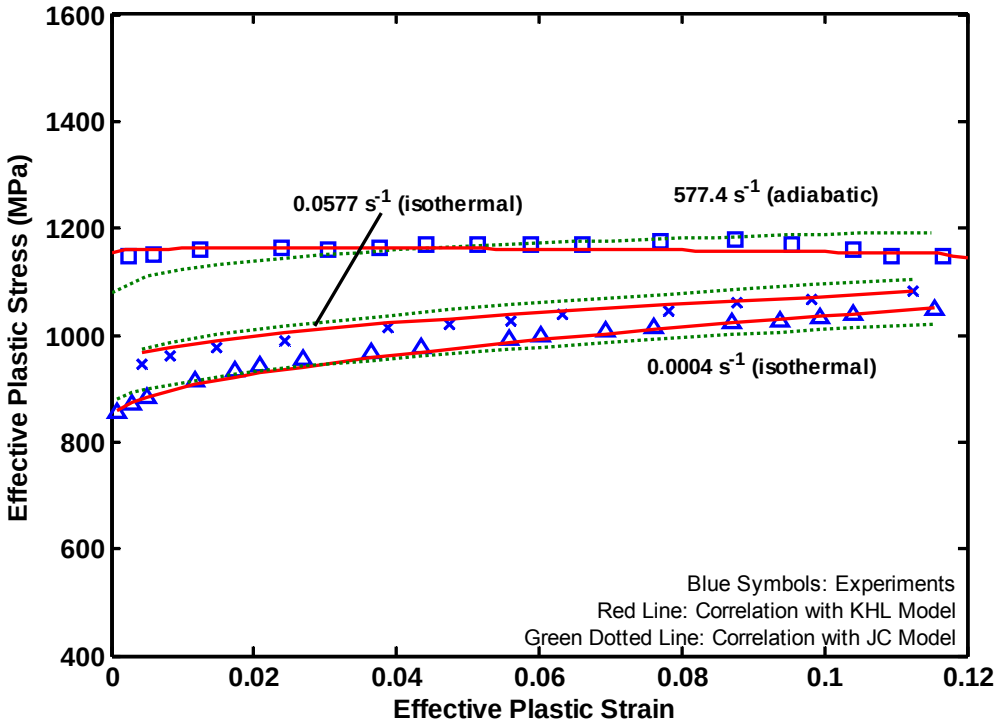

Fig. 2. KHL model and JC model correlations with experimental observations for experiments performed at room temperature [Data from Macdougall and Harding (1999)].

To determine the temperature dependence in the KHL and JC models, experiments were performed on a titanium alloy at different temperatures. The temperatures chosen for these experiments were both above and below the reference temperature which in this case was room temperature, but below $0.4T_m$. The experimental observations along with the model correlations are shown in Fig 3. Note the absence of any JC correlation for the experiment performed below the reference temperature of 233K; the KHL model is able to correlate the material response for that experiment also quite well. Overall, the KHL model was able to simulate the material behavior at these temperatures reasonably well whereas JC was unable to simulate for certain temperatures; also the correlations obtained through JC model were also not as good as the ones obtained by using KHL.

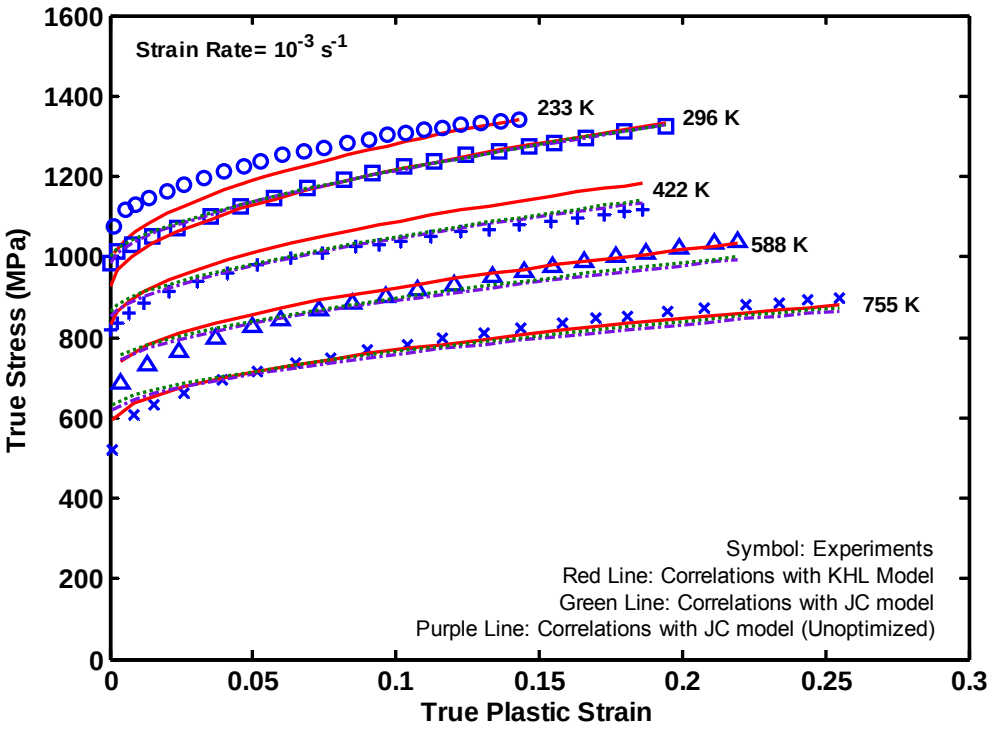

Fig. 3. KHL and JC model correlations for experiments performed at different temperatures for alloy 3 at the strain rate of 10-3 s-1. Note the absence of correlation at 233Kwith JC model in which the temperature term $(T\text{-}T_{ref})/(T_m\text{-}T_{ref})$ becomes negative.

From the current phase of investigation it is found that Ti–6Al–4V is non-linearly dependent on strain rate, as well as temperature. The KHL model is found to correlate better than JC model especially during dynamic deformation regime. The thermal softening at high strain rates, together with reduction in the work hardening rate with increase in strain rate and strain, is captured much better by the KHL model than the JC model. The temperature term of the modified KHL viscoplastic constitutive model is able to correlate well with the response at a temperature (233 K) which is lower than the reference temperature (296 K); the JC model is not valid in this case.

Executive Summary of Achievements II

Results from a series of experiments on three different titanium alloys, under quasi-static and dynamic loading conditions are presented. These alloys have been designated with different numbers i.e. as alloys 1, 2 and 3. Alloys 1 & 3 were manufactured using single electron beam melting process, resulting in higher oxygen content than the ELI version (alloy 2).

The strain-rates varied from 10^{-6} s^{-1} to 3378 $s^{-1,}$ while observations are made at temperatures from 233K to 755K. Differences in these alloys are observed in terms of thermal softening, work hardening, and strain-rate & temperature sensitivities. The Khan-Huang-Liang (KHL) model is used to effectively simulate the observed response obtained from these experiments. The model, with constants determined from the above experiments, is then used to predict strain-rate jump experimental results and also high temperature dynamic experiments for one of the alloys; the predictions are found to be very close to the observations. The chemical composition of the three alloys used in this investigation is shown below.

Material	Al	V	Fe	Y	H	N	O	C	Ti	Oeq
Alloy 1	6.26	4.16	0.14	<0.0003	0.0031	0.008	0.178	0.047	REM	0.229
Alloy 2	6.30	3.86	0.18	<0.0003	0.0026	0.003	0.112	0.045	REM	0.152
Alloy 3	5.97	4.09	0.15	<0.0003	0.0041	0.008	0.174	0.043	REM	0.222

Table 1. Chemical composition of the three Ti-6Al-4V alloys used

The equivalent oxygen content (O_{eq} = O+2N+0.75C), proposed Conrad et al. (1975) is also shown in the table above which gives the effect of dislocations-impurity interaction on the yield strength of the material. It can be seen clearly that alloy 1 and 3 are the higher oxygen content titanium alloys, while alloy 2 is the ELI version of the Ti-6Al-4V. The microstructure of these alloys was also determined before and after deformation using a scanning electron microscope (SEM). The specimens were cut along the compression axis of the specimen (the thickness direction of the plate). The initial microstructure of one of the higher oxygen content alloy (alloy 3) and the ELI version (alloy 2) are shown in Fig 4. It clearly shows distinct features in the microstructure of the two Ti-6Al-4V titanium alloys. Further studies by Conrad et al (1975) noted that the strengthening of the alloy due to these interstitials was dependent on, in decreasing order, Carbon, Oxygen and followed by Nitrogen. Effect of Hydrogen in most cases was neglected. They also found that between temperatures from 300 K to 800 K, the flow stress vs. temperature curve of α-titanium was almost parallel to that of Ti-6Al-4V alloy of nearly same interstitial content, concluding that alloying elements had insignificant effect on the temperature sensitivity in this range; the interaction of dislocations with interstitial impurities (C, N, O and H) had more effect on the response.

a)

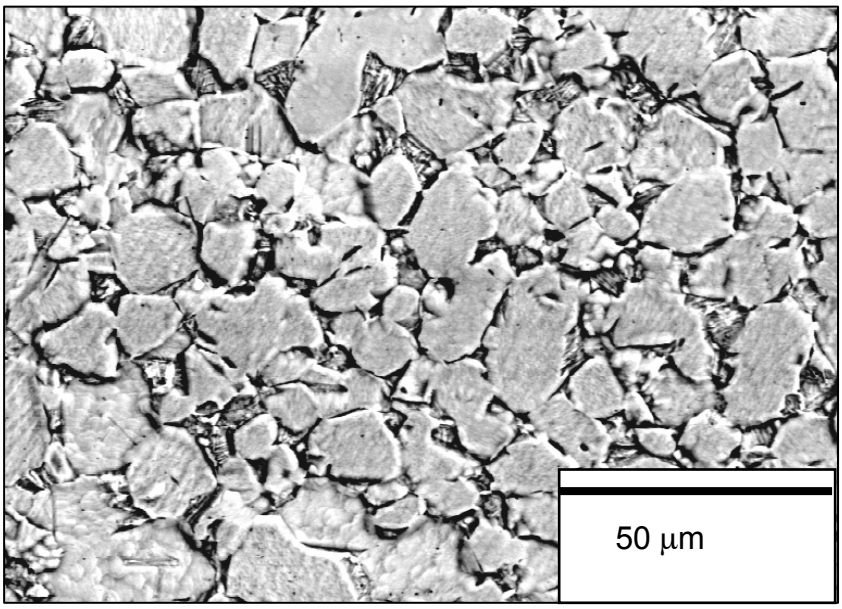

b)

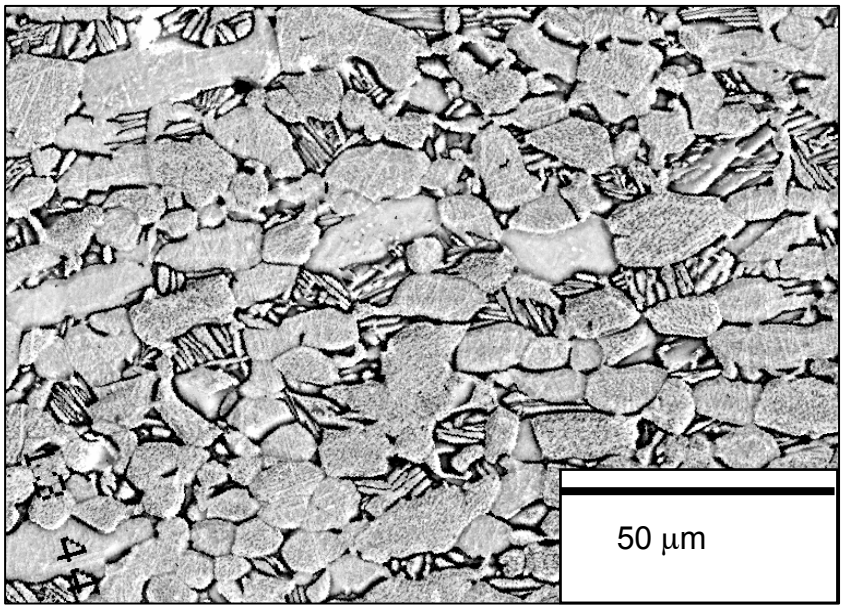

Fig. 4 Initial microstructures of the (a) ELI version of the titanium alloy (alloy 2), and (b) the higher oxygen content titanium alloy made from single electron beam melting process (alloy 3).

In the current investigation, it is observed from the measured responses that alloys 1 and 3 have higher flow stress as compared to the alloy 2. This is attributed to the fact that the interstitial solute content or the equivalent oxygen content (O_{eq}), which is known to strengthen the alloy, is higher in these alloys.

The material constants for this model are determined using several uniaxial quasi-static and dynamic experimental results at different strain rates at room temperature, and high & low temperature experimental results at one strain rate. This usually provides one with a set of initial material constants which can be used as input into a computer software which utilizes constrained optimization procedure using least square method to obtain a set of more refined material constants. The dynamic data before being input in the optimization scheme is converted into an equivalent isothermal data by calculating the instantaneous temperature rise in the material at any strain level and calculating stress increment for that temperature rise to get corresponding isothermal stress response. The material constants thus determined were used to predict a strain rate jump experiment, which was performed separately for each alloy. This experiment was not included in the calculation of the material constants. The strain rate jump experiment included at least two different strain rates in the quasi-static regime followed by a dynamic regime strain rate. The final material constants for the three alloys are given below.

	A **(MPa)**	***B*** **(MPa)**	n_1	n_0	***C***	***m***
Ti-6Al-4V Alloy 1	1100	857.5	0.5455	0.6086	0.02204	1.6236
Ti-6Al-4V Alloy 2	988	747.1	0.5455	0.3986	0.02204	1.2214
Ti-6Al-4V Alloy 3	1069	874.8	0.5455	0.4987	0.02204	1.3916

Table 2. KHL model material constants determined for the three Ti-6Al-4V Alloys used in the investigation

For alloy 1, five different strain-rate experiments were performed ranging from 10^{-6} s^{-1} to dynamic strain rate of 3100 s^{-1}. The material behavior was found to be strain rate sensitive and has a non linear work hardening response at low deformation levels transitioning to an almost linear response at higher deformation levels. Also, there is a slight reduction in work hardening rate with increasing strain rates in the quasi-static loading regime. There is no or little work hardening effect seen in the adiabatic dynamic experiment due to thermal softening. The room temperature experiments along with the model correlations can be seen in Fig 5. The observed response of the material is also a non-linear function of temperature. The increase in test temperature causes a drop in the flow stress. A slight decreasing work hardening rate behavior can be noticed as the temperature increases and also with an increase in the level of strain. The response of the alloy at various temperatures, along with the model correlations for different temperatures can be seen in Fig 6.

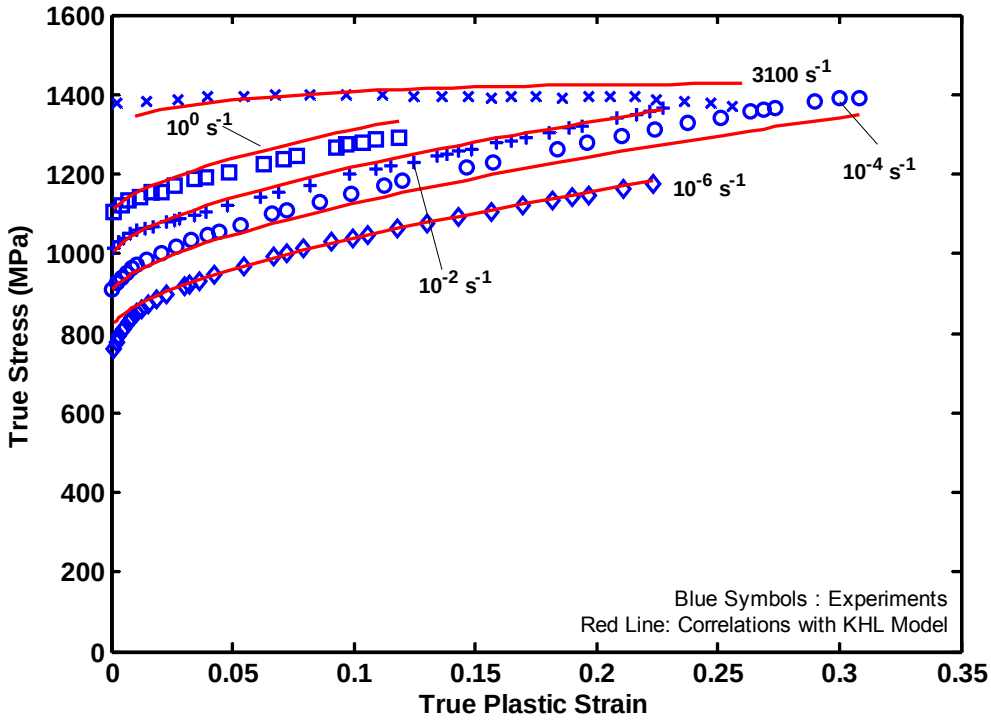

Fig. 5. KHL model correlations with the room temperature (296K) response of alloy 1 at different strain rates.

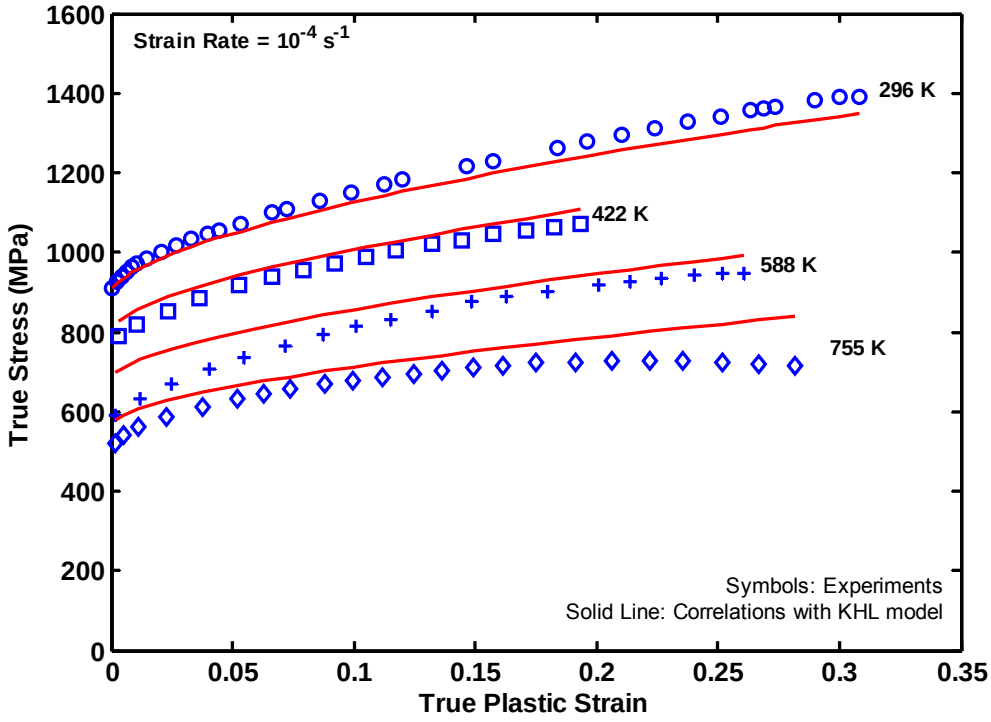

Fig. 6. KHL model correlations with the observed response of alloy 1 at different temperatures at constant strain-rate 10^{-4} s^{-1}

Experiments were also performed at high temperatures under dynamic loading conditions on alloy 3 and the response was modeled. The KHL model was able to successfully predict the material behavior at these temperatures and strain rates. The point to note is that these set of experimental observations were not included in calculating the material constants. The experimental observations and KHL predictions are shown in Fig 7. Overall KHL model is able to simulate different loading conditions at different strain rates and temperatures for all the alloys used in the investigation.

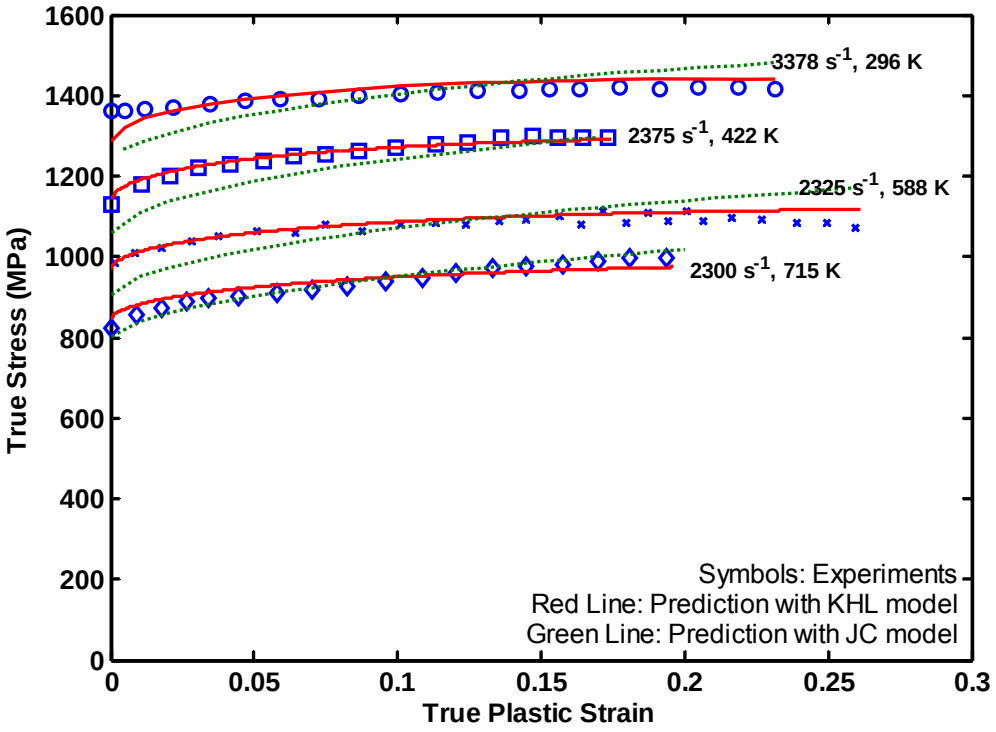

Fig. 7. KHL model predictions with the observed response of alloy 3 at high strain rates and different temperatures. All the predictions are adiabatic.

Executive Summary of Achievements III

A large number of studies have been carried out in understanding and modeling the response of these titanium alloys. These studies were focused mainly on the uniaxial response of the alloys at different strain rates and temperatures, and assuming isotropic behavior. However, it is well known that the stress states in these alloys while in use are definitely more complex and multiaxial in nature. Hence it becomes extremely important to understand the material behavior during these loading conditions. The uniaxial material responses and modeling act only as the first step towards understanding the

actual more complex conditions that exist and how they affect the corresponding responses.

Titanium alloys in the low and medium temperature regime consist mainly of the HCP α-phase with very little dispersed (BCC) β-phase in between the equiaxed α grains. These hexagonal closed packed (HCP) metals, especially in a plate geometry, are known to display plastic anisotropy and a strong strength differential in tension and compression. This is because of the interaction between crystallographic slip and deformation twinning (Cazacu et al., 2005). Twinning is also known to be dependent on the sign of the shear stresses. Also, anisotropy exists in these alloys mainly due to the strong crystallographic texture induced due to the rolling process. Therefore, multiaxial modeling of these HCP titanium alloys cannot be performed using definitions of the effective stress, strain and strain rate based on the isotropic J_2-flow theory as these alloys have been known to be anisotropic in nature. Similar conclusions were found by other researchers while studying the multiaxial response of α-titanium.

Anisotropy has been studied in great detail by many researchers over the past many decades. Hill (1948) was the first to quantitatively determine the yield surface for anisotropic materials. Hill's anisotropic model was primarily based on the generalization of the von-Mises yield criterion. Although this model has been useful because of its simplicity it was not able to capture the observed anisotropy in yield stress and the R-ratios together (Lademo et al. 1999). Other prominent anisotropic yield criteria are by Hosford (1979), Barlat and co workers (Barlat et al. 1991, 1997, 2003), Karafillis and Boyce (1993), Yoon et al. (2006), etc. These criteria dealt with the modeling of cubic crystals and assume same yield stress in tension and compression. Some anisotropic models have been proposed and used in the literature for HCP poly-crystals by Tomé and Lebensohn (2004), and Staroselsky and Anand (2003). Macroscopic criteria are generally less time consuming, such as the orthotropic criterion by Cazacu et al. (2005) which is based on the linear transformation of the Cauchy stress tensor deviator.

The present phase of investigation includes a comprehensive set of experiments for understanding the response of this alloy and consequently modeling the observed responses of these alloys at different strain rates. It is an extension of the previous investigation by Khan et al. (2004). In this investigation, the high strain rate torsion experiments are carried out using the modified Kolsky bar apparatus (Hartley et al., 1985). This is followed by compression on the same samples again at high strain rates, albeit at different operating temperatures. The quasi-static torsion experiments are carried out using the MTS axial/ torsion material testing system. The non-proportional loading experiments are performed using the channel die at small and intermediate strain-rate regime. During these experiments the stress state is designed to change from uniaxial to biaxial compression and the corresponding response is observed and recorded. Constitutive modeling of these observed responses is performed using the KHL model. The experimental data is first converted into effective stress and effective strain based on definitions of the orthotropic yield criteria proposed by Cazacu et al (2005).

In order to describe the strength differential and the anisotropy typically shown by hexagonally closed packed (HCP) metals and alloys, Cazacu et al. (2005), proposed a new phenomenological orthotropic criterion that could capture the response of the material in different directions accurately. This criterion was based on the linear transformation of the deviatoric part of the Cauchy stress tensor, $\boldsymbol{S}$ similar to previous studies by Barlat and co-workers (Barlat et al.1991; Barlat et al. 1997; etc) and had previously been used by many researchers (Lademo et al., 1999; Lademo et al., 2002; Abedrabbo et al., 2006, etc) successfully. The transformed tensor $\sum$ is defined as:

$$\sum = C[S] \tag{3}$$

where $\boldsymbol{C}$ is a 4^{th} order tensor. The orthotropic yield criterion is given as:

$$\left(|\Sigma_1| - k.\Sigma_1\right)^a + \left(|\Sigma_2| - k.\Sigma_2\right)^a + \left(|\Sigma_3| - k.\Sigma_3\right)^a = F \tag{4}$$

The exponent a, in the yield criterion is considered to be a positive integer (in our case a=2). The parameter k is a material constant, which for a fixed a, is determined by the ratio of the strength in tension and compression. The function F, gives the size of the yield locus. F can be defined either as a constant or a function of the total plastic strain (isotropic hardening).

Experimental results from uniaxial tension and compression yield stresses, in rolling and transverse to rolling directions, uniaxial compression in the 45° to the rolling direction and R-ratios in the rolling, and transverse to rolling directions for the compression case are used. These material constants are calculated using least square optimization technique in MATLAB. The value of the material constant k, used in this investigation is calculated from the ratio of the yield in tension and compression in the transverse to rolling direction. The experimental yield stresses for rolling and transverse to rolling as well as the yield surface generated from the orthotropic criteria are shown in Fig.8. The corresponding experimental R-ratios and the yield stresses at 45° to the rolling direction and in shear are shown along with the correlations from the model in Table 3.

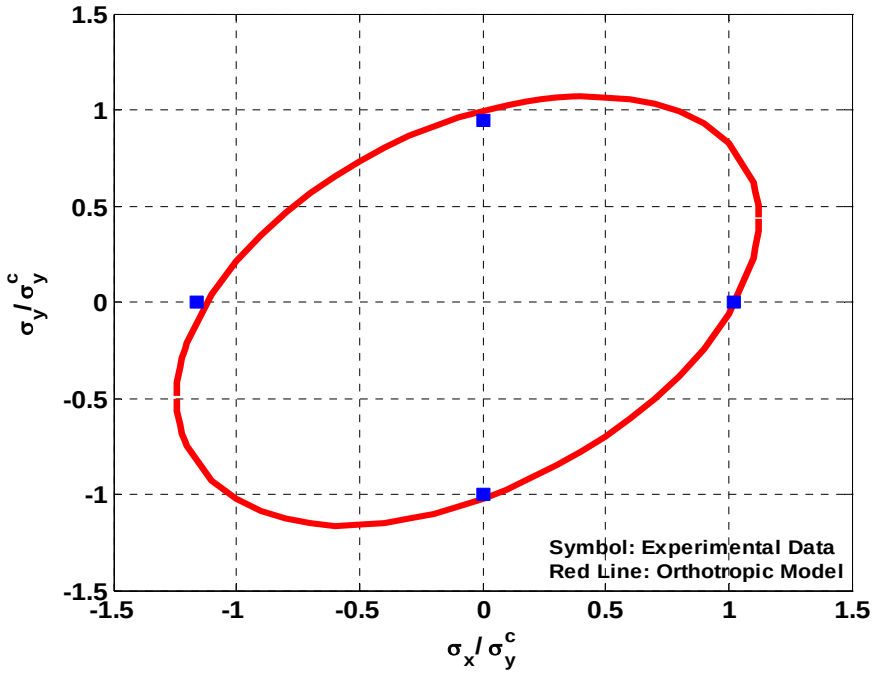

Fig. 8. Yield surface generated using the orthotropic yield criteria from Cazacu et al. (2005) for Ti-6Al-4V titanium alloy

Yield Stress	σ^T_0	σ^T_{90}	σ^C_0	σ^C_{90}	σ^C_{45}	σ_{xy}	r^C_0	r^C_{90}
Experimental Values	138.61	130.9	157.67	135.44	144.01	74.76	0.685	0.507
Normalized Exp. Values	1.02	0.97	1.16	1	1.06	0.55	0.685	0.507
Predicted Values	1.04	0.94	1.14	1.03	1.04	0.58	0.69	0.501

Table 3. Experimental and predicted values of the yield stresses and R-ratios under different loading conditions

It can be seen from the Fig. 8 and Table 3 that the orthotropic model works reasonably well for HCP metals in the development of the yield surface and that the values of R-ratios (which incorporates the flow rule) correlated by this model are extremely close to the experimental data. This implies that it is reasonable to use effective stress, strain and strain rate definitions using this orthotropic model.

The experimental results from quasi-static monotonic torsion, quasi-static jump torsion and dynamic torsion experiments were converted into effective stress (σ_e) using the definition of the yield function (Eqn. 4), so that the complexity of the stress state reduces to a single scalar quantity. In a similar manner the effective strain, (ε_e), and strain rates, ($\dot{\varepsilon}_e$), are also calculated from the experimental results by considering the principle of incremental work per unit volume (Khan and Huang, 1995). The experimental results were then plotted against the model predictions based on these definitions.

$$dW^p = \sigma_{ij} d\varepsilon_{ij}^p = \sigma_i d\varepsilon_i^p = \sigma_e d\varepsilon_e^p \tag{5}$$

Fig. 9 shows the experimentally observed multiaxial response of the alloy along with the model predictions (the material constants were not changed from the published values, Khan et al., 2004). The KHL model is able to predict the response of these quasi static as well as the dynamic torsion experiments reasonably well. The KHL predictions are made assuming adiabatic deformations for the 1.732 s^{-1} (shear strain rate) as well as the dynamic experimental results as an increase in the temperature were noticed during both experiments.

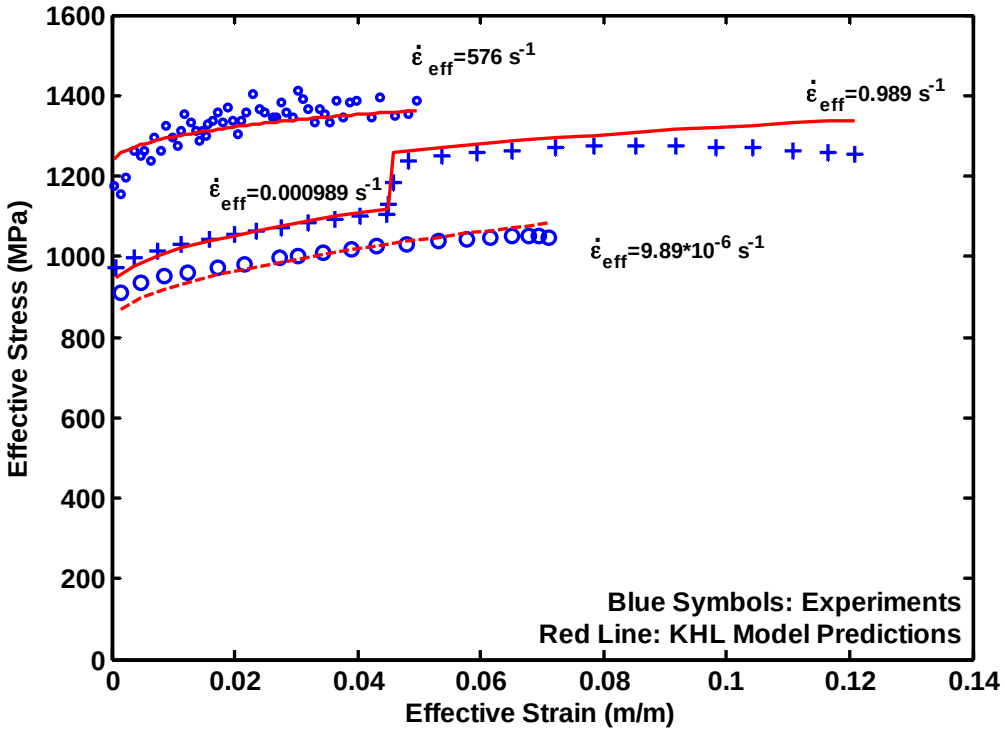

Fig. 9. Model predictions with the observed shear response of the titanium alloy converted to effective stress and strain during monotonic, strain-rate jump and dynamic torsion experiments at room temperature (296K). Dynamic and 0.989 s^{-1} effective strain rate predictions are based on assuming adiabatic deformation.

Fig. 10 shows the measured response of the alloy under dynamic torsion at room temperature, followed by dynamic compression at higher temperature (588 K). The KHL model predictions were converted for adiabatic case as was done in the previous case. The predictions are again in very good agreement with the actual observed material response for both types of dynamic loading conditions showing the capability of the model in capturing the observed behavior of the alloy under complex loading conditions when used in conjunction with the anisotropic criterion.

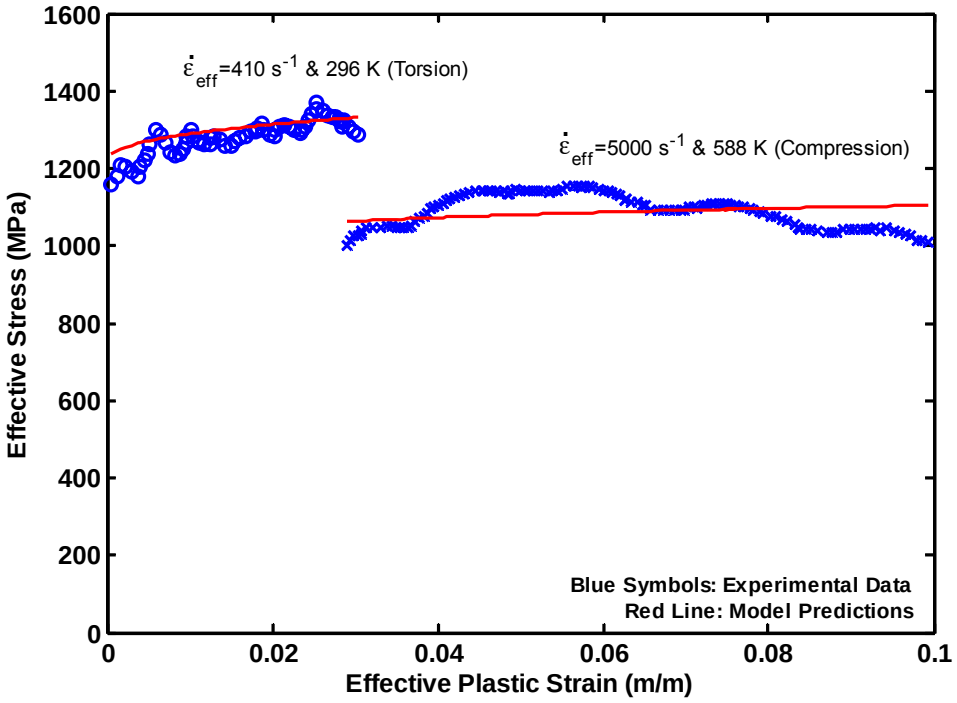

Fig. 10. Dynamic shear response at room temperature, followed by dynamic compression response at 588°K of the titanium alloy, and predictions using KHL model with the material constants determined from uniaxial compression experimental data.

The true stress and strain response of the alloy under non-proportional loading conditions, uni-axial to bi-axial compression, at 10^{-1} s^{-1} strain rate in the loading direction is shown in Fig. 11. The rise in the stress in the loading direction is clearly visible as the specimen becomes constrained once a certain predetermined level of deformation in the loading direction is achieved. Consequently, there is a corresponding rise in the stress in the constrained direction until the end of the experiment. Fig.12 shows the effective stress and effective strain responses for different strain rates in the loading directions along with the model predictions. Effective stresses, strains and strain rates are calculated based on the orthotropic yield criterion of Cazacu et al (2005) and the principle of incremental work per unit volume. The stresses and strains are then plotted with the model predictions. Again, the published values of constants [Khan et al (2004)] are used and are not modified using the present experimental results. The model prediction for the case

of 10^{-1} s^{-1} strain rate in the loading direction is converted assuming adiabatic deformation, as there was a significant increase in the temperature in the specimen noticed during the deformation. The model predictions are in excellent agreement with the experimentally observed responses for all strain rates. The strain rates used in the model calculations in all non proportional loading experiments are effective strain rates, and are computed using the three strain histories along with the principle of incremental work per unit volume.

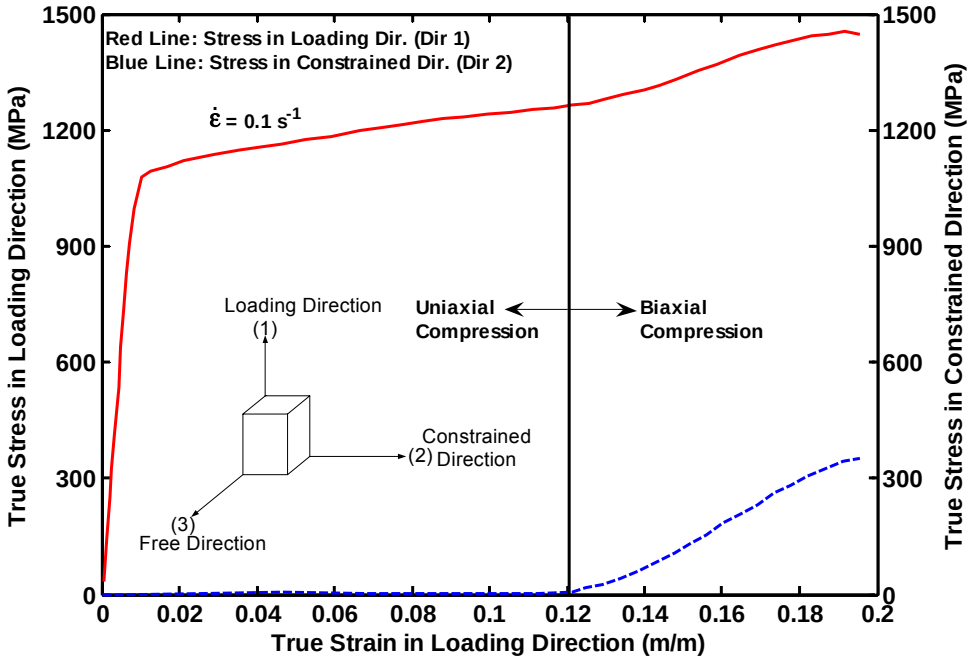

Fig. 11. True stress-strains for the non-proportional loading channel die experiment at 10^{-1} s^{-1} strain rate in the loading direction. Note the stress starts to increase in the direction 2 (constrained direction) from zero once the specimen comes in contact with the die walls at approximately 12% strain in the loading direction.

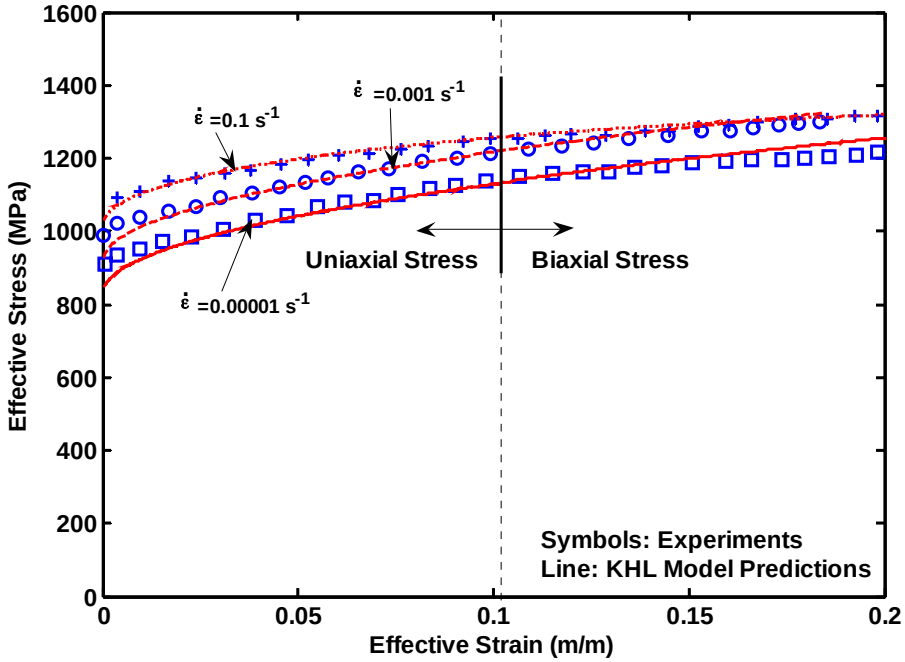

Fig. 12. Quasi static response of the titanium alloy under non proportional biaxial loading at room temperature converted to effective stress and strain based on an orthotropic yield criteria and predictions using KHL model with the material constants determined from uniaxial compression experimental data.

Using the set of model constants for this alloy which were calculated from the uniaxial responses at different strain rates and temperatures in an earlier paper (Khan et al. 2004), the capability of the model to predict accurately the observed new responses under the complex multiaxial loading conditions was demonstrated. The model was able to predict the material response under pure torsion, and torsion followed by compression extremely well using the effective stress, strain and strain rate definitions from a orthotropic yield criterion and principle of incremental work per unit volume. In the non proportional channel die experiments, the model was again able to predict the observed material responses under non-proportional loading conditions reasonably well.

References

Khan, A. S., Suh, Y. S., and Kazmi, R., "Quasi-static and dynamic loading responses and constitutive modeling of titanium alloys", International Journal of Plasticity, 20 (2004) 2233-2248.

Kazmi, R., Zupan, M., Khan, A. S., "Microstructure, response and constitutive modeling of several economical Ti-6Al-4V alloys over a wide range of strain rates and temperatures", in-print, 2006, International Journal of Plasticity.

Khan, A.S., Kazmi, R., Zhou, J., Farrokh, B. "Multiaxial and non-proportional loading response, anisotropy and modeling of titanium alloy (Ti-6Al-4V) over wide range of strain rates and temperatures", in-print, 2006, International Journal of Plasticity.

PUBLICATIONS IN REFEREED JOURNALS:

1. Akhtar S. Khan, Yeong Suh & Rehan Kazmi, 2004, "Quasi-static & Dynamic Loading Responses and Constitutive Modeling of Titanium Alloys", International Journal of Plasticity, Vol. 20, pp. 2233-2248.

2. Akhtar S. Khan, Rehan Kazmi, Marc Zupan, 2006 "Microstructure, response and constitutive modeling of several economical Ti-6Al-4V alloys over a wide range of strain rates and temperatures", in print, International Journal of Plasticity.

3. Akhtar S. Khan, Rehan Kazmi, Jiang Zhou, Babak Farrokh, 2006, "Multiaxial and non-proportional loading response, anisotropy and modeling of titanium alloy (Ti-6Al-4V) over wide range of strain rates and temperatures", in print, International Journal of Plasticity.

PUBLICATIONS IN CONFERENCE PROCEEDINGS:

1. Akhtar S. Khan, Jenifer Baker, Robert Matteson, Renee Tirocchi, 2002, " Response and Modeling of Titanium ELI over a Wide range of Temperatures and Strain Rates", in " Plasticity, Damage and Fracture at Macro, Micro and Nano Scales", Edited by A. S. Khan and O. Lopez-Pamies, NEAT Press, Fulton, MD, pp. 627-629.

PRESENTATIONS AT INTERNATIONAL CONFERENCES:

1. Renee Tirocchi, Akhtar S. Khan, Jenifer Baker, Robert Matteson, 2002: " Response and Modeling of Titanium ELI over a Wide range of Temperatures and Strain Rates", at Plasticity '02: The Ninth International Symposium on Plasticity and Its Current Applications, Wyndham Aruba Resort, Aruba, Jan. 3-8, 2002.

2. Khan, A. S., " Response of Ti-6Al-4V Alloys Over a wide Range of Strain-rates and Temperatures and Constitutive Modeling", IUTAM Symposium on Multi-Scale Modeling and Characterization of Elastic-Inelastic Behavior of Engineering Materials, October 20-25, 2002 (Invited Paper).

3. Akhtar S. Khan, 2005, " Thermo-mechanical Dynamic Response and Constitutive Modeling of Titanium Alloys," a Key-note Invited Lecture at the Eleventh International Symposium on Plasticity and Its Current Applications, Lihue, Kauai, Jan. 3-8, 2005.

4. Akhtar S. Khan, 2005, " Some critical Experimental Results for Constitutive Modeling" , a Plenary lecture at The Numisheet 2005, 6th International Conference and Workshop on Numerical Simulation of 3D Sheet Forming Processes, Detroit, August 15-19, 2005.

Technology Transfer

(i) The results of this project were presented at an informal seminar at TARDEC, Detroit, on October 28, 2003; the seminar was attended by TARDEC, ARL and ARO scientists with direct interests in this project, as well as by other scientists funded by ARO/TARDEC through complimentary projects.

(ii) Dr. D. Templeton sent copies of the presentation on a CD to other interested scientists at ARL.

(iii) The PI of this project has been in direct contact with Drs. Stephen Bilyk, Datta Dandekar and Hubert Meyer at ARL, and Dr. Raj Rajendran at ARO, about the results of this project.

(iv) An invited paper, based on these results, was presented at the IUTAM symposium At Marrakech, Morocco, 2002, which was attended by ARO scientists.

(v) An invited keynote lecture, based on this project, was delivered at the Tenth Int. Symp. On Plasticity and its Current Applications, Quebec City, July 2003; several ARL scientists attended the symposium.

Scientific Personnel and Degrees Awarded

Ms. Jennifer Baker and Mr. Rehan Kazmi worked as research assistants on the project during first year. Ms. Baker finished her M. S. degree in May 2002. She is now employed at Naval Lab. at Carderock. Mr. Kazmi continued on the project and defended his doctoral dissertation in February 2006. Mr. Jianbo Liu and Mr. Muneer Baig, doctoral students, also worked on this project. Drs. Yeong Sung Suh, Mohammed Abdel-Karim & Jianqui Zhou (post-doctoral research associates) and Dr. Akhtar S. Khan (PI) contributed to the project also.

Inventions

None.

Appendix I

(Khan, A. S., Suh, Y. S., and Kazmi, R., "Quasi-static and dynamic loading responses and constitutive modeling of titanium alloys", International Journal of Plasticity, 20 (2004) 2233-2248.)

QUASI-STATIC AND DYNAMIC LOADING RESPONSES AND CONSTITUTIVE MODELING OF TITANIUM ALLOYS

Akhtar S. Khan [*], Yeong Sung Suh[1], Rehan Kazmi,

Department of Mechanical Engineering, University of Maryland Baltimore County, Baltimore, MD 21250, USA

Abstract

The results from a systematic study of the response of a Ti–6Al–4V alloy under quasi-static and dynamic loading, at different strain rates and temperatures, are presented. The correlations and predictions using modified Khan–Huang–Liang (KHL) viscoplastic constitutive model are compared with those from Johnson–Cook (JC) model and experimental observations for this strain rate and temperature-dependent material. Overall, KHL model correlations and predictions are shown to be much closer to the observed responses, than the corresponding JC model predictions and correlations. Similar trend has been demonstrated for other titanium alloys using published experimental data [Mech. Mater. 33(8) (2001) 425; J. Mech. Phys. Solids 47(5) (1999) 1157].

[*] Corresponding author. Tel.: +1-410-455-3301; fax: +1-410-455-1052

e-mail address: khan@umbc.edu (A.S. Khan), suhy@hannam.ac.kr (Y. Sung Suh).

[1] On leave from Department of Mechanical Engineering, Hannam University, Daejeon 306-791, Republic of Korea.

Keywords: Constitutive behavior; Elastic–viscoplastic material; Finite dynamic strain; Titanium alloy; Split Hopkinson bar; Thermal softening; High strain-rate response; Kolsky bar

1. Introduction

Dynamic deformation has been of interest not only in impact and penetration related problems (Gilat & Cheng, 2002; Khan et al. 2002; Khan & Lopez-Pamies, 2002; Bjerke et al. 2002) but also in high speed machining (Molinari et al. 2002; Burns & Davies 2002; Titanium alloys have been studied by several investigators because of their use in aero-engine, gas turbines and other applications due to their high strength to weight ratio, ductility, and ability to withstand high temperatures and resist corrosion. Examples are Macdougall and Harding (1999), Meyers *et al*. (1994), Chichili *et al*. (1998), Cheng and Nemat-Nasser (2000). The first investigation mentioned above was on Ti-6Al-4V alloy,

while others were on commercially available pure alpha-titanium except in case of Cheng and Nemat-Nasser (2000), in which the microstructure, or phase, was not specified. The development of relatively economical Ti-6Al-4V alloy, with resulting high oxygen content, has sparked interest in its possible use in lightweight tanks (Montgomery and Wells, 2001); the conventional, more expensive Ti-6Al-4V alloy has been used primarily in aerospace components. The potential applications in armor, including ceramic tiles encapsulated in titanium alloys, have motivated several studies (Gray, 1997; Follansbee and Gray, 1989; Lesuer, 2000; Nemat-Nasser *et al*., 2001; Majorell *et al*., 2002).

In case of α-titanium, it has been demonstrated that the deformation mechanisms include glide systems with α-type dislocations in the h.c.p. structure, as well as, twinning shear which contributed to the overall strain (Meyers *et al*., 1994; Song and Gray, 1995; Chichili *et al*., 1998). In the only quantitative study of twinning, Chichili *et al*. (1998) have shown that twin number density increases drastically with increase in strain rate. They used length-to-diameter ratio of 1.6 for quasi-static experiments. The rate of increase of this density decreased with increase in strain at dynamic strain-rates of 10^3 s^{-1}, while this rate increased with deformation in the case of quasistatic loading (10^{-5} s^{-1}). Their results further demonstrated that loading at a particular temperature (and/or strain rate), unloading, and reloading at another temperature (and/or strain rate), resulted in a stress-strain curve which was significantly different than if the specimen was loaded at the latter temperature (and/or strain rate) right from the beginning. This study was performed over a wide range of strain rates (10^{-3}~10^3 s^{-1}) but over a very limited range of temperatures (77~298 K). Further, they did not provide the geometry of the specimens used in their split Hopkinson bar measurements.

The Ti-6Al-4V alloy consists of hcp α-grains, with a dispersion of stabilized bcc β phase around grain boundaries at room temperature. α phase transforms to β phase starting at 873 K (1110 F); above 1268 K (1825 F), the entire microstructure consists of equiaxed β grains (Majorell *et al*., 2002). This alloy, in addition to H, V, and Ti, contains O, Fe, Mo, C, Si, and Mn. Oxygen, nitrogen, and carbon contents are α stabilizers (Conrad *et al*., 1975), while vanadium, iron and molybdenum are β stabilizers. Conrad *et al*. (1975) proposed an equivalent oxygen content (O_{eq} = O+2N+0.75C); this equivalent impurity concentration gives the effect of dislocations-impurity interaction on the yield strength of the material. Investigation by Majorell *et al*. (2002) was on an untextured and a textured Ti-6Al-4V alloy rod that was manufactured by Allvac. This study was over a strain-rate range of 10^{-3} to 10 s^{-1} and a temperature range of 650~1345 K (710~1970 F). They did not observe any dynamic strain-aging at any of the temperatures or strain rates investigated. Further, athermal stress, *i.e.*, temperature insensitive response, was found at approximately 1255 K (1800 F); i.e. at a temperature when the material contained almost 100 % β phase. They did not specify specimen geometries used in their investigation. The equivalent oxygen content was 0.206 %.

In a study by Follansbee and Gray (1989), on a Ti-6Al-4V alloy, with an equivalent oxygen content of 0.23% (actual oxygen was 0.18%), the measurements were restricted to three temperatures with a range between 76 and 295 K and at only two strain rates

(10^{-3} and approx. 3000 s^{-1}). Their specimens on as-received and two heat-treated versions were made from a 13.8 mm thick plate; specimens were 4.8 mm in diameter and 5.2 mm long in case of quasistatic loading experiments, and 6.4 mm diameter with a length of 5.1 mm in a 12.7 mm diameter split Hopkinson bar experiment. This investigation did not include responses over a wide range of temperatures. Nemat-Nasser *et al*. (2001) study was on a commercial and two hot isostatically pressed Ti-6Al-4V alloys. The equivalent oxygen in the commercially pure alloy was 0.22 %. The geometry of the specimens was not specified and was presumably 5 mm in diameter and 5 mm long, for quasistatic and dynamic experiments. The diameters of the split Hopkinson bars (perhaps 12.7 mm) were not specified either in the paper. The measurements and assumptions in this investigation have raised several questions. First, they perform experiments on specimens from 77 K to 998 K in the dynamic strain rate regime of 2000 to 4000 s^{-1}. As discussed earlier, α-phase starts transforming to β-phase at 873 K. Thus, they performed experiments on presumably different materials in their range of temperatures, *i.e.*, with different amounts of α and β phases. Second, it is clear from the figures in their paper that at least some experiments had barreling due to insufficient lubrication. Third, they combine initial portions of multiple stages loading-unloading-reloading experiments using split Hopkinson bar technique, to obtain "isothermal" response, even when it is well known that initial portion(s) of the stress-strain curve is not accurate as force equilibrium in the specimen is not reached until elastic and plastic waves are reflected several times back and forth in the specimen. Using these loading-unloading and reloading experiments at different temperatures, they suggested that all (*i.e.* 100 %) of plastic work done was converted to heat. This suggestion is in direct contradiction to the measurements of Mason *et al*. (1994), Liao and Duffy (1998), Macdougall and Harding (1999) and Rosakis *et al*. (2000). As mentioned earlier, Chichili *et al*. (1998) and Follansbee and Gray (1989) have shown that the response of a material is different upon reloading to a different temperature (same strain rate), presumably due to history effects.

Similar inadequacies and contradictions are found in the published modeling efforts. The constitutive models used for high strain rate applications can be classified in two categories; the purely phenomenological ones, e.g. Johnson-Cook (J-C) (Johnson and Cook, 1983) and Khan-Huang-Liang (KHL) models (Khan and Huang, 1992; Khan and Liang, 1999; Khan and Zhang, 2000, 2001) and so called, "physically based models" *e.g.* the ones by Zerilli and Armstrong (1987), Mecking and Kocks (1981), *etc.*, that were used frequently by Follansbee and Gray (1989), and in a modified form by Nemat-Nasser *et al.* (2001). The latter group discusses the mechanisms of plastic deformation, mainly dislocations. However, the material constants are determined by not measuring any deformation mechanism related quantity, but by choosing constants to "fit" the uniaxial stress-strain curves at different strain rates and temperatures, just like the purely phenomenological models. In order to "fit" their model to the uniaxial stress-strain curves of two fairly close Ti-6Al-4V alloys, Nemat-Nasser *et al*. (2001) used athermal stress of 685 MPa while Follansbee and Gray (1989) used 100 MPa; Follansbee and Gray (1989) used a value of 10 MPa to analyze results of Paton et al. It is disappointing to note that almost six hundred percent difference in this value by these two set of researchers using models that are presumably based on the same "physics" for very similar materials. In the original Mecking and Kocks model, as used by Follansbee and Gray (1989), a highly

undesirable extrapolation to 0 K is necessary. In addition, the model has numerous material constants; it requires huge amount of resources and time to determine these constants. In the simplification or modification of this model by Nemat-Nasser *et al*. (2001), experiments are needed at very high temperatures where proper lubrication is extremely difficult, if not impossible, to attain, as is clearly evident in their paper. Since both categories of models, phenomenological and "so called physically based", determine material constants by "fitting" to the stress-strain responses at different temperatures and strain rates, the advantage of one over the other is merely number of material constants in each model. Any model with semi-infinite number of material constants will be able to approximate observed responses. Mecking and Kocks model, as used by Follansbee and Gray (1989) has 23 constants, while these constants range from 12 to 8 in case of Cheng and Nemat-Nasser (2000) and Nemat-Nasser *et al.* (2001), respectively, depending on whether they include modeling of dynamic strain aging or not. Johnson-Cook and Khan-Huang-Liang models have 5 and 6 constants, respectively. Johnson-Cook and Khan-Huang-Liang models are used in this investigation due to their advantage of fewer constants and their ability to model the observed material response as closely as with models with many more constants.

Modeling Approach

The material constants for both, the modified KHL (Khan-Huang-Liang) and JC (Johnson-Cook) models were determined. Using these material constants, correlations were obtained and compared to experimental results. The modified Khan-Huang-Liang (KHL) model is as follows.

$$\sigma = [A + B(1 - \frac{\ln \dot{\varepsilon}}{\ln D_0^p})^{n_1} (\varepsilon^p)^{n_0}](\frac{\dot{\varepsilon}}{\dot{\varepsilon}^*})^C (\frac{T_m - T}{T_m - T_r})^m \tag{1}$$

where σ is the stress and ε^p is the plastic strain. T_m, T, T_r are melting, current, and reference temperatures, respectively. $D_0^p = 10^6$ s^{-1} (arbitrarily chosen upper bound strain rate) and $\dot{\varepsilon}^* = 1$ s^{-1} (reference strain rate at which some material constants are determined). $\dot{\varepsilon}$ is the current strain rate. A, B, n_1, n_0, C and m are material constants. For Ti-6Al-4V alloys, the melting temperature is 1933 K (Nemat-Nasser *et al*., 2001). A major feature of this model, unlike the Johnson-Cook (JC) model, is that decreasing work-hardening with increasing strain rate can be accommodated through the material constant n_1. Previously, this model had a temperature dependence term (similar to JC model) as:

$$\left(1 - (\frac{T - T_r}{T_m - T_r})^m\right) \tag{2}$$

However, this term can not accommodate the case when the current temperature is lower than the reference temperature as then the above term within parenthesis becomes a

negative number raised to the power m. Therefore a modification was made as given in Equation (1). The Johnson-Cook (JC) model is given by the following equation.

$$\sigma = [A + B(\varepsilon^p)^{n_0}](1 + C \ln \frac{\dot{\varepsilon}}{\dot{\varepsilon}^*})\left(1 - (\frac{T - T_r}{T_m - T_r})^m\right) \tag{3}$$

In this case, various terms have the same definitions as Equation (1).

To determine the material constants for the model, uniaxial loading test results at different strain rates and temperatures were first used to obtain an initial set of values for the material constants, as described in Khan and Liang (1999). In order to get a refined set of material constants, the least squares and constrained optimization procedures were used to minimize the difference between correlated and actual data using MATLAB. The experimental results at low strain rates were first used to get a set of material constants using the least squares method. Then, higher strain rate data, measured under adiabatic condition, were correlated with the assumption that 90 % plastic work was dissipated to heat, to get a better set of material constants for both low and high strain rate material response using a constrained optimization procedure. This was iteratively performed until the constants converged. As for the dynamic data, thermal softening from the adiabatic deformation was effectively considered by converting the increment of temperature from the stress-strain curve using following equation:

$$\Delta T = \frac{\beta}{\rho C_p} \int_0^{\varepsilon_1^p} \sigma(\varepsilon^p) d\varepsilon^p \tag{4}$$

where β, ρ, C_p are the fraction of heat dissipation caused by the plastic deformation, mass density and specific heat at constant pressure, respectively. In fact, there are many arguments on the conversion of plastic work to heat during high strain rate deformation. Taylor and Quinny (1934) measured the fraction of heat conversion and found that it is of the order of 0.9 with copper specimens. Mason *et al*. (1993) measured it with dynamic experiments and demonstrated that it depended substantially on strain and strain rate. Kapoor and Nemat-Nasser (1998) measured the energy converted to heat using an infra-red method for Ta-2.5 % W alloy, commercially pure Ti, 1018 steel, 6061 Al and OFHC Cu. They argued that the infra-red measurement generally underestimated the conversion ratio (70% of conversion of work for Ta-2.5 % W, for example), they cooled down the specimen to the initial room temperature at certain strain and heated it to the temperature based on 100% heat conversion and then deformed the specimen at the same strain rate to check if the adiabatic curve was obtained. On this basis, they suggested that nearly all of the plastic work was converted into heat (*i.e*., β=1) within experimental error, concluding that the infra-red detection system recorded a lower (surface) temperature than the actual temperature of the specimen. Later, Nemat-Nasser *et al*. (2001) argued for this total heat conversion by measuring the thermomechanical response of a Ti-6Al-4V alloy (commercial Ti64). Macdougall and Harding (1999) calculated the proportion of work converted to heat based on their torsional dynamic test with an infrared technique

for Ti-6Al-4V specimens and concluded that β varied with increasing plastic strain from approximately 0.2 to approaching 0.7. Rittel (1999) and Rosakis *et al*. (2000) also indicated that β was a history-dependent quantity and depended strongly on both strain and strain rate for various engineering materials. There seems to be no agreement on a single value of β that works for variety of engineering materials; however most researchers still use 0.9, e.g. Lennon & Ramesh (2004). In this study, $\beta = 0.9$ was assumed.

For Ti-6Al-4V, the density is ρ = 4428 kg/m^3 (Lesuer, 2000). The heat capacity was expressed as a function of the temperature, (Military Handbook, 1998);

$$C_p = 559.77 - 0.1473T + 0.00042949T^2 \quad \text{J/(kg·K)} \quad (278\ \text{K} < T < 1144\ \text{K}) \qquad (5)$$

Finally, using these material constants for both models, predictions were made and compared to a strain-rate-jump experiment (10^{-5} to 10^{-1} to 1700 s^{-1}).

Material constants for both models were determined for two additional Ti-6Al-4V alloys (Nemat-Nasser *et al*., 2001; Macdougall and Harding, 1999). The first one was commercially available from Protech Metals (Nemat-Nasser *et al*., 2001), and the second one was used in torsion and tension tests by Macdougall and Harding, (1999), where the exact composition of the Ti-6Al-4V was not given.

Experimental Details

3.1 Material

The chemical composition of Ti-6Al-4V is shown in Table 1. This Ti-6Al-4V alloy is ductile and has a hexagonal close packed crystalline structure. The composition is slightly differed from the commercial Ti alloy that was used by Nemat-Nasser *et al* (2001), and is presented in Table 2.

3.2 Experimental Procedure

3.2.1 Room Temperature Compression Experiments

Quasistatic compression experiments were conducted using an MTS servo hydraulic axial/torsional material testing machine at strain rates of 10^{-5} s^{-1} to 1 s^{-1}, using cylindrical specimens. The specimens were machined from a plate (27.9 mm thick) of Ti-6Al-4V to 19.1 mm in length and 12.7 mm in diameter. The length dimension was in the thickness direction of the plate. It should be noted that the experiment at a strain rate of 1 s^{-1} was conducted in increments of 5 % strain, with 30 minutes between loading and reloading. This method allowed the specimen sufficient time to cool, ensuring an isothermal

response. For room temperature compression experiments, KFEL-2-120-C1 high elongation uniaxial strain gages, manufactured by Kyowa Ltd. (Japan), were mounted diametrically opposite to each other at the center of each specimen using Micro-Measurements Inc. adhesive AE-15. The MTS transducers directly supplied load and LVDT output data to the TestStar software. The interface between the load platens and the test specimens for each of the compression experiments was lubricated with Teflon sheets and Dow Corning high vacuum grease in order to achieve homogeneous deformation and thus avoid barreling of the specimen, maintaining a uniform, uniaxial stress state.

3.2.2 Compression Experiments at Different Temperatures

Quasistatic experiments at different temperature were conducted at 233, 296, 422, 588, and 755 K with a strain rate of 10^{-3} s^{-1}. The LVDT displacement supplied stroke data that included the total deformation of the MTS actuators, the loading platens, the grease lubricant, and the specimen. The interface between the load platens and the test specimens for each of the compression experiments was lubricated with high or low temperature grease, depending on the experiment temperature, in order to achieve uniformity in deformation and avoid barreling of the specimen, maintaining a uniform, uniaxial stress state. The stroke was corrected by running a blank experiment (without specimen).

3.2.3 Dynamic Compression Experiments

The Split Hopkinson Bar technique was used to attain dynamic measurements. The interfaces between the incident and transmitted bars and the test specimen were carefully lubricated with grease, in order to increase uniformity in deformation. The initial thickness and diameter of the specimen were 5.1 (in the direction of thickness of the plate) and 10.2 mm, respectively. The pressure and striker bars used for the experiment were made of hardened VascoMax C350 steel and the diameters were 12.7 mm.

3.2.4 Room Temperature Strain-Rate-Jump-Compression Experiments

In order to conduct the strain-rate-jump experiment, the specimen was loaded at an initial strain rate of 10^{-5} s^{-1}. The strain rate was then increased to 10^{-1} s^{-1} around 6.3 % strain. Upon unloading the specimen after quasistatic compression, around 14% strain, it was machined into two dynamic compression specimens with diameter 10.2 mm and thickness 5.1 mm. The split Hopkinson pressure bar technique was then used to obtain the response of the material in the third stage of loading at a strain rate of 1700 s^{-1}.

Results and Discussion

4.1 Experimental Results

Fig. 1 includes the measured true stress-true plastic strain curves shown with symbols (the plastic strain was converted from the total strain measurement) at different strain rates and at room temperature. As seen in Fig. 1, the material response at various strain rates indicates that the material is strain rate dependent. Fig. 2 gives the measured true stress - true plastic strain curves (also shown with symbols) at different temperatures and at a strain rate of 10^{-3} s^{-1}. Figures 1 to 3 include results using the Alloy 1 (see Table 1). Figure 4 contains results of Nemat-Nasser et al. for Alloy 2, while Figures 5 & 6 represents results of Macdougall & Harding (1999).

4.2 Determination of Material Constants

In order to determine the material constants, all data were included in the least squares method and constrained optimization procedure. Isothermal dynamic response was obtained, and included in the optimization procedure, from adiabatic measurements using $\beta = 0.9$. In case of JC model, the material constants were determined by two methods, the published non-optimized approach and also the optimized method used for KHL method. Tables 3 and 4 include material constants for KHL and JC models, determined for Ti-6Al-4V alloy and for two alloys from the studies of the data extracted from Nemat-Nasser *et al*. (2001) and Macdougall and Harding (1999).

4.2.1 Correlations and Predictions with Ti-6Al-4V (Alloy 1)

The quasistatic and dynamic measurements at a temperature of 296 K and at various strain rates, along with correlations by KHL and JC models are shown in Fig. 1. Although the correlations with both models are reasonably good for the quasistatic case, the KHL model correlates better with the dynamic response, while the JC model differs substantially from the measured response in terms of initial yield stress and work hardening rate at this high strain rate deformation. It was observed that even with the optimized material constants, JC model did not correlate well with the dynamic response. This is due to the fact that JC model fails to correlate the decreasing work hardening rate as the strain rate increases. This is described elsewhere in detail (Liang and Khan, 1999), in which it was shown that in the JC model, the work hardening rate at certain strain would increase when strain rate increases. That is, the JC model is not appropriate for modeling any material where the work hardening rate decreases with increasing strain rate, such as tantalum, (Chen and Gray, 1995). With Ti-6Al-4V, too, it can be observed from the material behavior at different strain rates that the work hardening rate decreases as the strain rates increases.

In Fig. 2, quasistatic measurements (at a strain rate of 10^{-3} s^{-1}) at various temperatures, with correlations using KHL and JC models are shown, respectively. Material constants for JC model determined using published conventional methods, *i.e.*,

without the optimization, led to slight deviation from the measured response. Overall, the KHL model gave somewhat better correlation than the JC model, except for 422 K. The JC model has a major drawback that it cannot be used at temperatures lower than the reference temperature at which material constants are determined. Note the absence of correlation at 233 K in JC model as, $(T - T_{ref})/(T_m - T_{ref})$ becomes negative.

A strain-rate-jump experiment was performed at 296 K with strain rate from 10^{-5} s^{-1} to 10^{-1} s^{-1}, followed by an experiment at a strain rate of 1700 s^{-1}. The measured response was compared with predicted ones by using KHL and JC models (Fig. 3). This experimental response was not included in the determination of material constants. The predictions were made assuming that 10^{-5} s^{-1} span is under isothermal conditions and 10^{-1} s^{-1} and 1700 s^{-1} experiment are under adiabatic condition. Especially at a strain rate of 1700 s^{-1}, and initial segment at 10^{-5} s^{-1}, KHL model predictions are in better agreement with the measured response than the JC model, which over predicts the experimental results at these two strain rates.

4.2.2 Correlations with Nemat-Nasser et al.'s data (Alloy 2)

In Fig. 4, quasistatic and dynamic measurements (at a strain rate of 10^{-3} s^{-1}) for various temperatures with the correlations using KHL and JC models are shown. These measurements were made on a commercially available Ti-6Al-4V alloy, obtained from Protech Metals. As shown in Table 2, the composition of this material is somewhat different from that of the Ti-6Al-4V alloy studied in the present work (Alloy 1), see Table 1. Since the quasistatic data to determine the initial material constants were not available, the parameters were directly optimized using the parameters obtained for the other alloy as an initial input. For all the cases, KHL model gives better correlation.

4.2.3 Correlations and Predictions Using Macdougall and Harding's data (Alloy 3)

The data from torsional experiments were extracted and converted to von Mises effective stress and effective plastic strain assuming $\bar{\sigma} = \tau\sqrt{3}$ and $\bar{\varepsilon}^p = \gamma/\sqrt{3}$ where τ and γ are shear stress and shear strain, respectively. The material constants determined from the correlation with three torsional measurements: $\dot{\gamma}$ = 1000, 0.1, and 0.0007 s^{-1} (which correspond to effective von Mises strain rates, $\dot{\bar{\varepsilon}}$ = 577.4, 0.0577, and 0.0004 s^{-1}, respectively). These constants are given in Tables 3 & 4. Since the data near failure may be affected by necking (tensile loading), or buckling in case of torsional loading, these data near failure are not included in the analysis. In Fig. 5, quasistatic and dynamic torsional measurements with effective strain rates, $\dot{\bar{\varepsilon}}$ = 577.4, 0.0577, and 0.0004 s^{-1} at a temperature of 293 K are shown along with correlations using KHL and JC models. The material constants were determined from the same experimental results. Again, KHL model correlations are better than those with JC model especially at higher strain rates. Based on the material constants determined only from the torsion experiments, a comparison between tensile dynamic data at a strain rate, $\dot{\varepsilon}$ = 2000 s^{-1}, and predicted adiabatic stress/strain responses using KHL and JC models at a temperature of 293 K are

shown in Fig. 6. Again, KHL model gives better prediction; especially the thermally softened work-hardening due to heat dissipation is more closely predicted with KHL model.

Conclusions

A comprehensive study on quasi-static and dynamic responses of Ti-6Al-4V Titanium (Alloy 1) alloy from monotonous and strain-rate-jump compression experiments was performed. Quasistatic experiments, using MTS machine, at room temperature were conducted on cylindrical titanium specimens at strain rates of 10^{-5}, 10^{-3} and 1 s^{-1}, and at temperatures of 233 K, 296 K, 422 K, 588 K, and 755 K at a strain rate of 10^{-3} s^{-1}. Dynamic response was measured using the split Hopkinson pressure bar (SHPB) technique at strain rates of 3378 s^{-1} at room temperature. Experimental results from uniaxial loading experiments were used to determine material constants for the KHL and JC constitutive models for this titanium alloy. It was found that Ti-6Al-4V is nonlinearly dependent on strain rate, as well as temperature.

The KHL model was found to correlate better than JC model especially during dynamic deformation regime. The thermal softening at high strain rates, together with reduction in the work hardening rate with increase in strain rate and strain, was captured much better by the KHL model than the JC model. The temperature term of the modified KHL viscoplastic constitutive model was able to correlate well with the response at a temperature (233 K) which was lower than the reference temperature (296 K); the JC model was not valid in this case.

Material constants of the KHL and JC models, determined previously were used for predictions of the observed material response in a strain-rate-jump experiment to examine the validity of the two models. The test was performed at 296 K with strain rate from 10^{-5} s^{-1} to 10^{-1} s^{-1} and then to 1700 s^{-1}. Again KHL model provided better agreement with the measured response than the JC model.
In addition to this alloy, results from two more titanium alloys were obtained from the existing publications (Nemat-Nasser *et al*., 2001; Macdougall and Harding, 1999) and compared with correlations and predictions by using KHL and JC models. Once again, the KHL model was closer to the observed response than JC model especially at high strain rates and at different temperatures.

Acknowledgements
The first author is grateful for the funding of this project by the Army Research Office under cooperative agreement DAAD19-01-1-0635, under the direction of Dr. Bruce LaMattina (Solid Mechanics Program). The first author is also thankful to Dr. Douglas Templeton, Team Leader of Emerging Technologies at US Army TARDEC for funding of the project and guidance. Various help and comments of Dr. Raj Rajendran at the Army Research Office is also gratefully acknowledged.

Table 1: Chemical Composition of Ti-6AL-4V (alloy 1) in the present investigation

Element	**Ti**	**Y**	**N**	**C**	**H**	**Fe**	**O**	**Al**	**V**
% wt Composition	Bal.	<0.0003	0.008	0.043	0.0041	0.15	0.174	5.97	4.09

Table 2: Chemical composition of commercial Ti-6Al-4V (alloy 2) used by Nemat-Nasser et al. (2001)

Element	**Ti**	**Y**	**N**	**C**	**H**	**Fe**	**O**	**Al**	**V**
% wt Composition	Bal.	<0.001	0.01	0.01	0.0006	0.21	0.19	6.21	3.61

Table 3: KHL model material constants determined for the Ti-6Al-4V (alloy 1) and the data extracted from Nemat-Nasser et al. (2001), alloy 2, and Macdougall and Harding (1999), alloy 3

	A **(MPa)**	***B*** **(MPa)**	n_1	n_0	***C***	***m***
Ti-6Al-4V Alloy 1	1069	874.8	0.5456	0.4987	0.02204	1.3916
Ti-6Al-4V Alloy 2	1097	1004.7	0.4993	0.6268	0.02219	1.4796
Ti-6Al-4V Alloy 3	1004	325.1	1.9015	0.5263	0.02204	1.1206

Table 4: JC model material constants determined for the Ti-6Al-4V (alloy 1) and the data extracted from Nemat-Nasser et al. (2001), alloy 2, and Macdougall and Harding (1999), alloy 3

	A **(MPa)**	***B*** **(MPa)**	n_0	***C***	***m***
Ti-6Al-4V Alloy 1 (with optimization)	1104	1036	0.6349	0.01390	0.7794
Ti-6Al-4V Alloy 1 (without optimization)	1080	1007	0.5975	0.01304	0.7701
Ti-6Al-4V Alloy 3	1119	838.6	0.4734	0.01921	0.6437
Ti-6Al-4V Alloy 4	984	520.3	0.5102	0.015	0.8242

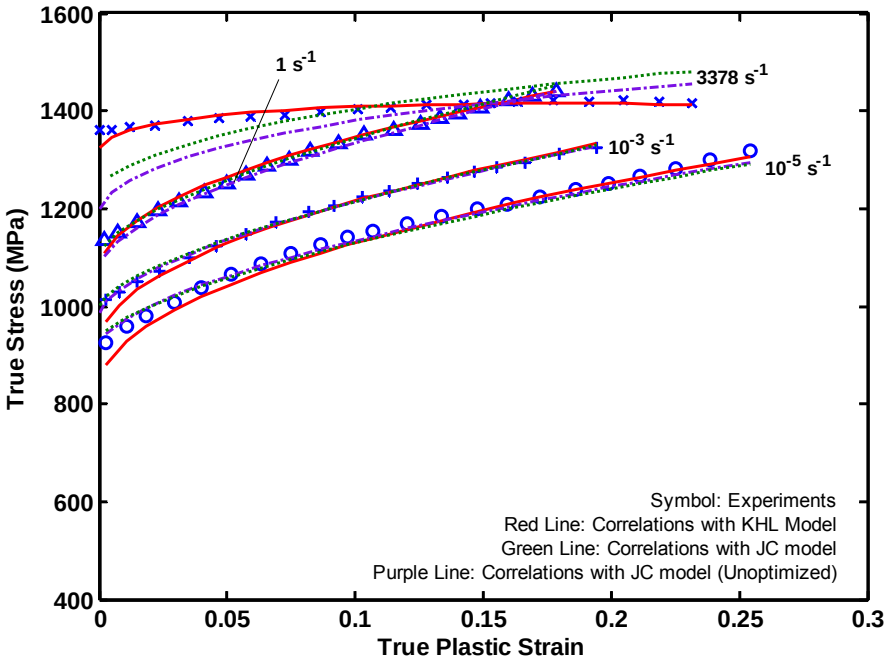

Figure 1: Quasi-static and dynamic loading experimental results (at a temperature of 296K) for different strain rates with correlations using KHL and JC models; the correlations with JC model were shown with and without optimization to determine the material constants.

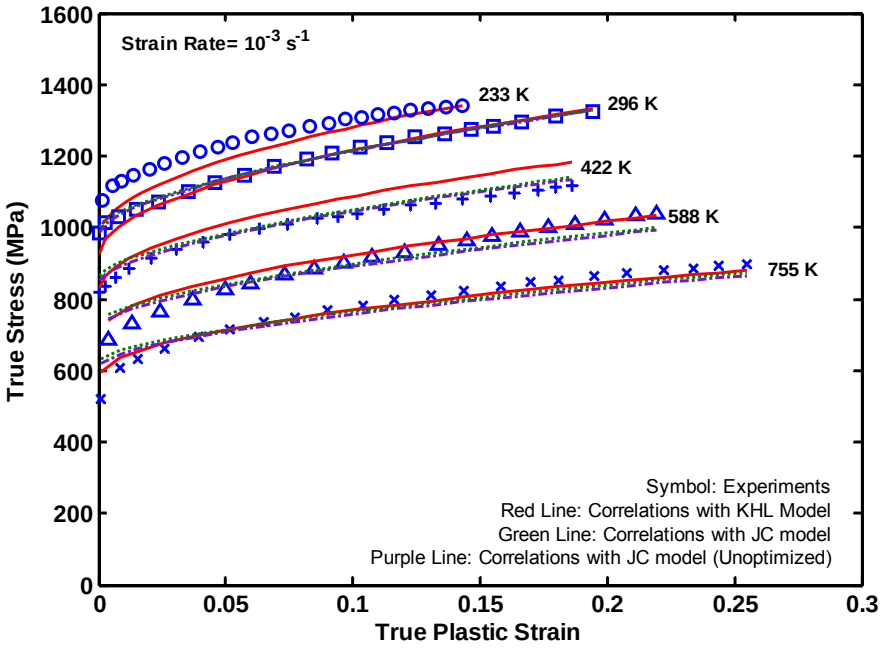

Figure 2: Quasi-static measurements (at a strain rate of 10^{-3} s^{-1}) for various temperatures with correlations using KHL and JC models; the correlations with JC model were shown with and without optimization to determine the material constants. Note the absence of correlation at 233 K with JC model in which $(T-T_{ref})/(T_m-T_{ref})$ becomes negative.

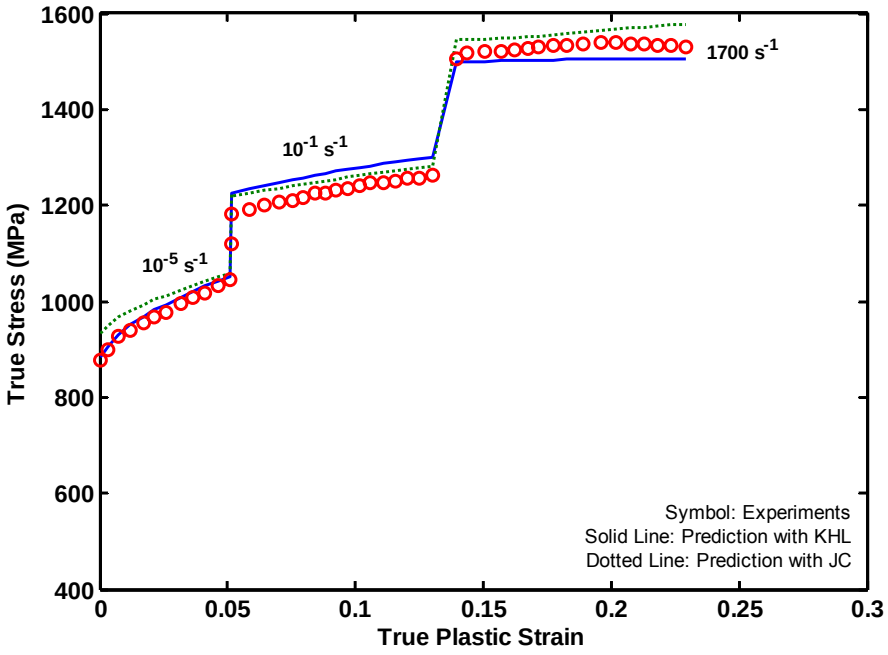

Figure 3: A comparison of a strain-rate-jump experiments results with predictions using KHL and JC models. The test was performed at 296 K with strain rate from 10^{-5} s^{-1} to 10^{-1} s^{-1} and to 1700 s^{-1}. The predictions were made assuming that 10^{-5} s^{-1} region is under isothermal conditions, while 10^{-1} s^{-1} and 1700 s^{-1} regions are under adiabatic conditions. Material constants for JC model used here were determined with optimization.

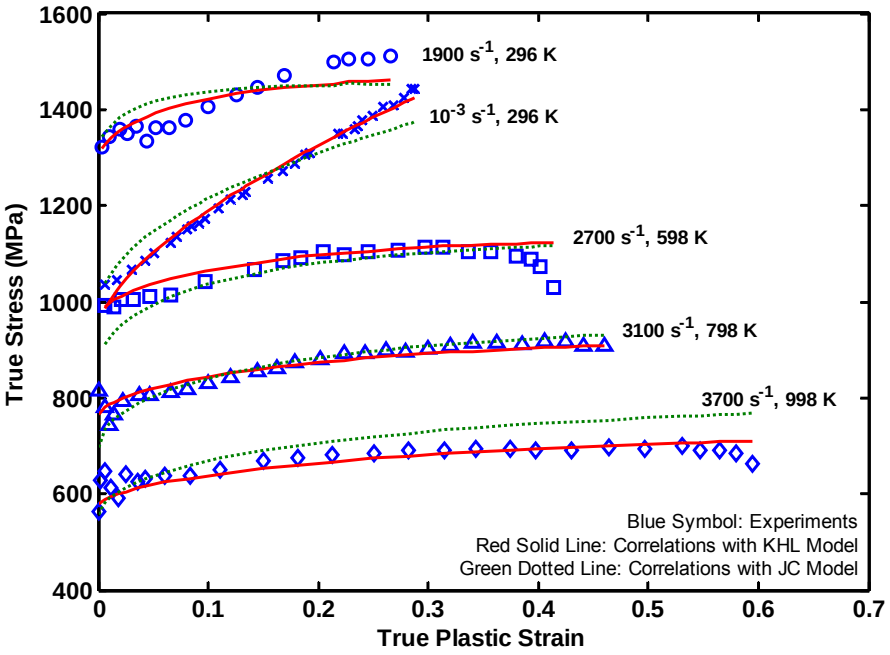

Figure 4: Quasi-static (at a strain rate of 10^{-3} s^{-1}) and dynamic measurements for various strain rates and temperatures (Nemat-Nasser et al. 2001) with correlations using KHL and JC model. Material constants for JC model used here were determined with optimization.

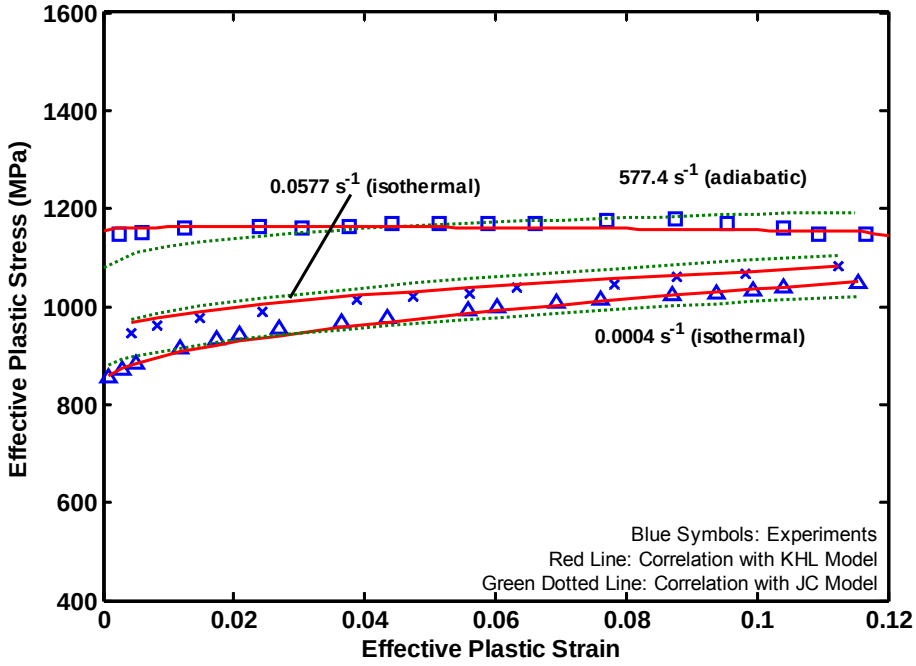

Figure 5: Quasi-static and dynamic torsional measurements for effective strain rates, $\dot{\bar{\varepsilon}} =$ 577.4, 0.0577, and 0.0004 s^{-1} at a temperature of 293 K (Macdougall and Harding, 1999) with correlations using KHL and JC models. Material constants for JC model used here were determined with optimization.

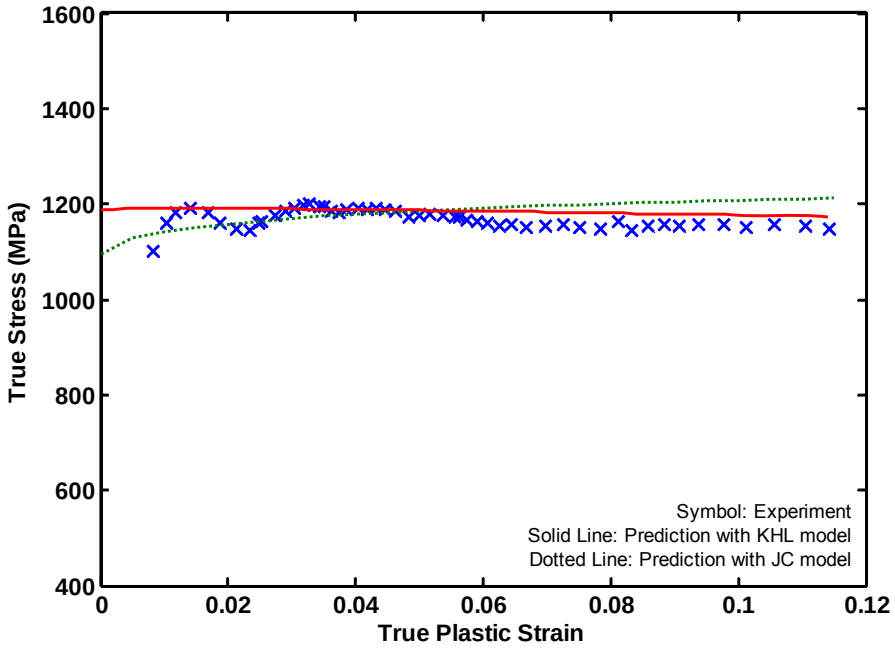

Figure 6: Comparison between tensile dynamic data with a strain rate, $\dot{\varepsilon}$=2000 s^{-1}, and predicted adiabatic responses using KHL and JC models t a temperature of 293 K. The material constants were optimally determined from the correlation with torsional experiments.

References

Bjerke, T., Li, Z., Lambros, J., 2002. Role of plasticity in heat generation during high rate deformation and fracture of polycarbonates. International Journal of Plasticity 18 (4), 549–567.

Burns, T.J., Davies, M.A., 2002. On repeated adaiabatic shear band formation during high speed machining. International Journal of Plasticity 18 (4), 487–506.

Chen, S.R., Gray III, G.T., 1995. Constitutive behavior of tungsten experiments and modeling. In: Bose, A., Dowding, R.J. (Eds.), Second International Congress on Tungsten and Refractory Metals, McLean, VA, Metal Powder Industries Federation, Princeton, NJ, p. 489.

Cheng, J., Nemat-Nasser, S., 2000. A model for experimentally observed high-strain-rate dynamic strain aging in titanium. Acta Materialla 48 (12), 3131–3144.

Chichili, D.R., Ramesh, K.T., Hemker, K.J., 1998. The high strain rate response of alpha-titanium: experiments, deformation mechanisms and modeling. Acta Meterialia 46 (3), 1025–1043.

Conrad, H.M., Doner, M., de Meester, B., 1973. Critical review deformation and fracture. In: International Conference on Titanium, Proceedings of Titanium Science and Technology. Massachusetts Institute of Technology, Boston, p. 969.

Follansbee, P.S., Gray III, G.T., 1989. An analysis of the low temperature, low and high strain-rate deformation of Ti–6Al–4V. Metallurgical Transactions A 20 (5), 863–874.

Gilat, A., Cheng, C.-S., 2002. Modeling torsional split Hopkinson bar tests at strain rates above 10,000 per sec. International Journal of Plasticity 18 (5–6), 787–799.

Gray III, G.T., 1997. Influence of strain rate and temperature on the structure, property behavior of high purity titanium. Journal of Physics IV France 7 (3), C3-423–C3-429.

Johnson, G.R., Cook, W.H., 1983. A constitutive model and data for metals subjected to large strains, high strain rates and high temperatures. In: Proceedings of the Seventh International Symposium on Ballistic, The Hague, The Netherlands, 1983, p. 541.

Kapoor, R., Nemat-Nasser, S., 1998. Determination of temperature rise during high strain rate deformation. Mechanics of Materials 27 (1), 1–12.

Khan, A.S., Huang, S., 1992. Experimental and theoretical study of mechanical behavior of 1100 aluminum in the strain rate range 10_5–104 s_1. International Journal of Plasticity 8 (4), 397–424.

Khan, A.S., Liang, R., 1999. Behaviors of three BCC metal over a wide range of strain rates and temperatures: experiments and modeling. International Journal of Plasticity 15 (10), 1089–1109.

Khan, A.S., Zhang, H., 2000. Mechanically alloyed nanocrystalline iron and copper mixture: behavior and constitutive modeling over a wide range of strain rates. International Journal of Plasticity 16 (12), 1477–1492.

Khan, A.S., Zhang, H., 2001. Finite deformation of a polymer: experiments and modeling. International Journal of Plasticity 17 (9), 1167–1188.

Khan, A.S., Colak, O.U., Centala, P., 2002. Compressive failure strengths and modes of woven S2-glass reinforced polyester due to quasi-static and dynamic loading. International Journal of Plasticity 18 (10), 1337–1357.

Khan, A.S., Lopez-Pamies, O., 2002. Time and temperature-dependent response and relaxation of a soft polymer. International Journal of Plasticity 18 (10), 1359–1372.

Lennon, A.M., Ramesh, K.T., 2004. The influence of crystal structure on the dynamic behavior of materials at high temperatures. International Journal of Plasticity 20 (2), 269–290.

Lesuer, D.R., 2000. Experimental investigations of material models for Ti–6Al–4V titanium and 2024-T3 aluminum. In: Final Report, DOT/FAA/AR-00/25, US Department of Transportation, Federal Aviation Administration.

Liang, R., Khan, A.S., 1999. A critical review of experimental results and constitutive models for BCC and FCC metals over a wide range of strain rates and temperatures. International Journal of Plasticity 15 (9), 963–980.

Liao, S.-C., Duffy, J., 1998. Adiabatic shear bands in a TI–6Al–4V titanium alloy. Journal of the Mechanics and Physics of Solids 46 (11), 2201–2231.

Macdougall, D.A.S., Harding, J., 1999. A constitutive relation and failure criterion for Ti6Al4V alloy at impact rates of strain. Journal of the Mechanics and Physics of Solids 47 (5), 1157–1185.

Majorell, A., Srivatsa, S., Picu, R.C., 2002. Mechanical behavior of Ti–6Al–4V at high and moderate temperatures – Part I: experimental results. Materials Science and Engineering A 326 (2), 297–305.

Mason, J.J., Rosakis, A.J., Ravichandran, G., 1994. On the strain and strain rate dependence of the fraction of plastic work converted into heat: an experimental study using high speed infrared detectors and the Kolsky bar. Mechanics of Materials 17 (2-3), 135–145.

Mecking, H., Kocks, U.F., 1981. Kinetics of flow and strain-hardening. Acta Metallurgica 29 (11), 1865–1875.

Meyers, M.A., Subhash, G., Kad, B.K., Prasad, L., 1994. Evolution of microstructure and shear-band formation in A-hcp titanium. Mechanics of Materials 17 (2-3), 175–193.

Military Handbook, Metallic Materials and Elements for Aerospace Vehicle Structures, MIL-HDBK-5H, DOD and FAA, 1998.

Molinari, A., Musquar, C., Sutter, G., 2002. Adiabatic shear banding in high speed machining of Ti–6Al–4V: experiments and modeling. International Journal of Plasticity 18 (4), 443–459. Montgomery, J.S., Wells, M.G.H., 2001. Titanium armor applications in combat vehicles. JOM 53 (4), 29– 32.

Nemat-Nasser, S., Guo, Wei-Guo, Nesterenko, Vitali, F., Indrakanti, S.S., Gu, Ya-Bei, 2001. Dynamic response of conventional and hot isostatically pressed Ti–6Al–4V alloys: experiments and modeling. Mechanics of Materials 33 (8), 425–439.

Rittel, D., 1999. On the conversion of plastic work to heat during high strain rate deformation of glassy polymers. Mechanics of Materials 31 (2), 131–139.

Rosakis, P., Rosakis, A.J., Ravichandran, G., Hodowany, J., 2000. A thermodynamic internal variable model for the partition of plastic work into heat and stored energy in metals. Journal of Mechanics and Physics of Solids 48 (3), 581–607.

Song, S.G., Gray III, G.T., 1995. Structural interpretation of the nucleation and growth of deformation twins in Zr and Ti – I. Application of the coincidence site lattice (CSL) theory to twinning problems in H.C.P. structures. Acta Metallurgica et Materialia 43 (6), 2325–2337.

Taylor, G.I., Quinney, H., 1934. The latent energy remaining in a metal after cold working. Proceedings of the Royal Society Series A 143, 307–326.

Zerilli, F.J., Armstrong, R.W., 1987. Dislocation-mechanics-based constitutive relations for material dynamics calculations. Journal of Applied Physics 61 (5), 1816–1825.

Appendix II

(Kazmi, R., Zupan, M., Khan, A. S., "Microstructure, response and constitutive modeling of several economical Ti-6Al-4V alloys over a wide range of strain rates and temperatures", in-print, 2006, International Journal of Plasticity.)

EFFECT OF OXYGEN CONTENT AND MICROSTRUCTURE ON THE THERMO-MECHANICAL RESPONSE OF THREE TI-6AL-4V ALLOYS: EXPERIMENTS AND MODELING OVER A WIDE RANGE OF STRAIN-RATES AND TEMPERATURES

Rehan Kazmi, Akhtar S. Khan * and Marc Zupan

Department of Mechanical Engineering, University of Maryland Baltimore County, Baltimore, MD 21250, USA

Abstract

Results from a series of experiments on three different titanium alloys, under quasi-static and dynamic loading conditions are presented. The Ti-6Al-4V titanium alloys include the ELI version and two with higher oxygen content. The strain-rates varied from 10^{-6} s^{-1} to 3378 s^{-1} while observations were made at temperatures from 233K to 755K. The initial and deformed microstructures are also given. Differences in these alloys are observed in terms of thermal softening, work hardening, and strain-rate & temperature sensitivities. The Khan-Huang-Liang (KHL) model is used to effectively simulate the observed response obtained from these experiments. The model, with constants determined from the above experiments, is then used to predict strain-rate jump experimental results and also high temperature dynamic experiments for one of the alloys; the predictions are found to be very close to the observations.

* Corresponding author. Tel.: +1-410-455-3301; fax: +1-410-455-1052
e-mail address: khan@umbc.edu

Keywords

Dynamic compression, Thermal softening, Compression split-Hopkinson bar, Titanium alloys, Strain rate sensitivity, KHL model, Interstitial impurities, Oxygen influence

Introduction

Since the introduction of titanium and titanium alloys in the early 1950s they have become important materials for aerospace, energy, and chemical industries. They are used chiefly for parts that require good corrosion resistance, moderate strength up to 588 K, and lightweight. Titanium alloys, especially Ti-6Al-4V, an $\alpha+\beta$ type titanium alloy is a largely used alloy in many industries because of its extremely attractive properties like high specific strength, good deformability, reasonable ductility and ability to withstand high temperatures and resistance to corrosion. It is primarily used in aero-engine, gas turbines and other applications. The development of a relatively economical Ti-6Al-4V alloy, with a low interstitial content has prompted a lot of interest in its possible use in armor tanks because of improved ductility, whereas the conventional more expensive Ti-6Al-4V alloy has been used primarily in aerospace components chiefly because of its high strength to weight ratio. This advantage has also been contemplated in various

applications like armor, including ceramic tiles encapsulated in these titanium alloys. Several experimental studies have been carried out on similar materials, which included quasi-static and dynamic experimentation (Follansbee and Gray, 1989; Lee and Lin, 1997 & 1998; da Silva and Ramesh, 1997; Lesuer, 2000; Nemat-Nasser *et al*., 2001; Majorell *et al*., 2002).

Since the mechanical properties of this alloy are heavily influenced by its impurities and heat treatment it is imperative that this alloy be understood in terms of the microstructure, constituents, and the processing history. The unalloyed titanium exists in mainly two forms, α-titanium (hcp structure) at room temperature, and at high temperatures it exists as β-titanium (bcc structure). The α phase (primary and secondary) is more dominant in the temperature ranging from 300 K to 800 K, while the amount of β phase starts to increase thereon and is almost totally β-phase at about 1270 K, which is called the β transus temperature [Majorell *et al*., 2002]. The α phase is much harder than the β phase, so the drop in stress levels upon increase of temperatures can be noticed with increasing β content. However, formability increases as the phase changes from α to β. Aluminum and Vanadium are added to titanium to stabilize the two phases. Aluminum, oxygen, nitrogen, and carbon are the α stabilizers, while vanadium, iron and manganese are the β stabilizers. Planar slip is more dominant in the lower temperature range (<500 K). The slip occurs on the basal, prismatic and the pyramidal planes. At temperatures below 800 K, Al transforms the primary α into secondary α precipitates. The secondary α phase has a higher dislocation density than primary α and has a smaller grain size. This basically suggests that it is harder than primary α phase [Picu *et al*., 2002]. Also, studies by Conrad and Wang (1979), where they studied high purity titanium against titanium with 7.4% Al, suggested an increase in the flow stress with the addition of Al content. This is because the increase in the presence of Al concentration enhances the production of secondary α phase, which consequently makes the alloy harder. They also showed that there was an inverse dependency of stress to the grain size for the same material. The effect of grain size on the yield and flow stress of titanium was found to obey the Hall-Petch relation (Conrad, 1984). Also, the strain hardening of the alloy is more due to the presence of the lamellar Widmanstätten microstructure of the secondary α phase. However, Sargent and Conrad (1970) noticed that the addition of aluminum does not alter the rate controlling mechanism and the aluminum contributes only to the athermal components of the flow stress whereas the rate controlling mechanism is the thermally activated component overcoming of the interstitial solute atoms. De Meester and Döner and Conrad (1975), found that between temperatures from 300 K to 800 K the flow stress vs. temperature curve of α-titanium was almost parallel to that of Ti-6Al-4V alloy of nearly same interstitial content, concluding that alloying elements had nothing to do with temperature sensitivity in this range and that the interaction of dislocations with interstitial impurities (C, N, O and H) were more responsible. They also concluded that the deformation kinetics and the related parameters for the Ti-6Al-4V alloy are the same as those for unalloyed titanium.

Chichilli *et al*. 1998 found that twinning, an important dislocation mechanism, occurred at all temperatures below 773 K for α-titanium; at high strain rates, the density of twins significantly increased. There was no twinning seen for Ti-6Al-4V alloys even at low temperatures of 100 K (Paton *et al*. 1976), suggesting that increase in aluminum

content inhibited twinning. However, at room temperature, there was some twinning observed by Follansbee and Gray (1989) at strain rate of 5000 s^{-1} in grains which were larger than the average size.

Conrad *et al*. (1975) proposed an equivalent oxygen content (O_{eq} = O+2N+0.75C), which gives the effect of dislocations-impurity interaction on the yield strength of the material. They also noted that the strengthening of the alloy due to these interstitials was dependent on, in decreasing order, Carbon, Oxygen and followed by Nitrogen. Effect of Hydrogen in most cases was neglected. Majorell *et al*. (2002) studied the deformation characteristics and response of a textured and untextured Ti-6Al-4V alloy rod that was manufactured by Allvac. This study was over a strain-rate range of 10^{-3} to 10 s^{-1} and a temperature range of 650~1345 K (710~1970 F). They did not observe any dynamic strain aging at any of the temperatures or strain rates investigated. The equivalent oxygen content of the specimen was 0.206% and the average grain size of the specimen was 20 μm. They also included the equivalent oxygen content and aluminum impurities in the thermal stress component and the grain size effect in the athermal stress component.

The aim of this study is to compare the responses of the three alloys and subsequently present the modeling capability of the KHL model (Khan and Liang, 1999), which was modified further in an earlier paper (Khan et al. 2004), for three titanium alloys. Comparisons of KHL model correlation and predictions with Johnson-Cook model (Johnson and Cook, 1983) were also given in that paper for one of the alloys presented here, and also alloys used by Nemat-Nasser *et al*. (2001), & Macdougall and Harding (1999). The reader is referred to papers by Abed and Voyiadjis (2005) & Uenishi and Teodosiu (2004), for other modeling approaches.

Experimental Procedure

2.1 Material

Three titanium alloys with different compositions are included in this study of the effect of impurities on the stress-strain response of the material under different loading conditions. The alloys were in as received condition in the form of plates, and specimens were machined to a diameter of 0.5 in. (12.7mm) and length 0.75 inches (19.05 mm). The dynamic specimens were machined to discs with 0.4 in. (10.16 mm) diameter and 0.2 in (5.08 mm) thickness. The loading direction in all these specimens was the thickness direction (axis of cylinders) of the plate. The chemical composition of these three different alloys is given in Table1. These alloys have been designated with different numbers i.e. as alloys 1, 2 and 3. The equivalent oxygen content for alloys 1, 2 and 3 were found to be 0.229, 0.152 and 0.222 respectively. Alloys 1 & 3 were manufactured using single electron beam melting process, resulting in higher oxygen content than the ELI version (alloy 2).

2.2 Microstructure Evaluation

The microstructure of these alloys was determined before and after deformation using a scanning electron microscope (SEM). The specimens were cut along the compression axis of the specimen (the thickness direction of the plate). The preparation of the specimens involved polishing using a Buehler Metaserv grinding-polishing machine. Different grits of carbide paper were used for grounding starting from 240, 400, 600, 800, to 2400. The specimens were then polished again using a Struers DP-Plus micro cloth with slurry of 0.3 μm alumina to get a mirror-like finish. It was eventually etched with Kroll's reagent (a solution of 1% HF, 2% HNO_3 and 97% distilled H_2O), for about 5 min.

The photomicrographs of the initial and deformed microstructures revealed an alpha-beta type microstructure, which is typical for the alloy (Fig. 1 and 2). It confirms that the alloys went through different annealing and cooling processes with higher amount of transformed β content in alloy 3. This alloy has gone through annealing at higher temperatures (~ 1750F). Its microstructure consists of the hcp α grains and a transformed β with a lamellar Widmanstätten structure dispersed between these primary globular α grains. The higher annealing temperature along with higher rate of cooling, is responsible for the increased transformed β content as compared to the other alloys. The percentage of lamellar transformed β is lower in alloy 2 relative to alloy 3. However, the aluminum content, which is an α phase stabilizer, is higher in alloys 1 and 2 than alloy 3. Also, the average grain size for the titanium alloys was approximately 9 μm as calculated using intercept method (ASTM E112-96).

The deformed photomicrographs of alloys 2 and 3 are shown in Figures 1(b) and 2(b), respectively. The specimen chosen for the microstructural examination were deformed at somewhat higher temperatures (422 K) for alloys 3 than in case of alloy 2, which was deformed at room temperature (296 K). The strain rate during the deformation of alloy 2 was 1 s^{-1} whereas for alloy 3 it was 10^{-3} s^{-1}. The deformed microstructures in both cases show elongated hcp α grains. The β grains in the samples displayed no apparent change in the substructure and this was same for all the alloys independent of the level of deformation or loading conditions. This was consistent with the other researchers (Follansbee and Gray, 1989). Also, very little to almost no twinning was observed in the alloys. This is also consistent with other studies (Follansbee and Gray, 1989), where the authors found deformation twins only at very high strain rate (5000 s^{-1}) experiments. The reason behind this behavior is that at very high strain rate or at very low temperatures, higher stresses are required to cause plastic deformation and since the dislocation mobility is low at these conditions, the deformation twins develop as a consequence. However, in the case of low strain rate and high temperatures, dislocation mechanisms are supposed to be the dominating components in the deformation mechanism of the alloys through planar slips with almost negligible amounts of deformation twins.

The photomicrographs of deformed samples under dynamic loading conditions at various temperatures for alloy 3 are also shown in the Fig 3. The specimens are cut along the compression axis for this investigation. The samples show that elongation of grains occurs for the deformed sample perpendicular to the loading axis. The grain elongation

ratio, as per ASTM standard E112-96, for this alloy was calculated for undeformed and deformed samples and is shown in Table 3. Also, the average grain size for each of the photomicrographs for this alloy are calculated and shown in the table. The average grain size was found to decrease with increasing strain rates. It is believed that for high strain rate and high temperature deformations, the energy generated causes dynamic recrystallization of the platelet type alpha into globular primary alpha grains (422K and 715K) as the platelet type alpha content is lowest in these samples.

2.3 Quasi-Static Experiments

2.3.1 Room temperature experiments

The quasi-static experiments performed were in compression. Cylindrical specimens were made out of the base plates into dimensions of approximately 0.75 in. (19.05 mm) in length and 0.5 in. (12.7 mm) diameter with the longitudinal axes in the thickness direction. Care was taken during the machining of the specimens that no plastic work hardening is introduced on the surface and the last three machining cuts were one thousands of an inch. These specimens were then subjected to different strain rates ranging from 10^{-6} to 1 s^{-1} on the MTS servo hydraulic axial/torsional material testing machine. The 1 s^{-1} experiment was performed as a load-unload-reload experiment with increments of 5% strains with a 30-minute interval between each consecutive loading, to obtain an isothermal response of the material. For these room temperature compression experiments, KFEL-2-120-C1 high elongation uniaxial strain gages, manufactured by Kyowa Ltd. (Japan), were mounted diametrically opposite to each other at the center of each specimen using an AE-15 (Micro Measurements Inc.) epoxy resin. The gages were then connected to the MTS TestStar software through signal conditioners. The strains obtained using strain gages were corrected before conversion into true plastic strain for Wheatstone bridge non-linearity and gage factor variation (Huang and Khan, 1991). The MTS transducers directly supplied load data to the software. The interface between the fixtures and the test specimens for each of the compression experiments was lubricated with Teflon sheets and a high vacuum grease in order to achieve uniformity in deformation and avoid barreling of the specimen, maintaining a uniform, uniaxial stress state.

2.3.2 Experiments at different temperatures

The stress-strain response was observed during experiments at temperatures of 233, 422, 589, and 755 K at a strain rate of 10^{-4} s^{-1} for alloys 1 and 2, whereas for alloy 3, strain rate of 10^{-3} s^{-1} was used to perform these experiments. Alumina bars were attached to the grips of the MTS using Vascomax C-350 steel fixtures. The specimen was placed between the alumina bars. A thermocouple was cemented to the center of the specimen to monitor the temperature throughout the experiment. Once the desired temperature was reached, it was kept constant for 30 minutes so that steady state conditions existed and consequently ensured a uniform temperature throughout the specimen. Extreme high temperature grease was applied between the specimen and the ceramic bars to reduce frictional effects and have uniaxial stress state throughout the length of the experiment.

The LVDT of the MTS supplied stroke data in the form of displacement and force was supplied by the force transducers. The displacement data supplied by the machine included machine elastic deformations, the deformation of the ceramic bars and the variation in thickness of the layer of grease. This measurement in displacement was corrected by running a "blank experiment", i.e. without the specimen and keeping all the other parameters approximately same. The displacement for the blank experiment was then subtracted from the experiment displacement at each load to get the actual displacement of the specimen. The remaining calculations were done using this corrected displacement.

For the low temperature experiments, dry ice in form of small granules was used. A chamber was placed around the specimen with dry ice. The temperature of the specimen was monitored using the same technique as in the case of high temperature experiments. The specimen temperature went down to 233 K and remained steady during the test. Low temperature grease was used as lubricant between the specimen and the alumina bars. Corrections for the displacement were performed similar to that of high temperature experiments

2.4 Dynamic experiments at room temperature

Dynamic experiments on the alloy were performed using the compression split-Hopkinson pressure bar technique (SHPB), which is a widely used technique for high strain-rate experiments. Details of this technique can be found in Khan and Liang (1999). The diameter of these bars, made from Vascomax C-350 steel, was a constant 0.5 in. (12.7 mm). The specimen was machined to the shape of a disc and was sandwiched between the incident and transmitted bars. The dimensions of the specimens used for dynamic experiments were 0.2 in. (5.1 mm) in thickness and 0.4 in. (10.2 mm) in diameter. The interfaces of these incident and transmitted bars with the specimen were lubricated with grease to reduce friction and to maintain a uniform stress state in the specimen. The strain gages mounted on the bars were manufactured by Kyowa Inc., Japan. These gages were bonded diametrically opposite to each other using an epoxy resin. The position of the gages was such that there was no interaction of the incident, reflected and transmitted waves with each other. These gages were connected to a Nicolet 440 oscilloscope through a potentiometer circuit. The stresses and the corresponding strains in the specimen are calculated using the incident, reflected and transmitted waves signals. More detailed information about the split-Hopkinson can be found elsewhere (Follansbee, 1979).

For high temperature deformations, the disk specimens were heated to a predetermined temperature. Thermocouples were cemented to the outside surface of the specimens to monitor the current temperatures. Once the desired temperature was achieved, it was held constant for about 15 minutes at that value to insure uniformity of heating at the surface and the core of the samples. The Hopkinson bars were kept cooler using cooling devices. The temperature in the bars was kept constant around room temperature so as not to cause any significant change in the elastic modulus.

During high strain rate experiments most of the heat generated by the plastic work is entrapped within the specimen making it somewhat relatively soft, this process is called thermal softening. Thermal softening is a function of the specific heat capacity at constant pressure, mass density and the deformation in the specimen. The rest of the heat generated is used up to change the microstructure, e.g. increase the dislocation density. Thus, high strain-rate deformation is adiabatic and there is a significant increase in the temperature of the specimen during deformation. The effect of this softening is significant and cannot be neglected. The temperature rise in the specimen can be calculated by the following equation:

$$\Delta T = \frac{\beta}{\rho C_p} \int_0^{\varepsilon} \sigma(\varepsilon) d\varepsilon \tag{1}$$

In this study, the fraction of plastic work converted to heat is taken to be 0.9, which implies that 90% of the plastic work done during the deformation is assumed to be converted to heat and is responsible for the rise in the temperature of the specimen. ρ and C_p are the mass density and the specific heat at constant pressure for the alloy. This relation is used to convert the original experimental response at high strain rates under adiabatic heating to corresponding isothermal behavior. The density for the titanium (Ti-6Al-4V) alloys is 4428 kg/m^3 (Lesuer, 2000) and the specific heat capacity at constant pressure for the alloys can be expressed as a function of the temperature of the material (Military Handbook, 1998).

$$C_p = 559.77 - 0.1473T + 0.00042949T^2 \ \ \text{J/(kg·K)} \qquad (278\ \text{K} < T < 1144\ \text{K}). \tag{2}$$

2.5 Compressive Strain rate jump experiments

Compressive strain rate jump experiments were performed on the titanium alloys as a part of this comprehensive study. The quasi-static regime part of the experiment was initially performed on the MTS. The strain rate of the samples, once loaded to a certain level of strain, was changed abruptly and the corresponding response of the alloy was recorded. After the predetermined level of strain was achieved, the sample was unloaded and machined to a disc form for a dynamic compression experiment using the split-Hopkinson pressure bar technique.

2. Modeling Procedure

The KHL model utilizes a systematic method of determining initial material constants (see Khan and Liang, 1999), which are used as input in a program to obtain refined material constants by employing an optimization technique and to predict the material response over a wide range of strain rates and temperatures. There are six different material constants, which define the material behavior with respect to yield strength, strain hardening, strain rate sensitivity, temperature sensitivity and strain hardening sensitivity to strain rate. The model is more suited for modeling the material response as compared to JC model, which fails to provide observed decreasing work hardening

behavior in some materials with increasing strain rate. More detailed advantages of this model over JC model are given in Khan *et al.* (2004). The KHL constitutive equation is given as:

$$\sigma = \left[A + B\left(1 - \frac{ln\,\dot{\varepsilon}}{ln\,D_0^p} \right)^{n_1} \varepsilon_p^{\,n_0} \right] \left(\frac{\varepsilon}{\dot{\varepsilon}^*} \right)^c \left(\frac{T_m - T}{T_m - T_{ref}} \right)^m \tag{3}$$

where, σ is the true (Cauchy) stress and ε^p is the true plastic strain. T_m, T, T_{ref} are melting, current, and reference temperatures, respectively. $D_0^p = 10^6$ s^{-1} (arbitrarily chosen upper bound strain rate) and $\dot{\varepsilon}^* = 1$ s^{-1}(reference strain rate, at a reference temperature of T_{ref}, usually room temperature, at which material constants A, B and n_0 are determined). $\dot{\varepsilon}$ is the current strain rate. n_1, C and m are additional material constants. For Ti-6Al-4V alloys, the melting temperature was taken to be 1933 K (Nemat-Nasser *et al*., 2001). The reference temperature was the constant room temperature for experiments at 296K.

The material constants for this model are determined using several uniaxial quasi-static and dynamic room temperature experimental results at different strain rates and high & low temperature experimental results at one strain rate. This usually provides one with a set of initial material constants which can be used as input into a programming software which utilizes constrained optimization procedure using least square method to obtain a set of more refined material constants. The dynamic data before being input in the optimization scheme is converted into an equivalent isothermal data by calculating the instantaneous temperature rise in the material at any strain level using Eq (1) and calculating stress increment for that temperature rise to get corresponding isothermal stress response. The material constants thus determined were used to predict a strain rate jump experiment, which was performed separately for each alloy. This experiment was not included in the calculation of the material constants. The strain rate jump experiment included at least two different strain rates in the quasi-static regime followed by a dynamic regime strain rate.

3. Results and correlations with the constitutive model

The comprehensive observed response of the alloys are given by symbols (e.g. ▽,◊,×,+,o, etc.), in Fig 4-13. For alloy 1 five different strain-rate experiments were performed ranging from 10^{-6} s^{-1} to dynamic strain rate of 3100 s^{-1}. The material behavior was found to be strain rate sensitive and has a non linear work hardening response at low deformation levels transitioning to an almost linear response at higher deformation levels. Also, there is a slight reduction in work hardening rate with increasing strain rates in the quasi-static loading regime. The JC model, with no provisions to replicate such behavior was found earlier not as good as the corresponding KHL model (Khan et al., 2004). There is no or little work hardening effect seen in the adiabatic dynamic experiment due to thermal softening. The observed response of the material is also a non-linear function of temperature. The increase in test temperature causes a drop in the flow stress. A slight decreasing work hardening rate behavior can be noticed as the temperature increases and also with an increase in the level of strain. This is consistent with other studies on the alloy (Majorell et al., 2002, Lee and Lin, 1997, etc.). This kind of behavior is amplified in

the experiment performed at 755 K temperature. The flow stresses in the alloy is also found to be more sensitive to temperature of the material than to the strain rate as also found by Nemat-Nasser *et al*. (2001) in a similar alloy. For alloy 2 experiments were performed at strain rates ranging from 10^{-6} s^{-1} to 2926 s^{-1}. A low temperature experiment at 233 K was also performed for this alloy. Other quasi-static experiments at different temperatures were performed at 422 K, 588 K and 755 K. All of these experiments were well below beta transus temperature (~1270K) to ensure that the material did not change phases during the experiments. Similarly, different strain-rate and temperature experiments were performed for alloy 3. For room temperature experiments the range of strain rate was from 10^{-5} s^{-1} to 3378 s^{-1}. Experiments at different temperatures (233K, 422K 588K and 755K) on this alloy were performed at a strain rate of 10^{-3} s^{-1}.

4.1 Correlations and predictions for alloy 1

The correlations obtained for room temperature experiments are also shown in Fig. 4 using lines (——, ---, – · –, etc.). The various material constants obtained for this alloy using MATLAB software, utilizing the least square method with constrained optimization, are shown in Table 2. The constants, depicting the strain rate sensitivity of work hardening n_1 and the strain rate sensitivity parameter C, were kept same for all three alloys. In spite of putting these extra constraints in the optimization procedure the KHL model was able to successfully correlate with the material response over large strains and displaying excellent capability in simulating decreased work hardening behavior with increasing strain rate. The various correlations for different temperatures, using lines, can be seen in Fig. 5. Here too, the model correlates reasonably well with the data. Further, in Fig. 6, a strain rate jump experiment from 10^{-5} s^{-1} to 10^{-1} s^{-1}, followed by another jump at a dynamic strain rate of 1816 s^{-1}, is predicted by the model. This experiment was performed at room temperature. These results were not used in the calculation of the material constants, earlier. The predictions from the model are shown by a solid line; the model predicts the observed response very closely in this strain rate jump experiment.

4.2 Correlations and predictions for alloy 2

The various material constants for this alloy are given in Table 2. Here again, the two material constants, n_1 and C, were kept same as it was assumed that the heat treatment and slight changes in composition only changes constants A, B, n_0 and m. Results of the correlations can be seen in Fig. 7. The model is in good agreement with the experimentally observed response during the quasi-static room temperature experiments throughout the deformation regime. The dynamic response is also fairly close to the correlations, including the replication of the reduced work hardening throughout the deformation. The model correlations for observed responses at different temperatures are given in Fig. 8. The model is again in good agreement with the experimentally observed responses for the low (233 K) as well as other high temperature experiments. Similar to alloy 1, a strain rate jump experiment was performed on this alloy from 10^{-5} s^{-1} to 1 s^{-1} and then back to 10^{-5} s^{-1}, before performing a dynamic experiment on the same specimen.

Again, this experiment was not used to determine the material constants. The model predictions are in good agreement for all strain rates and to all levels of strain as shown in Fig 9. In predictions, the responses were assumed adiabatic for the strain rate of 1 s^{-1} and also the dynamic strain rate regime portion of the experiment.

4.3 Correlations and predictions for alloy 3

The response modeling for alloy 3 was performed similar to the other two alloys. The material constants thus obtained after refinement of the initial constants are given in Table 2. The measured responses during four room temperature quasi-static experiments, and the dynamic experiment also at room temperature are shown in Fig. 10 along with the correlations obtained for this alloy. The correlations are in excellent agreement with the observed responses. For the dynamic case, the isothermal values were converted into adiabatic response before plotting for comparison with the adiabatic dynamic results. This was done in the cases of other two alloys as well. The correlations with the experimental results at different temperatures and at the strain rate of 10^{-3} s^{-1} are provided in Fig. 11. The observations and the model correlations are again in good agreement with each other at all temperatures. Furthermore, as in the case of the other two alloys, a strain rate jump experiment was performed at a strain rate of 10^{-5} s^{-1} to 10^{-1} s^{-1} followed by a dynamic strain rate experiment at 1700 s^{-1} on the same specimen. Predictions were performed based on the material constants obtained for the alloy from other experimental results. The experimental results along with the predictions are compared in Fig. 12. As, in all the previous cases the predictions are in good agreement with the observed results. The predictions for the strain rate of 10^{-1} s^{-1} were converted into corresponding adiabatic response, before comparison, as there was a temperature increase noticed in the specimen during the experiment. Dynamic strain rate regime predictions are also converted similarly in order to obtain the adiabatic response.

Predictions for high strain rate experiments are also shown for different temperatures in Fig. 13. These predictions were also converted to adiabatic response and plotted along with the experimental results. The predicted response is again in excellent agreement with the experimental observations.

Overall, the correlations and predictions using are very close to measured experimental responses for a large range of strain rates and temperatures. Further, it was observed from the measured responses that alloy 1 and 3 had higher flow stress as compared to the alloy 2. This is attributed to the fact that the interstitial solute content or the equivalent oxygen content (O_{eq}), which is known to strengthen the alloy, is higher in these alloys (Conrad *et al*., 1975). Alloy 2 is the ELI grade alloy and has a lower flow stress response during the various experiments. The work hardening in the alloys 1 and 3 were found to be quite similar but higher than that of alloy 2 and this is also confirmed in Table 2, where the material constants (B and n_0) are listed. However there is a slightly different response of the alloys at different temperatures, this characteristic is also highlighted in Table 2, where the three alloys have different temperature sensitivity parameter. From the above observations it can be concluded that the interstitial impurities have significant effect on the flow stress and work hardening response of the alloys, and

these additions also affect the temperature sensitivity of the alloys. This is consistent with the findings of other researchers (de Meester and Döner and Conrad, 1975). Also, the interstitial content has no apparent effect on the work hardening sensitivity of strain rate, as well as the overall strain rate sensitivity of the material.

Conclusions

In the present paper, the quasi-static and dynamic responses of the three titanium alloys were studied in a systematical manner over large ranges of strain rates and temperatures. The alloys were found to be more sensitive to change in temperature than strain rate. The KHL model was utilized to model the observed behavior of these three different alloys over this range. The model was found to be fairly accurate to capture closely all the important features observed for these alloys. Material constants of the KHL model were determined for all three alloys; previously determined values were used for predictions of the observed material response in strain-rate jump experiments (all alloys) and high strain rate experiments at different temperatures for alloy 3 to show the applicability of the model. Two of the six constants determined were kept same for all three alloys, suggesting that the strain rate sensitivity and the strain rate effect on the work hardening of the alloys were independent of the interstitial content and small differences in the initial microstructures of these alloys. The yield strength, work hardening and the temperature sensitivity though were found to be somewhat different for these three different alloys and it was concluded that the amount of interstitial content and the initial microstructure had been responsible for these variations in the observed responses.

Acknowledgements

The first author is grateful for the funding of this project by the Army Research Office under cooperative agreement DAAD19-01-1-0635, under the direction of Dr. Bruce LaMattina (Solid Mechanics Program). The first author is also thankful to Dr. Douglas Templeton, Team Leader of Emerging Technologies at US Army TARDEC for funding of the project and guidance. Various help and comments of Dr. Raj Rajendran at the Army Research Office are also gratefully acknowledged. Also, the assistance in performing some experiments by previous graduate students, Jennifer Baker and Robert Matteson, along with current graduate student Babak Farrokh is greatly appreciated.

Table 1

Chemical composition of the three Ti-6Al-4V alloys used

Material	Al	V	Fe	Y	H	N	O	C	Ti	Oeq
Alloy 1	6.26	4.16	0.14	<0.0003	0.0031	0.008	0.178	0.047	REM	0.229
Alloy 2	6.30	3.86	0.18	<0.0003	0.0026	0.003	0.112	0.045	REM	0.152
Alloy 3	5.97	4.09	0.15	<0.0003	0.0041	0.008	0.174	0.043	REM	0.222

Table 2

KHL model material constants determined for the three Ti-6Al-4V Alloys used in the investigation

	A **(MPa)**	***B*** **(MPa)**	n_1	n_0	***C***	***m***
Ti-6Al-4V Alloy 1	1100	857.5	0.5455	0.6086	0.02204	1.6236
Ti-6Al-4V Alloy 2	988	747.1	0.5455	0.3986	0.02204	1.2214
Ti-6Al-4V Alloy 3	1069	874.8	0.5455	0.4987	0.02204	1.3916

Table 5

Grain Elongation Ratio and average grain size for deformed and undeformed samples of alloy 3

Sample	**Undeformed**	**10^{-3} s^{-1} 422 K**	**Dynamic 296K**	**Dynamic 422K**	**Dynamic 715K**
Grain Elongation Ratio	0.89	0.36	0.63	0.50	0.44
Average Grain Size (μm)	9.86	9.37	9.80	9.07	7.91

a)

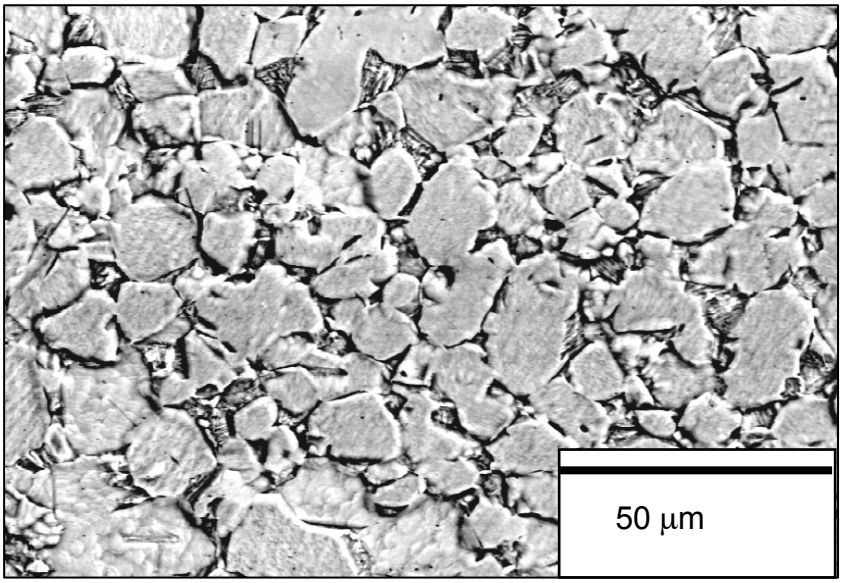

b)

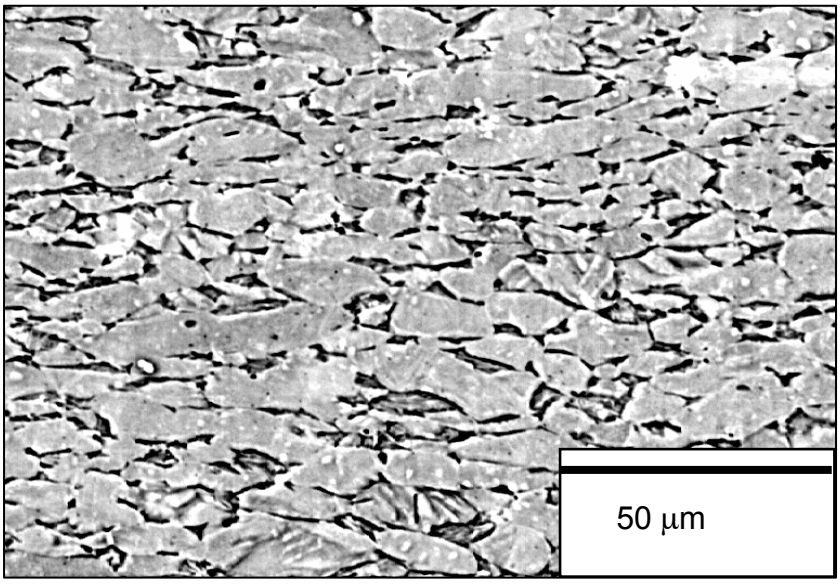

Figure 1. (a) Undeformed and (b) 18% deformed Ti-6Al-4V alloy 2 at 296K and 10^0 s^{-1} strain rate showing the globular α with dispersed β along the grain boundaries.

a)

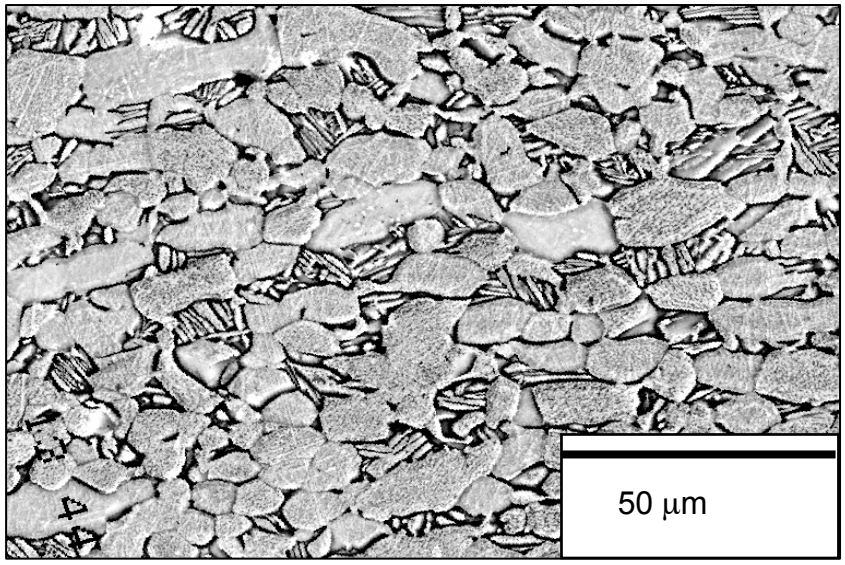

b)

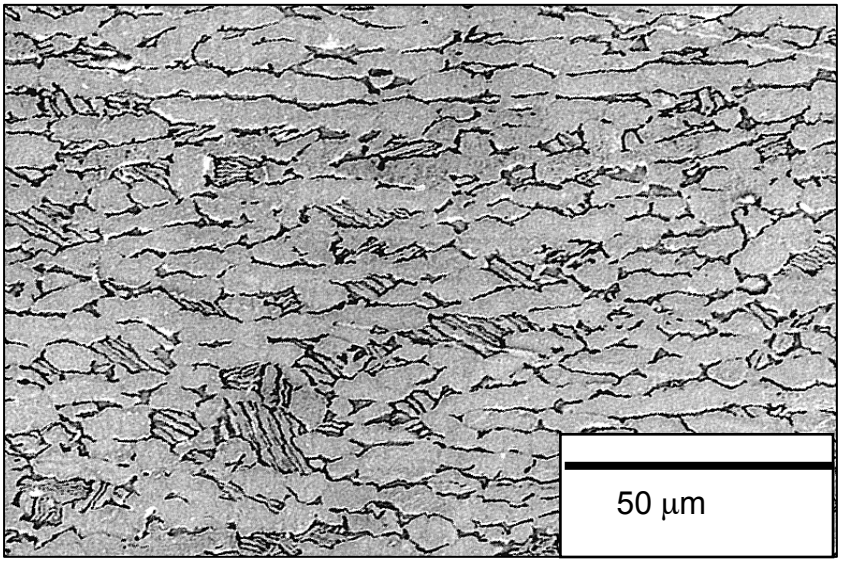

Figure 2. (a) Undeformed and (b) 20% deformed Ti-6Al-4V alloy 3 at 422K and 10^{-3} s^{-1} strain rate showing the globular α with dispersed transformed β (Widmanstätten structure).

a)

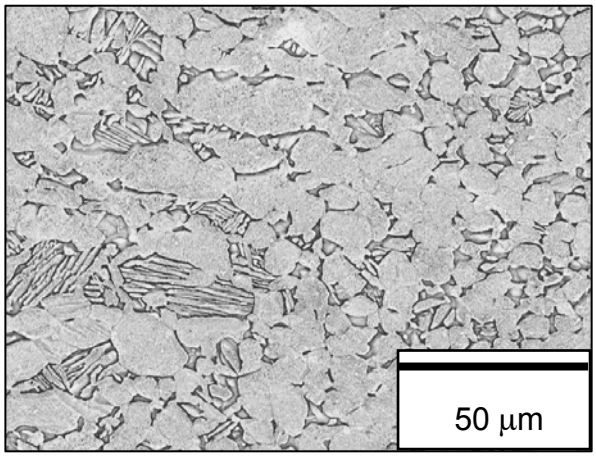

b)

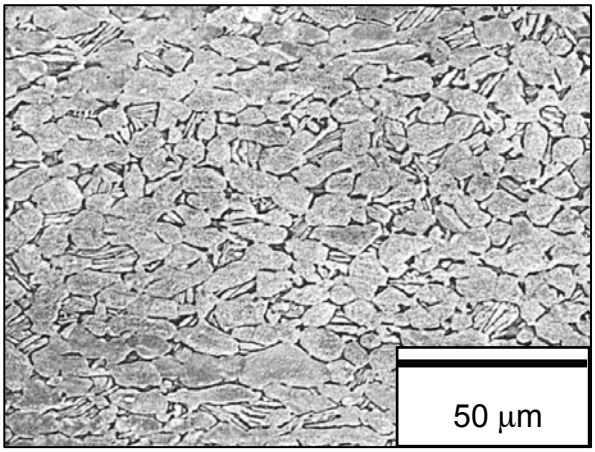

c)

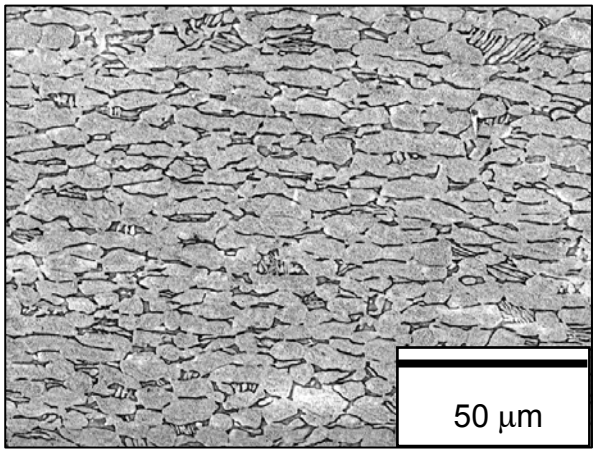

Figure 3. Deformed samples of alloy 3 at high strain rates and different temperatures. a) at 296 K, b) at 422 K and c) at 715 K (compression along vertical direction).

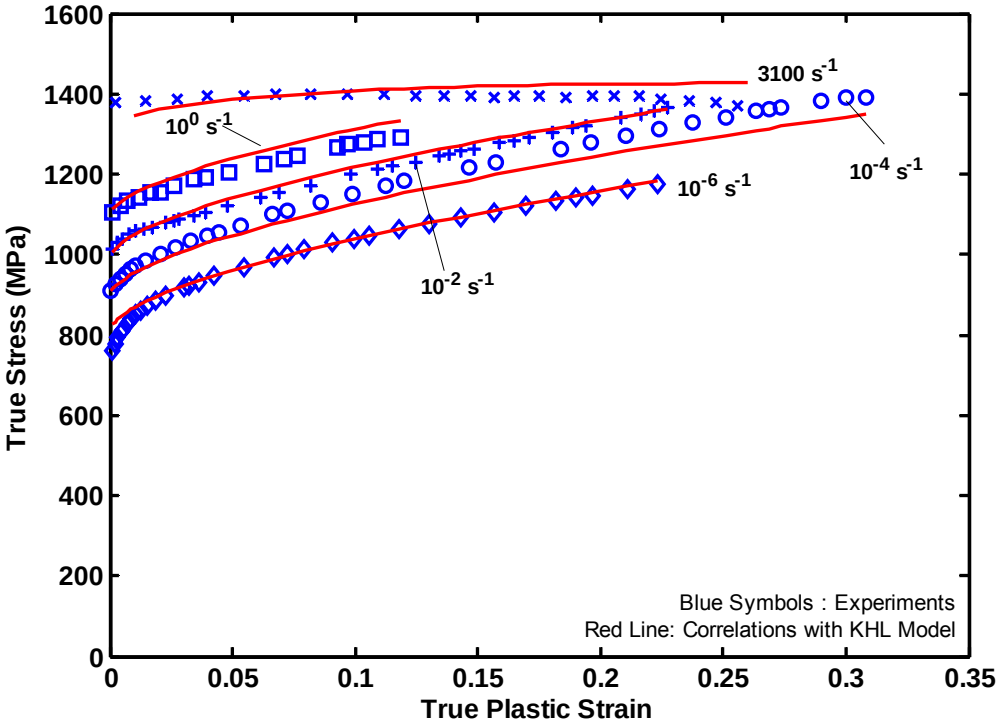

Figure 4. KHL model correlations with the room temperature (296K) response of alloy 1 at different strain rates.

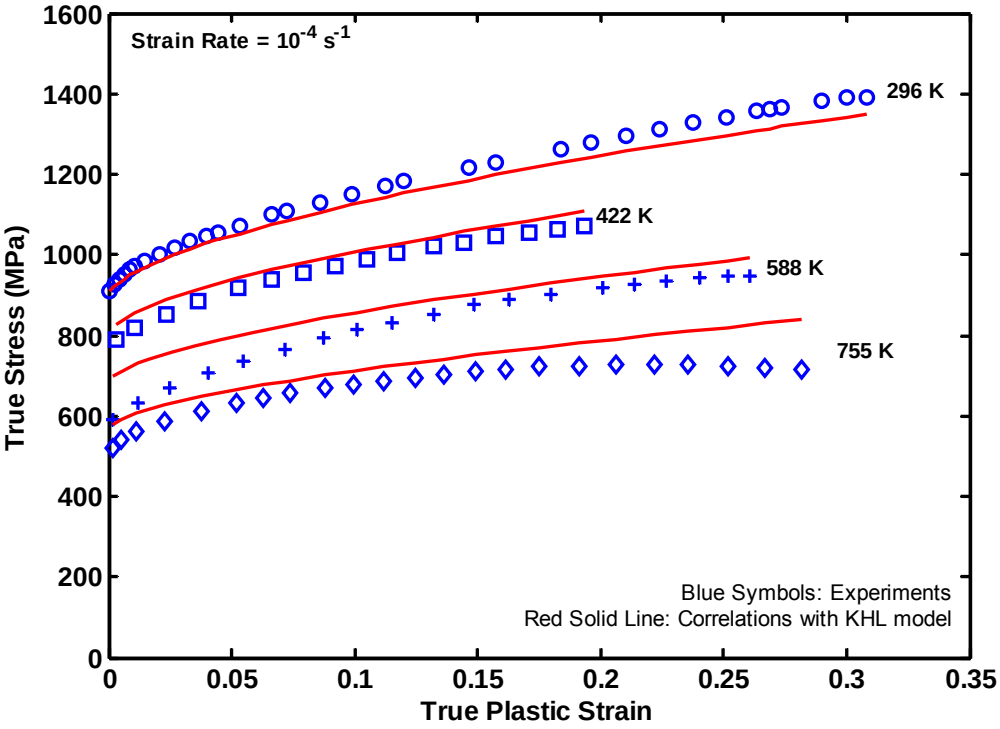

Figure 5. KHL model correlations with the observed response of alloy 1 at different temperatures at constant strain-rate 10^{-4} s^{-1}

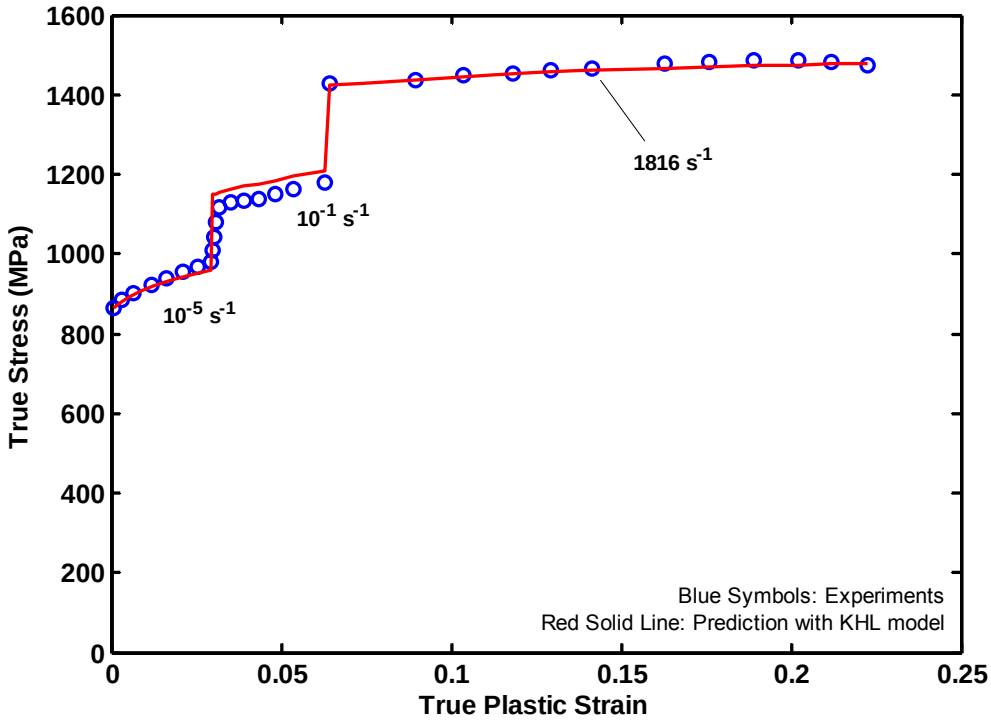

Figure 6. KHL model predictions with the observed response of alloy 1 during a strain-rate jump experiment at room temperature (296K). Dynamic predictions are adiabatic.

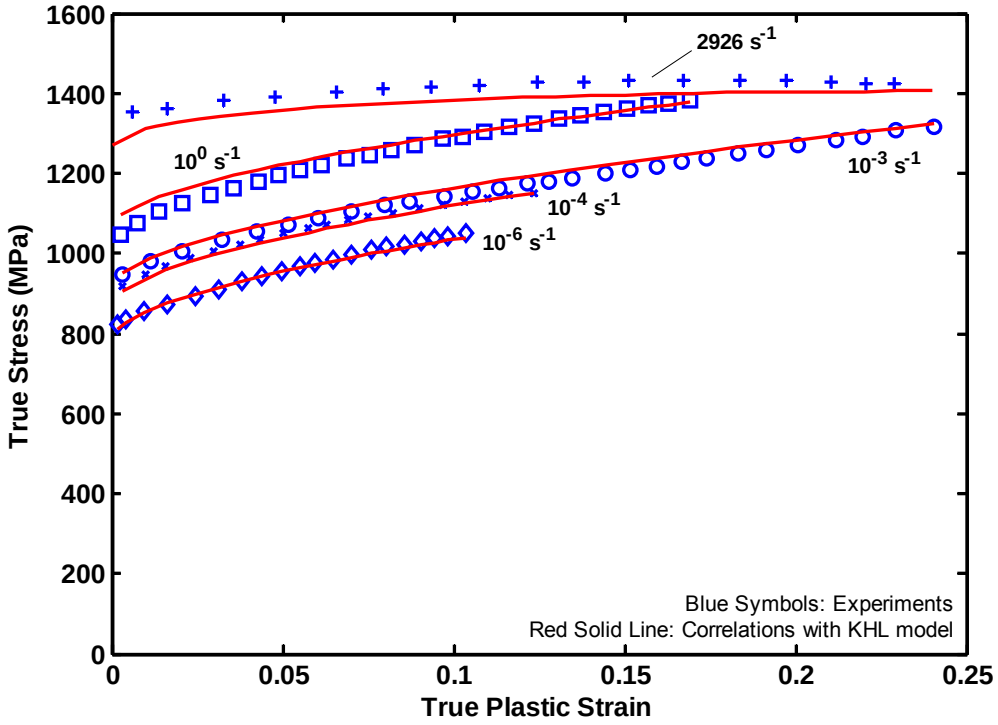

Figure 7. KHL model correlations with the room temperature (296K) response for alloy 2 at different strain rates.

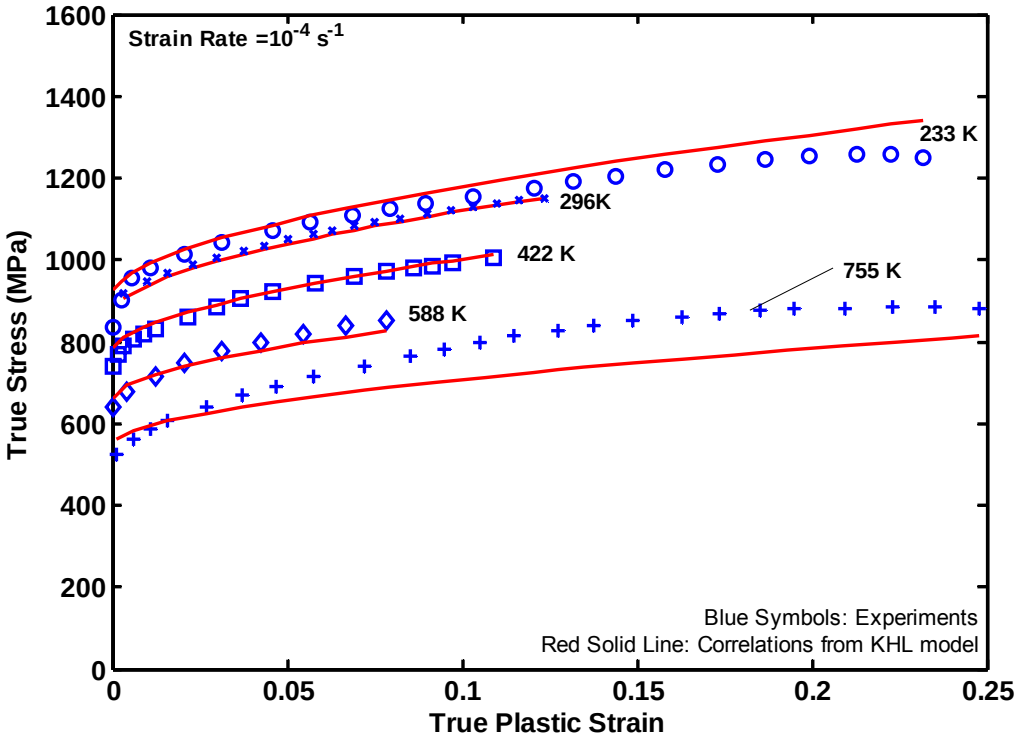

Figure 8. KHL model correlations with the observed response of alloy 2 at different temperatures at constant strain-rate 10^{-4} s^{-1}

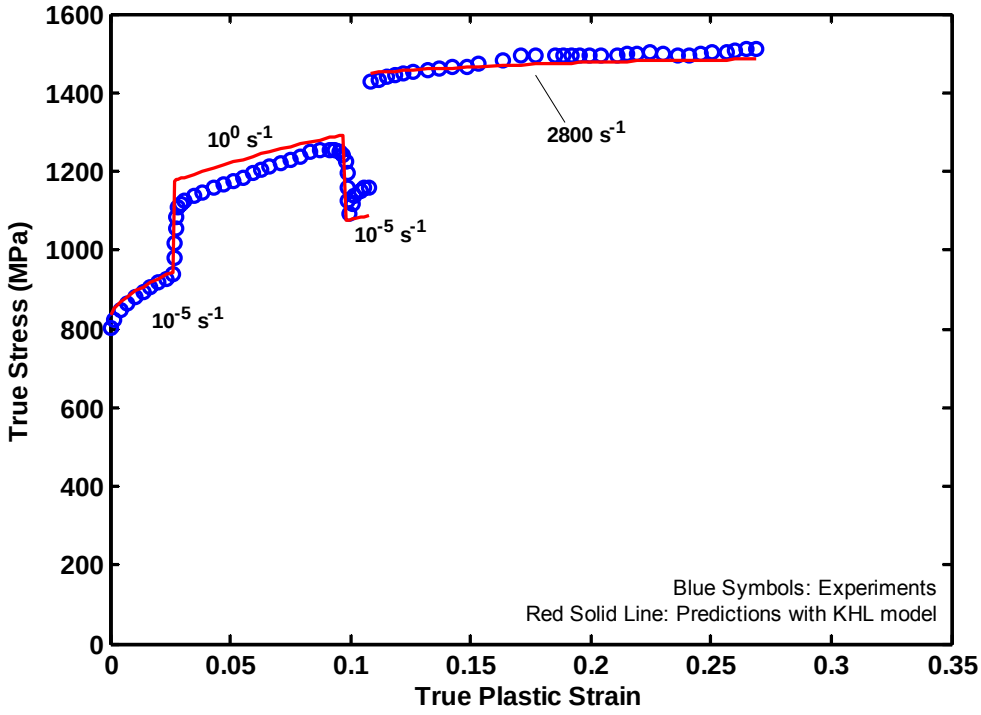

Figure 9. KHL model predictions with the observed response of alloy 2 during a strain-rate jump experiment at room temperature (296K). Dynamic predictions are adiabatic.

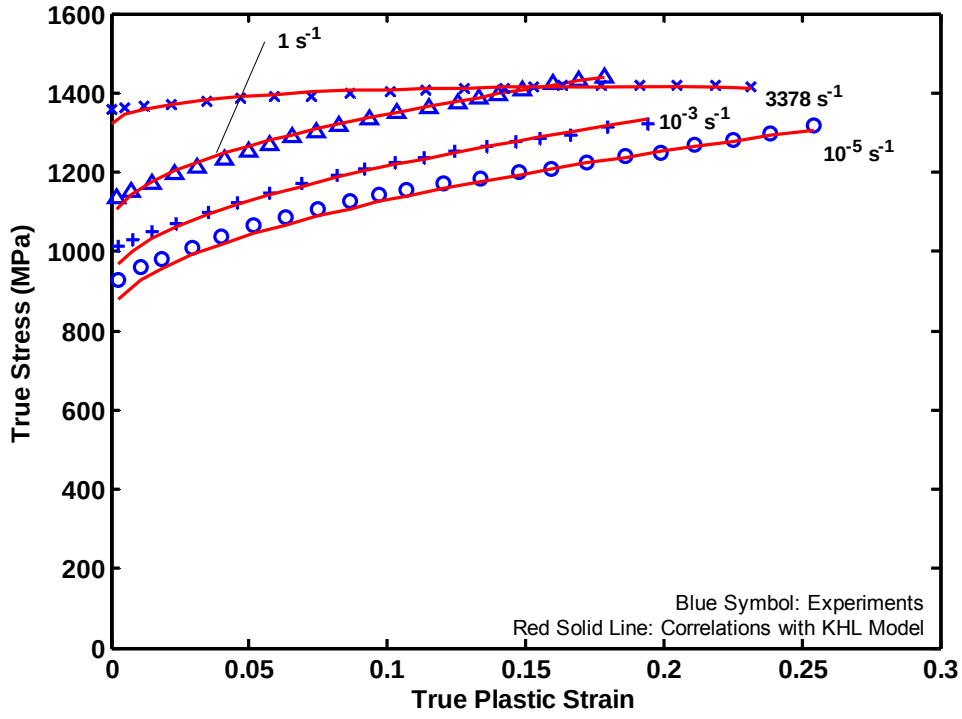

Figure 10. KHL model correlations with the room temperature (296K) response for alloy 3 at different strain rates. (Published data: Khan et al., Int J. Plas 20, 2004)

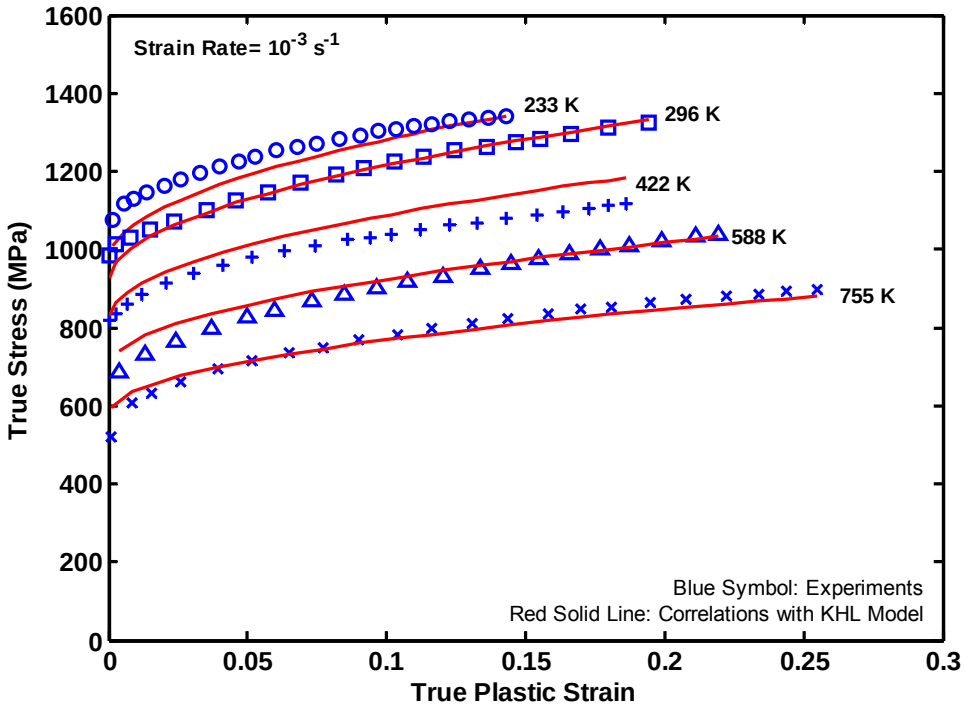

Figure 11. KHL model correlations with the observed response of alloy 3 at different temperatures at constant strain-rate 10^{-3} s^{-1}. (Published data: Khan et al., Int J. Plas 20, 2004)

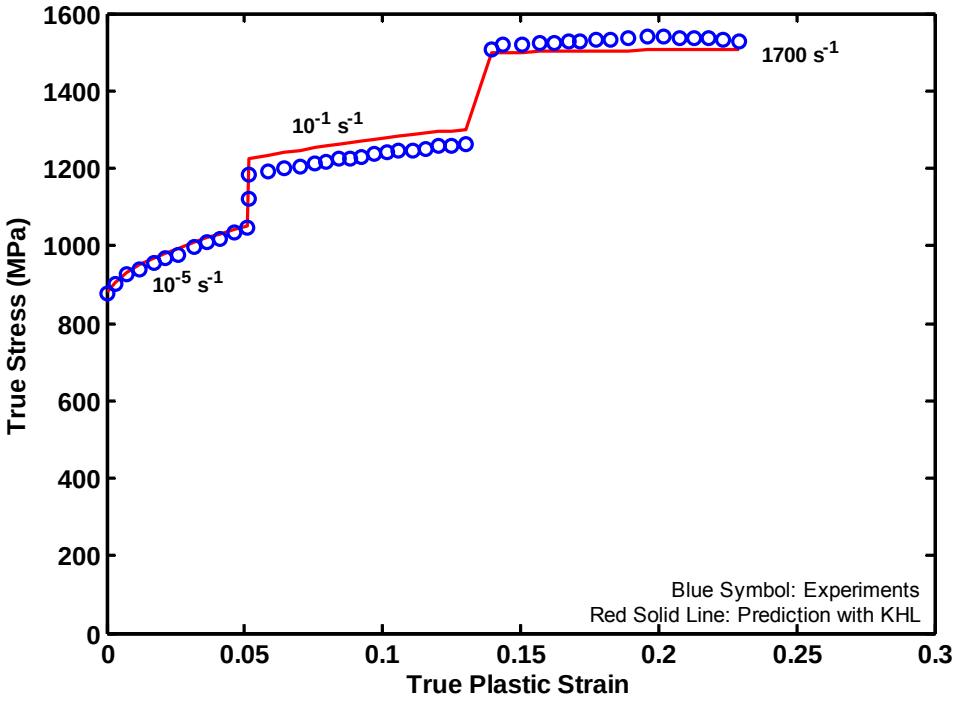

Figure 12. KHL model predictions with the observed response of alloy 3 during a strain-rate jump experiment at room temperature (296K). Dynamic predictions are adiabatic. (Published data: Khan et al., Int J. Plas 20, 2004).

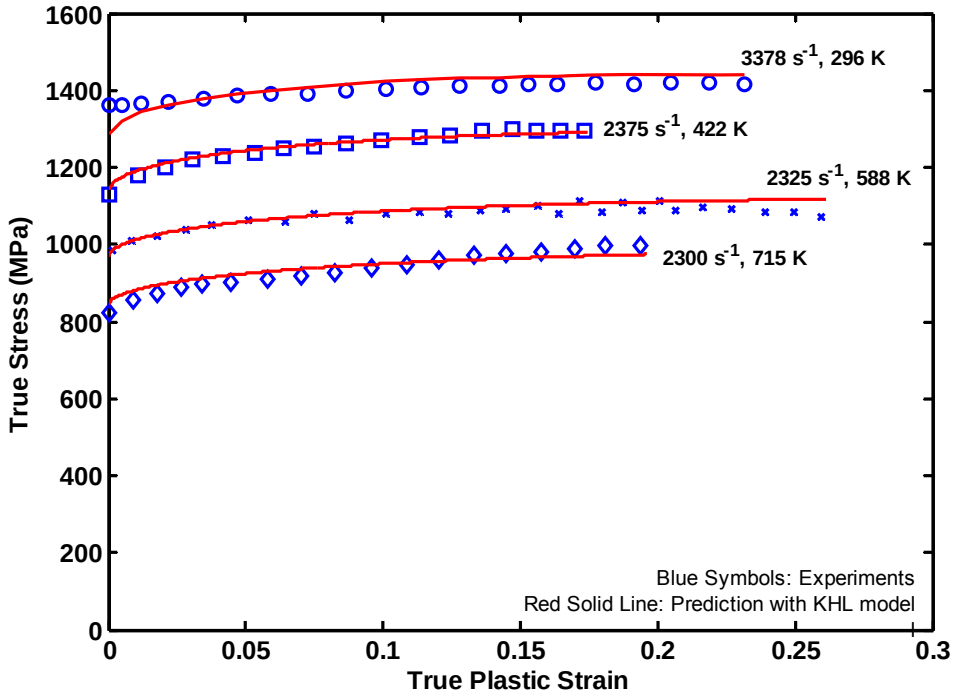

Figure 13. KHL model predictions with the observed response of alloy 3 at high strain rates and different temperatures. All the predictions are adiabatic.

References

Abed, F. H., Voyiadjis, G. Z., 2005. Plastic deformation modeling of AL-6XN stainless steel at low and high strain rates and temperatures using a combination of bcc and fcc mechanisms of metals. International Journal of Plasticity, 21(8), 1618-1639

ASTM International 1996. Standard Test Methods for Determining the Average Grain Size. Designation E 112-96. July 1996. PA, USA.

Burns, T.J., Davies, M.A., 2002. On repeated adaiabatic shear band formation during high speed machining. International Journal of Plasticity 18 (4), 487–506.

Davis, J. R., 1998. In: Metals Handbook Desk Editions, 2nd Edition, ASM International.

Chen, S. R. and Gray, III, G. T., 1995. Constitutive behavior of tungsten experiments and modeling. In: Bose, A., Dowding, R. J. (Eds.), 2nd International Congress on Tungsten and Refractory Metals, McLean, VA, Metal Powder Industries Federation, Princeton, NJ, p. 489.

Chichili, D. R., Ramesh, K. T., Hemker, K. J., 1998. The high strain rate response of Alpha-Titanium: Experiments, deformation mechanisms and modeling. Acta Meterialia 46 (3), 1025-1043.

Conrad, H., M., Doner, M., de Meester, B., 1973. Critical review deformation and fracture. In: International Conference on Titanium, Proceedings of Titanium Science and Technology, Massachusetts Institute of Technology, Boston, p. 969.

Conrad. H., Wang, K., 1978. Solid solution strengthening of titanium by aluminum at low temperatures. 5th Int. Conf. Strength of Materials and Alloys. 1978. 1067-1072.

Conrad, H., 1984. Plastic flow and fracture of titanium at low temperatures. Cyrogenics, June 1984. 293-304.

Conrad, H., 1981. Thermally activated rate controlling mechanisms during plastic flow of titanium from 0 K to T_m. Thermodynamics and Kinetics of Metallurgical Processes. ICMS-1981. 371-399.

De Meester, B., Doner, M., Conrad, H., 1975. Deformation kinetics of the Ti-6Al-4V alloy at low temperatures. Metallurgical Transactions A. Vol. 6A, 1975-65.

Follansbee, P. S., 1979. High strain rate compression testing. American Society for Metals, Mechanical Testing, Metals Handbook, 9th Edition 8, pp. 190-205.

Follansbee, P. S., Gray, G. T. III, 1989. An analysis of the low temperature, low and high strain-rate deformation of Ti-6Al-4V. Metallurgical Transactions A, 20A (5), 863-874.

Johnson, G. R., Cook, W. H., 1983. A constitutive model and data for metals subjected to large strains, high strain rates and high temperatures. In: Proceedings of the Seventh International Symposium on Ballistic, The Hague, The Netherlands, 1983, p. 541.

Khan, A.S., Huang, S., 1992. Experimental and theoretical study of mechanical behavior of 1100 aluminum in the strain rate range 10^{-5}–10^{4} s^{-1}. International Journal of Plasticity 8 (4), 397–424.

Khan, A. S., Huang, S., 1995. Continuum Theory of Plasticity. John Wiley & Sons, New York.

Khan, A. S., Liang, R., 1999. Behaviors of three BCC metal over a wide range of strain rates and temperatures: Experiments and modeling. International Journal of Plasticity 15 (9), 1089-1109.

Khan, A. S., Suh, Y. S., Kazmi, R., 2004. Quasi-static and dynamic loading responses and constitutive modeling of titanium alloys. Int. J. of Plasticity 20 (2004) 2233-2248.

Lee, W.S., Lin, M. T., 1997. The effects of strain rate and temperature on the compressive deformation behavior of Ti-6Al-4V alloy. J. Met. Processing Tech. 71 (1997) 235-246.

Lee, W. S., Lin, C. F., 1998. Plastic deformation and fracture behavior of Ti-6Al-4V alloy loaded with high strain rate under various temperatures. Materials Science & Engineering. A241 (1998) 48-59.

Lesuer, D. R.. 2000. Experimental investigations of material models for Ti-6Al-4V Titanium and 2024-T3 Aluminum. In: Final Report, DOT/FAA/AR-00/25, U. S. Department of Transportation, Federal Aviation Administration.

Liang, R., Khan, A.S., 1999. A critical review of experimental results and constitutive models for BCC and FCC metals over a wide range of strain rates and temperatures. International Journal of Plasticity 15 (9), 963–980.

Macdougall, D. A. S., Harding, J., 1999. A constitutive relation and failure criterion for Ti-6Al-4V alloy at impact rates of strain. Journal of the Mechanics and Physics of Solids 47 (5), 1157-1185.

Majorell, A., Srivatsa, S., Picu, R. C., 2002. Mechanical behavior of Ti-6Al-4V at high and moderate temperatures - Part I: Experimental results. Materials Science and Engineering A326 (2), 297-305.

Makel, D. D., Eylon, D. 1990. The effect of microstructure on localized melting at separation in Ti-6Al-4V tensile samples. Metallurgical Transactions A. Vol. 21A, Dec. 1990-3127.

Mecking, H., Kocks, U. F., 1981. Kinetics of flow and strain-hardening. Acta Metallurgica 29 (11), 1865-1875.

Meyers, M. A., Subhash. G., Kad, B. K., Prasad, L. 1994. Evolution of microstructure and shear -band formation in A-hcp titanium. Mechanics of Materials 17 (2-3), 175-193.

Military Handbook, Metallic Materials and Elements for Aerospace Vehicle Structures, MIL-HDBK-5H, DOD and FAA, 1998.

Molinari, A., Musquar, C., Sutter, G., 2002. Adiabatic shear banding in high speed machining of Ti–6Al–4V: experiments and modeling. International Journal of Plasticity 18 (4), 443–459.

Montgomery, J. S., Wells, M. G. H., 2001. Titanium armor applications in combat vehicles. JOM, 53 (4), 29-32.

Nemat-Nasser, S., Guo, Wei-Guo, Nesterenko, Vitali F., Indrakanti, S. S., Gu, Ya-Bei, 2001. Dynamic response of conventional and hot isostatically pressed Ti-6Al-4V alloys: Experiments and modeling. Mechanics of Materials, 33 (8), 425-439.

Nemat-Nasser, S., Guo, Wei-Guo, 2003. Thermomechanical response of DH-36 structural steel over a wide range of strain rates and temperatures. Mechanics of Materials, 35 (2003), 1023-1047.

Okazaki, K., Conrad, H., 1982. Mechanisms of plastic deformation and superplasticity. Titanium and titanium alloys: Scientific and Technology Aspects. Vol. 1, 1982. 429-466.

Paton, N.E., Baggerly, R.G., and Williams, J.C., 1976. AFOSR Final Report, Rockwell International.

Picu, R. C., Majorell, A., 2002. Mechanical behavior of Ti-6Al-4V at high and moderate temperatures - Part II: constitutive modeling. Materials Science and Engineering A326 (2002), 306-316.

Uenishi, A., Teodosiu, C., 2004. Constitutive modeling of the high strain rate behavior of interstitial-free steel. International Journal of Plasticity, 20(4-5) 2004, 915-936.

Appendix III

(Khan, A.S., Kazmi, R., Zhou, J., Farrokh, B. "Multiaxial and non-proportional loading response, anisotropy and modeling of titanium alloy (Ti-6Al-4V) over wide range of strain rates and temperatures", in-print, 2006, International Journal of Plasticity.)

MULTIAXIAL & NON-PROPORTIONAL LOADING RESPONSE, ANISOTROPY AND MODELING OF TI-6AL-4V TITANIUM ALLOY OVER WIDE RANGES OF STRAIN RATES AND TEMPERATURES

Akhtar S. Khan*, Rehan Kazmi, Jianqiu Zhou and Babak Farrokh

Department of Mechanical Engineering, University of Maryland Baltimore County, Baltimore, MD 21250, USA

Abstract

Multiaxial experiments on Ti-6Al-4V titanium alloys are presented. Different loading conditions are applied in order to get the comprehensive response of the alloy. The strain rates are varied from the quasi-static regimes to dynamic regimes and the corresponding material response is obtained. The specimen is deformed to large strains in order to study the material behavior under finite deformation at various strain rates. Torsional Kolsky bar is used to achieve material strain rates up to 1000 s^{-1}. The non-proportional loading experiments comprise of an initial uniaxial loading to a certain level of strain then followed by biaxial loading, using a channel-type die at various rates of loadings, as well as dynamic torsion followed by dynamic compression. All the non-proportional experiments are carried out at room temperature. Experiments are also performed to investigate the anisotropic behavior of the alloy. An orthotropic yield criterion proposed by Cazacu et al. (2005) for anisotropic hexagonal closed packed materials with strength differential is used to generate the yield surface. Based on the definition of the effective stress of this yield criterion, the observed material response for the different loading conditions under large deformation is modeled using the Khan-Huang-Liang (KHL) equation assuming isotropic hardening. The model constants used were pre-determined from the extensive uniaxial experiments presented in the earlier paper [Int. J. Plast., 20 (2004), 2233-2248]. The model predictions are found to be extremely close to the observed material response.

* Corresponding author. Tel.: +1-410-455-3301; fax: +1-410-455-1052

E-mail address: khan@umbc.edu (A.S. Khan)

Keywords

Kolsky bar; Multiaxial experiments; Titanium alloys; Constitutive behavior; High strain rate; Non-proportional loadings; Anisotropy

1. Introduction

Titanium alloys have found a wide variety of usage in the aerospace industry because of its high strength to weight ratio. Medical industry has uses for titanium in surgical equipment and implants because of its biocompatibility. Petrochemical industry has also found immense usage for this alloy because of its high corrosion resistance. The defense industry is interested in advancing the application of these alloys to armor systems. This is because of the high strength to weight ratio and the corrosion resistance of these alloys encourage its use in armor of tanks and as compartments for the fuel and ammunitions. These alloys come in different grades depending on the impurity contents. The ELIs or the extra low interstitials are more popular in ground applications because of their increased deformability and fracture resistance thus favoring the ballistic properties. Although this grade of alloy has a slightly lesser strength than the ones used for aerospace applications, however, it is cheaper than conventional Ti-6Al-4V titanium alloy.

A large number of studies have been carried out in understanding and modeling the response of these titanium alloys (Follansbee and Gray, 1989; Lesuer, 2000; Nemat-Nasser et al. 2001; Picu and Majorell, 2002; Lee and Lin, 1997; Khan et al. 2004). These studies were focused mainly on the uniaxial response of the alloys at different strain rates and temperatures. However, it is well known that the stress states in these alloys while in use are definitely more complex and multiaxial in nature. Hence it becomes extremely important to understand the material behavior during these loading conditions. The uniaxial material responses and modeling act only as the first step towards understanding the actual more complex conditions that exist and how they affect the corresponding responses.

There have been a few studies understanding the torsional behavior of the Ti-6Al-4V titanium alloys which are available in the literature. Liao and Duffy (1998), performed a series of high strain rate ($\gamma \sim 10^3$ /sec) torsion experiments to study the process of initiation and formation of adiabatic shear bands in conventional Ti-6Al-4V titanium alloy. The temperature rise in the alloys during deformation was also measured. Macdougall and Harding (1999) have also performed a series of torsional experiments on thin tubular Ti-6Al-4V specimens to achieve the response of these alloys in shear. They also measured the temperature rise in the specimens. Constitutive modeling was performed using Zerilli-Armstrong (ZA) model; high strain rate torsional response of the alloys and the material constants were incorporated into the ABAQUS/*explicit* FE code to predict the tensile response of the alloys. They concluded that the ZA model was unable to model the markedly reduced work hardening behavior at high strain rate torsion deformation. They also suggested that strain rate and temperature dependence of work hardening required a modification in the model. Chichili et al. (2004) have studied the torsional high strain rate response of α-titanium. They performed compression-torsion Kolsky bar experiments at high rates. The specimens used in their study were of two different kinds. First one was the conventional thin tubular specimen (Marchand and Duffy, 1988) and the other specimen is solid and had a circumferential notch in the test section to study shear localization.

Non-proportional loading experiments are useful in determining the multiaxial response of the material when subject to complex loading conditions. Bridgman (1946) was first to study the material response during two dimensional compressive experiments on steel. He used two independent hydraulic presses to apply compressive loads to two mutually perpendicular faces of a rectangular block specimen, the third face was free to deform. Florenz (1969) modified this experiment to replace one of the hydraulic presses with almost rigid tool steel walls. The load was applied in one direction and the tool steel walls applied a stress on that face by constraining the deformation in that direction; however he did not measure the stress in the constrained direction. This version of experiments is often called the channel die experiments. This experiment was modified by Khan and Wang (1990) in which all the non-zero stresses and strains were accurately measured in all three directions for annealed aluminum. Later it was used by Khan and Liang, (2000) to observe the response of Aermet, Ta and Ta-2.5W under these loadings.

Titanium alloys in the low and medium temperature regime consist mainly of the HCP α-phase with very little dispersed (BCC) β-phase in between the equiaxed α grains. These hexagonal closed packed (HCP) metals are known to display plastic anisotropy and a strong strength differential in tension and compression. This is because of the interaction between crystallographic slip and deformation twinning (Cazacu et al., 2005). Twinning is also known to be dependent on the sign of the shear stresses (Hosford, 1998). Also, anisotropy exists in these alloys mainly due to the strong crystallographic texture induced due to the rolling process (Hosford, 2005). Therefore, multiaxial modeling of these hcp titanium alloys cannot be performed using definitions of the effective stress, strain and strain rate based on the isotropic J_2-flow theory as these alloys have been known to be anisotropic in nature. Similar conclusions were found by Chichili et al. (2004) while studying the multiaxial response of α-titanium .

Anisotropy has been studied in great detail by many researchers over the past many decades. Hill (1948) was the first to quantitatively determine the yield surface for anisotropic materials. Hill's anisotropic model was primarily based on the generalization of the von-Mises yield criterion. Although this model has been useful because of its simplicity it was not able to capture the observed anisotropy in yield stress and the R-ratios together (Lademo et al. 1999). Other prominent anisotropic yield criteria are by Hosford (1979), Barlat and co workers (Barlat et al. 1991, 1997, 2003), Karafillis and Boyce (1993), Yoon et al. (2006), etc. These criteria dealt with the modeling of cubic crystals and assume same yield stress in tension an compression. Some anisotropic models have been proposed and used in the literature for hcp polycrystals by Tomé and Lebensohn (2004) and Staroselsky and Anand (2003). Macroscopic criteria are generally less time consuming, such as the orthotropic criterion by Cazacu et al. (2005) which is based on the linear transformation of the Cauchy stress tensor deviator.

The present study includes a comprehensive set of experiments for understanding the response of this alloy and consequently modeling the observed responses of these alloys at different strain rates. It is an extension of the previous investigation by Khan et al. (2004). In this investigation, the high strain rate torsion experiments were carried out using the modified Kolsky bar apparatus (Hartley et al., 1985). This was followed by

compression on the same samples again at high strain rates albeit at different operating temperatures. The quasi-static torsion experiments were carried out using the MTS axial/ torsion material testing system. The non-proportional loading experiments were performed using the channel die at small and intermediate strain-rate regime. During these experiments the stress state was designed to change from uniaxial to biaxial compression and the corresponding response was observed and recorded. Constitutive modeling of these observed responses was performed using the KHL model. The experimental data was first converted into effective stress and effective strain based on definitions of the orthotropic yield criteria proposed by Cazacu et al (2005). For an alternative constitutive modeling technique the reader is referred to Abed and Voyiadjis, (2005).

2. Experimental Procedure

2.1 Material

The titanium alloy used in this study is Ti-6Al-4V with high oxygen content. The equivalent oxygen content, O_{eq} = O+2N+0.75C (DeMeester et al.1975), of this alloy is 0.222 %. This alloy was manufactured using single electron beam melting process, resulting in higher oxygen content than the ELI grade. The chemical composition of this titanium alloy is shown in Table 1.

2.2 Quasi-static free-end torsional experiments

Torsion specimens for quasi-static loading were machined as shown in Figure 1(a). The specimens were in the form of a thin hollow tube with a square flange to minimize any radial variation in the shear stress in the test section (Hosford, 2005). A female slot similar to the square flange was machined in the fixture holding the specimen. The geometry used is somewhat similar to the hexagonal flanges used by Liao and Duffy, (1998) for dynamic torsional experiments. Strain gage rosettes were mounted on the test section of the specimen. These gages were bonded at an angle of $\pm 45^0$ degrees to the vertical axis. The torque experienced by the torsional transducer during rotation of the lower fixture in an angle controlled mode, and the axial displacement were also recorded. The shear stress and strain were calculated as in Khan and Liang, (2000). The axial force was zero during the experiment. Experiments were performed at different strain rate using this experimental setup. The gage section wall thickness and length were 0.018 in. (0.4752 mm) and 0.125 in. (3.175 mm), respectively. In one experiment the shear strain rate was kept constant at 1.732×10^{-5} s^{-1}. A strain rate jump experiment was also performed where the shear strain rate was abruptly changed from initially 1.732×10^{-3} s^{-1} to 1.732 s^{-1} at approximately 8.5 % plastic shear strain.

2.3 Dynamic torsional experiments

Dynamic torsion experiments were performed using the modified torsional Kolsky bar (TSHB) setup. The specimens were machined as shown in Figure 1(b). The schematic diagram of the apparatus used is also shown in Figure 2. The torsional Kolsky bar works

on the same principle as the compression bar with the following differences. A section of the incident bar CD (Figure 2) is quasi-statically pre-torqued. The bolt holding the clamp at D is ruptured, thus releasing a shear wave in the incident bar. The strain gages on the incident and transmitted bars are mounted at $\pm 45^0$ to the axis of these bars. These strain gages are connected to a Nicolet 440 digital oscilloscope using a potentiometer circuit. The specimen is glued to the incident and transmitted bars using a high strength adhesive. The shear stress and strain rate are obtained by using Eqns. (1) and (2).

$$\tau(t) = \frac{GR_b^3}{d_s^2 h}\gamma_T \qquad \ldots (1); \qquad \dot{\gamma}(t) = \frac{c_o' d_s}{LR_b}\gamma_R \qquad \ldots (2)$$

where G is the shear modulus of the bar, R_b is the bar diameter, c_0' is the shear wave speed, d_s is the mean diameter of the specimen, L and h are the length and the thickness of the test section of the specimen, respectively. Also, γ_T and γ_R are the transmitted and reflected shear strains, respectively. The shear strain rate is integrated over time to get the shear strains. Correlating the stress and strain with respect to time gives the shear stress-strain response of the material under dynamic torsional loading.

The diameter of the incident and transmitted bars used in the experiment is 0.84 in (21.34 mm). These bars were made from hardened Vascomax-C350 steel. Hollow tubular specimens are used as in the case of quasi-static torsional experiments. The inside diameter of the specimen is approximately 0.5 in. (12.7 mm) and the outside diameter is 0.536 in. (13.6 mm), approximately. A more detailed discussion of this experimental technique can be found in the literature (Hartley et al. 1985).

2.4 Dynamic torsion-compression experiments

Dynamic torsion compression experiments were performed on the titanium alloys using the TSHB technique as described above. Once the hollow tubular specimen was deformed plastically under torsional loading, the test section was machined in a form of a circular ring. The ring was used as a specimen and compressed under dynamic loading conditions using the compression split-Hopkinson bar technique (SPHB). This technique was used for obtaining the response of the specimens at room temperature and also at different temperatures. The details of the SPHB technique can be found in Liang and Khan (1999) and also in Follansbee (1979). All dynamic torsion experiments were performed at room temperature; however, the subsequent dynamic compression experiments using the rings machined from the specimens after dynamic torsional loadings were performed at room and higher temperatures. In these experiments, the specimens were heated to known temperatures (300F and 600F) and then loaded in compression at dynamic strain rates. The diameter of the incident, transmitted and projectile bars of the split-Hopkinson pressure bar (SHPB) apparatus was 0.5 in. (12.7 mm). These bars were made from Vascomax-C350 steel heat treated to maximum hardness.

2.5 Non-Proportional Loading Experiments

Non-proportional compressive loading experiments were performed on the titanium alloys at strain rates of 10^{-5}, 10^{-3} and 1 s^{-1} in the loading direction. The specimens were machined in the form of a rectangular block of dimensions 0.72 in. (18.29 mm) in height (loading direction), 0.4 in. (10.16 mm) and 0.5 in. (12.7 mm) in the other two directions. The schematic diagrams of the channel die for the non-proportional loading experiments and the rectangular block specimen are shown in Figure 3. It consists of a hardened Vascomax-C350 steel die with removable side plate inserts, a removable base plate and a plunger or loading block also made from the same material. The plate inserts and base plate are made removable so that the specimen can be taken out easily after the experiment. The specimen is placed inside the die as shown in the apparatus. Initially the specimen is subjected to uniaxial deformation in direction 1 (before the gap between specimen and die plate inserts in direction 2 closes). The direction 1 is the loading direction as shown in the schematic. Then, after some pre-designed finite deformation, the block is subjected to large deformations under biaxial compression due to constraint in the other direction (direction 2). The 3rd direction is free of stress as the specimen deforms freely in that direction. The amount of finite uniaxial deformation can be controlled by choosing the right dimension of the specimen in the 2nd direction (approximately 10% in the present experiments). Uniaxial loading is applied through the MTS material testing system through a hardened loading block also called the plunger. The dimension of this plunger is selected so that there is neither any pinching nor any appreciable plastic flow through any space between the plunger and the hardened steel plates. Strain gages were mounted on the specimen in the loading direction to record the strain in that direction. Clip gages were used to record the strain in the direction 3, or the direction in which the specimen is free to deform. These gages are made by bonding uniaxial strain gages at exactly the same location on the tension and compression side of a cantilever beam made from very thin blade strips of high strength steel. These strips are connected to the die in the form of a cantilever beam as shown in Figure 3. Steel pins were used to connect the specimen to the blade strips of the clip gages. Once the load is applied on the specimen in the direction 1, the pins start to move outward in the direction 3 due to the Poisson effect. This causes the clip gages or the cantilever beams (blade strips) to bend outward. The gages on the inside surface of the beams (or strips) experience tensile elastic deformation while the gages on the outside surface experiences an equal amount of compressive strains. The gages are then connected in a full Wheatstone bridge arrangement so the magnitude of these strains are added and thus quadrupled. These cantilever beam clip gages are calibrated before the experiment by moving them (known amounts) to get strains in the specimen in this direction. In order to measure the stress in the direction 2, high pressure manganin gages (LM-SS-110FB-048) manufactured by Vishay Micro-Measurements Division are used. These gages are bonded to the surface of the removable steel plate inserts, facing the die. Once the level of deformation in the specimen is such that it starts to push against the hardened steel plates these gages experience an increase in the pressure (stress), which is recorded using the teststar software of the MTS. These gages are also calibrated prior to experiment. The amount of lubrication is very critical on the removable walls, the base plate and plunger during these experiments, as experienced by others as well (Bridgman, 1946 and Bell,

1988). In our case, high vacuum grease manufactured by Dow Corning was used together with graphite powder. This ensured that there was no bulging or reverse barreling during the experiment and thus the deformation was uniform.

2.6 Uniaxial Experiments in Different Directions

In order to determine the level of anisotropy in the alloy, uniaxial quasi-static compression experiments were performed in different directions of the plate. The principal axes of orthotropy are denoted *x*, *y* and *z*, where *x* axis direction represents the rolling direction of the plate, *y* direction is transverse to the rolling direction in plane of rolling and *z* direction is the thickness direction of the plate. For the determination of the in-plane anisotropy, uniaxial quasi-static compression experiments were performed in the rolling direction, 45° to rolling direction and transverse to rolling direction. Strain values were recorded for the loading and transverse to loading directions also in order to calculate the corresponding R-ratios. Additionally, tension experiments were also performed in the rolling and transverse to rolling directions. All the experiments for anisotropic analysis were performed at a constant strain rate of 10^{-3} s^{-1}. The 0.2% offset definition of yield was used for calculation of the yield strength of the alloy. This definition is found suitable for this alloy, as unlike FCC metals (aluminum, etc) it has a well defined yield stress at 0.2 % offset.

3. Orthotropic Yield Criteria and Constants

In order to describe the strength differential and the anisotropy typically shown by hexagonally closed packed (hcp) metals and alloys, Cazacu et al. (2005), proposed a new phenomenological orthotropic criterion that can capture the response of the material in different directions accurately. The authors developed the criterion initially for materials with strength differential, i.e., different strength in tension and compression and extended it for anisotropic materials. This criterion is based on the linear transformation of the deviatoric part of the Cauchy stress tensor, $\boldsymbol{S}$ similar to previous studies by Barlat and co-workers (Barlat et al.1991; Barlat et al. 1997; etc) and has previously been used by many researchers (Lademo et al., 1999; Lademo et al., 2002; Abedrabbo et al., 2006, etc) successfully. The transformed tensor $\sum$ is defined as:

$$\sum = C[S] \tag{3}$$

where $\boldsymbol{C}$ is a 4^{th} order tensor. The orthotropic yield criterion is given as:

$$\left(|\Sigma_1| - k.\Sigma_1\right)^a + \left(|\Sigma_2| - k.\Sigma_2\right)^a + \left(|\Sigma_3| - k.\Sigma_3\right)^a = F \tag{4}$$

The exponent *a*, in the yield criterion is considered to be a positive integer (in our case *a*=2). The parameter *k* is a material constant, which for a fixed *a*, is determined by the ratio of the strength in tension and compression. The function *F*, gives the size of the yield locus. *F* can be defined either as a constant or a function of the total plastic strain (isotropic hardening). The parameter *k*, is defined as;

$$k = \frac{1-h}{1+h} \tag{5}$$

where h is given by,

$$h\left(\frac{\sigma_t}{\sigma_c}\right)=\left[\frac{\left[-2^a+2\left(\frac{\sigma_t}{\sigma_c}\right)^a\right]}{\left[2-2^a\left(\frac{\sigma_t}{\sigma_c}\right)^a\right]}\right]^{1/a} \tag{6}$$

For a 2-D case, the transformation tensor $\boldsymbol{C}$, is given by

$$C=\begin{bmatrix} C_{11} & C_{12} & C_{13} & \\ C_{12} & C_{22} & C_{23} & \\ C_{13} & C_{23} & C_{33} & \\ & & & C_{66} \end{bmatrix} \tag{7}$$

The principal anisotropic stress tensor components are given as:

$$\Sigma_1=\frac{\Sigma_{xx}+\Sigma_{yy}}{2}+\sqrt{\left(\frac{\Sigma_{xx}-\Sigma_{yy}}{2}\right)^2+\Sigma_{xy}^2} \tag{8}$$

$$\Sigma_2=\frac{\Sigma_{xx}+\Sigma_{yy}}{2}-\sqrt{\left(\frac{\Sigma_{xx}-\Sigma_{yy}}{2}\right)^2+\Sigma_{xy}^2} \tag{9}$$

$$\Sigma_3=\Sigma_{zz} \tag{10}$$

According to the linear transformation, $\Sigma=C[S]$, the non-zero components of the anisotropic stress tensor are given as,

$$\begin{bmatrix}\Sigma_{xx}\\ \Sigma_{yy}\\ \Sigma_{zz}\\ \Sigma_{xy}\end{bmatrix}=\begin{bmatrix} C_{11} & C_{12} & C_{13} & 0\\ C_{12} & C_{22} & C_{23} & 0\\ C_{13} & C_{23} & C_{33} & 0\\ 0 & 0 & 0 & C_{66}\end{bmatrix}\times\begin{bmatrix}s_x\\ s_y\\ s_z\\ s_{xy}\end{bmatrix} \tag{11}$$

Where, s_x, s_y, s_{xy} and s_z are the components of the deviatoric Cauchy stress tensor. Upon expansion Eqn (11) leads to

$$\Sigma_{xx}=\left(\frac{2}{3}C_{11}-\frac{1}{3}C_{12}-\frac{1}{3}C_{13}\right)\sigma_{xx}+\left(-\frac{1}{3}C_{11}+\frac{2}{3}C_{12}-\frac{1}{3}C_{13}\right)\sigma_{yy} \tag{12}$$

$$\sum_{yy} = \left(\frac{2}{3}C_{12} - \frac{1}{3}C_{22} - \frac{1}{3}C_{23}\right)\sigma_{xx} + \left(-\frac{1}{3}C_{12} + \frac{2}{3}C_{22} - \frac{1}{3}C_{23}\right)\sigma_{yy} \tag{13}$$

$$\sum_{zz} = \left(\frac{2}{3}C_{13} - \frac{1}{3}C_{23} - \frac{1}{3}C_{33}\right)\sigma_{xx} + \left(-\frac{1}{3}C_{13} + \frac{2}{3}C_{23} - \frac{1}{3}C_{33}\right)\sigma_{yy} \tag{14}$$

$$\sum_{xy} = C_{66}.\sigma_{xy} \tag{15}$$

Applying the various stress states, the yield stress in tension and compression along the rolling direction x (0°), according to the orthotropic criterion are given as

$$\sigma_0^T = \left\{\frac{F}{\left[\left|\Phi_1\right| - k.\Phi_1\right]^a + \left[\left|\Phi_2\right| - k.\Phi_2\right]^a + \left[\left|\Phi_3\right| - k.\Phi_3\right]^a}\right\}^{1/a} \tag{16}$$

$$\sigma_0^C = \left\{\frac{F}{\left[\left|\Phi_1\right| + k.\Phi_1\right]^a + \left[\left|\Phi_2\right| + k.\Phi_2\right]^a + \left[\left|\Phi_3\right| + k.\Phi_3\right]^a}\right\}^{1/a} \tag{17}$$

where,

$$\begin{aligned}
\Phi_1 &= \left(\frac{2}{3}C_{11} - \frac{1}{3}C_{12} - \frac{1}{3}C_{13}\right) \\
\Phi_2 &= \left(\frac{2}{3}C_{12} - \frac{1}{3}C_{22} - \frac{1}{3}C_{23}\right) \\
\Phi_3 &= \left(\frac{2}{3}C_{13} - \frac{1}{3}C_{23} - \frac{1}{3}C_{33}\right)
\end{aligned} \tag{18}$$

Similarly, the tensile and compressive yield stresses in the transverse direction (90°), *y*, are given by,

$$\sigma_{90}^T = \left\{\frac{F}{\left[\left|\Psi_1\right| - k.\Psi_1\right]^a + \left[\left|\Psi_2\right| - k.\Psi_2\right]^a + \left[\left|\Psi_3\right| - k.\Psi_3\right]^a}\right\}^{1/a} \tag{19}$$

$$\sigma_{90}^{C}=\left\{\frac{F}{\left[\left|\Psi_1\right|+k.\Psi_1\right]^a+\left[\left|\Psi_2\right|+k.\Psi_2\right]^a+\left[\left|\Psi_3\right|+k.\Psi_3\right]^a}\right\}^{1/a} \tag{20}$$

where,

$$\Psi_1=\left(-\frac{1}{3}C_{11}+\frac{2}{3}C_{12}-\frac{1}{3}C_{13}\right)$$

$$\Psi_2=\left(-\frac{1}{3}C_{12}+\frac{2}{3}C_{22}-\frac{1}{3}C_{23}\right) \tag{21}$$

$$\Psi_3=\left(-\frac{1}{3}C_{13}+\frac{2}{3}C_{23}-\frac{1}{3}C_{33}\right)$$

The stress state in material coordinates for a compression experiment in the 45° direction is given as $\sigma_{xx}=-\frac{\sigma_{45}^{C}}{2},\sigma_{yy}=-\frac{\sigma_{45}^{C}}{2}$ and $\sigma_{xy}=-\frac{\sigma_{45}^{C}}{2}$

Based on this, the principal values of the transformed tensor for this experiment are given as:

$$\Sigma_1=\sigma_{45}^{C}\left[\left(\frac{-\Phi_1-\Psi_1-\Phi_2-\Psi_2}{4}\right)+\sqrt{\left(\frac{-\Phi_1-\Psi_1+\Phi_2+\Psi_2}{4}\right)^2+\frac{C_{66}^2}{4}}\right]=\sigma_{45}^{C}.[A] \tag{22}$$

$$\Sigma_2=\sigma_{45}^{C}\left[\left(\frac{-\Phi_1-\Psi_1-\Phi_2-\Psi_2}{4}\right)-\sqrt{\left(\frac{-\Phi_1-\Psi_1+\Phi_2+\Psi_2}{4}\right)^2+\frac{C_{66}^2}{4}}\right]=\sigma_{45}^{C}.[B] \tag{23}$$

$$\Sigma_3=\sigma_{45}^{C}\left[\frac{-\Phi_3-\Psi_3}{2}\right]=\sigma_{45}^{C}.[C] \tag{24}$$

where,

$$A=\left[\left(\frac{-\Phi_1-\Psi_1-\Phi_2-\Psi_2}{4}\right)+\sqrt{\left(\frac{-\Phi_1-\Psi_1+\Phi_2+\Psi_2}{4}\right)^2+\frac{C_{66}^2}{4}}\right]$$

$$B = \left[\left(\frac{-\Phi_1 - \Psi_1 - \Phi_2 - \Psi_2}{4} \right) - \sqrt{\left(\frac{-\Phi_1 - \Psi_1 + \Phi_2 + \Psi_2}{4} \right)^2 + \frac{C_{66}^2}{4}} \right]$$

$$C = \left[\frac{-\Phi_3 - \Psi_3}{2} \right]$$

Finally, the yield stress for compression experiment at 45° to rolling direction is given as

$$\sigma_{45}^{C} = \left\{ \frac{F}{\left[|A| - k.A \right]^a + \left[|B| - k.B \right]^a + \left[|C| - k.C \right]^a} \right\}^{1/a} \tag{25}$$

Furthermore, yielding under pure shear parallel to the orthotropy axes is given by

$$\sigma_{xy} = \left\{ \frac{F}{\left[|C_{66}| + k.C_{66} \right]^a + \left[|C_{66}| - k.C_{66} \right]^a} \right\}^{1/a} \tag{26}$$

The R-ratio for different orientations of the specimen is defined as the ratio of the incremental transverse to thickness strain and is given as

$$r_\theta = \frac{d\varepsilon_w}{d\varepsilon_t} \tag{27}$$

Through constancy of volume assumption this can also written as

$$r_\theta = \frac{d\varepsilon_w}{-\left(d\varepsilon_l + d\varepsilon_w \right)} \tag{28}$$

here, $d\varepsilon_w$ and $d\varepsilon_l$ are the incremental width and longitudinal plastic strain respectively. For isotropic materials the R-ratios are normally equal to unity. Through intense mathematics and use of associated flow rule (incorporating the assumption that the plastic potential coincides with the yield function), the R-ratios can be written for the different directions as follows

$$r_0^C = -\frac{\left(-1-k\right)^a.\Phi_1^{a-1}.\Psi_1 + \left(1-k\right)^a.\left(\Phi_2^{a-1}.\Psi_2 + \Phi_3^{a-1}.\Psi_3\right)}{\left(-1-k\right)^a.\Phi_1^{a-1}.\left(\Psi_1 + \Phi_1\right) + \left(1-k\right)^a.\left(\Phi_2^{a-1}.\Psi_2 + \Phi_3^{a-1}.\Psi_3 + \Phi_2^a + \Phi_3^a\right)} \tag{29}$$

$$r_{90}^C = -\frac{\left(-1-k\right)^a.\Psi_2^{a-1}.\Phi_2 + \left(1-k\right)^a.\left(\Psi_1^{a-1}.\Phi_1 + \Psi_3^{a-1}.\Phi_3\right)}{\left(-1-k\right)^a.\Psi_2^{a-1}.\left(\Phi_2 + \Psi_2\right) + \left(1-k\right)^a.\left(\Psi_1^{a-1}.\Phi_1 + \Psi_3^{a-1}.\Phi_3 + \Psi_1^a + \Psi_3^a\right)} \tag{30}$$

The exponent *a*, is chosen to be 2, as it was also used by Cazacu et al. (2005) for other Ti alloys. This orthotropic yield criterion, for a fixed exponent *a*, utilizes 7 material constants for a plane stress (2D) case. Correspondingly, determination of these material constants requires seven experimental results. For a more detailed explanation of this yield criterion, the reader is referred to the original paper by Cazacu et al. (2005).

Experimental results from uniaxial tension and compression yield stresses in rolling and transverse to rolling directions, uniaxial compression in the 45° to the rolling direction and R-ratios in the rolling, and transverse to rolling directions for the compression case are used. These material constants were calculated using least square optimization technique in MATLAB. The value of the material constant *k*, used in this investigation was calculated from the ratio of the yield in tension and compression in the transverse to rolling direction. Table 2, shows the material constants which were calculated using least square optimization method. The yield stresses determined from these experiments and R-ratios along with the values predicted by the model based on the optimized material constants can be seen in Table 3. Figure 4 shows the yield surface for the orthotropic yield criteria based on the material constants calculated for our case. Figure 5 shows the normalized yield stress correlations from the orthotropic criterion along with the normalized experimental yield stresses at in different directions in plane of the plate. It can be seen from the Figure 4 and 5 and Table 3 that the orthotropic model works reasonably well for hcp metals in the development of the yield surface and that the values of R-ratios (which incorporates the flow rule) correlated by this model are extremely close to the experimental data. This implies that it is reasonable to use effective stress, strain and strain rate definitions using this orthotropic model.

4. Experimental Results and Constitutive Model Predictions

The Khan-Huang-Liang constitutive model is used to simulate the observed behavior of the titanium alloys under the complex multiaxial loadings at various strain rates and temperatures. The detailed modeling procedure for the above model can be found in Khan and Liang, (1999) & Khan et al. (2004). The constitutive model is expressed as

$$\sigma = \left[A + B\left(1 - \frac{ln\,\dot{\varepsilon}}{ln\,D_0^p} \right)^{n_1} \varepsilon_p^{\,n_0} \right] \left(\frac{\varepsilon}{\dot{\varepsilon}^*} \right)^c \left(\frac{T_m - T}{T_m - T_{ref}} \right)^m \tag{27}$$

where, σ, ε^p, $\dot{\varepsilon}$ are the effective stress, effective plastic strain and strain rate, respectively. T_m, T, T_{ref} are melting, current, and reference temperatures in degrees Kelvin, respectively. $D_0^p = 10^6$ s^{-1}(arbitrarily chosen upper bound strain rate) and $\dot{\varepsilon}^* = 1$ s^{-1}. A, B, n_1, n_0, C and m are the material constants. For Ti-6Al-4V alloys, the melting temperature was taken to be 1933 K (ASM Handbook, 1994). The reference temperature was room temperature (296K). These material constants have been previously determined from uniaxial experimental results at different strain rates and temperatures for the same alloy (Khan et al., 2004).

The experimental results from quasi-static monotonic torsion, quasi-static jump torsion and dynamic torsion experiments are shown in Figure 6, along with the model predictions (the material constants were not changed from the published values, Khan et al., 2004). The experimental results in these multiaxial stress states were converted into effective stress (σ_e) using the definition of the yield function (Eqn. 4), so that the complexity of the stress state reduces to a single scalar quantity.

In a similar manner the effective strain, (ε_e), and strain rates, ($\dot{\varepsilon}_e$), are also calculated from the experimental results by considering the principle of incremental work per unit volume (Khan and Huang, 1995). The experimental results were then plotted against the model predictions based on these definitions.

$$dW^p = \sigma_{ij} d\varepsilon_{ij}^p = \sigma_i d\varepsilon_i^p = \sigma_e d\varepsilon_e^p \tag{28}$$

The KHL model is able to predict the response of these quasi static as well as the dynamic torsion experiments reasonably well (Fig. 6). The KHL predictions are made assuming adiabatic deformations for the 1.732 s-1 (shear strain rate) as well as the dynamic experimental results as an increase in the temperature were noticed during both experiments. The reader is referred to another paper (Khan et al., 2004) for a detailed discussion of the calculation of the temperature rise in the specimen.

Figure 7 shows the observed response of the alloy under dynamic torsion loading followed by dynamic compression at room temperature. Here again, the stress obtained using the KHL constitutive model is converted for adiabatic case for both the loading conditions (torsion and compression) as the effective strain rate of the experiment is in the dynamic regime and thus the deformation is adiabatic resulting in thermal softening. The KHL model predictions are again found to be in excellent agreement with experimentally observed response of the alloy.

Figure 8 shows the measured response of the alloy under dynamic torsion followed by dynamic compression at higher temperature (422 K). The KHL model predictions were converted for adiabatic case as is done in the previous case. The predictions are again in very good agreement with the actual observed material response for both types of dynamic loading conditions showing the capability of the model in capturing the observed behavior of the alloy under complex loading conditions when used in conjunction with the anisotropic criterion.

Figure 9 shows the experimental results of the alloy during dynamic torsion followed by dynamic compression at 588 K. The model predictions are again converted to adiabatic case for both loadings. The differences between predictions and the observed responses are reasonably small.

The true stress and strain response of the alloy under non-proportional loading conditions at 10^{-1} s^{-1} strain rate in the loading direction is shown in Figure 10. The rise in the stress in the loading direction is clearly visible as the specimen becomes constrained once a certain predetermined level of deformation in the loading direction is achieved.

Consequently, there is a corresponding rise in the stress in the constrained direction until the end of the experiment. Figure 11 shows the effective stress and effective strain responses for different strain rates in the loading directions along with the model predictions. Effective stresses, strains and strain rates are calculated based on the orthotropic yield criterion of Cazacu et al (2005) and the principle of incremental work per unit volume. The stresses and strains are then plotted with the model predictions. Again, the published values of constants [Khan et al (2004)] are used and are not modified using the present experimental results. The model prediction for the case of 10^{-1} s^{-1} strain rate in the loading direction is converted assuming adiabatic deformation, as there was a significant increase in the temperature in the specimen noticed during the deformation. The model predictions are in excellent agreement with the experimentally observed responses for all strain rates. The strain rates used in the model calculations in all non proportional loading experiments are effective strain rates, and are computed using the three strain histories along with the principle of incremental work per unit volume.

5. Conclusions

Quasi static and dynamic torsion experimental results, dynamic torsion loadings followed by dynamic compression experiments at different strain rates and temperatures were presented in this study on a single electron beam melt Ti-6Al-4V titanium alloy. Non proportional loading experiments at various strain rates were also presented. These experimental results formed a comprehensive data to display the behavior of the alloy under various complex loading conditions.

Using the set of model constants for this alloy which were calculated from the uniaxial responses at different strain rates and temperatures in an earlier paper (Khan et al. 2004), the capability of the model to predict accurately the observed new responses under the complex multiaxial loading conditions was demonstrated. The model was able to predict the material response under pure torsion and torsion followed by compression extremely well using the effective stress, strain and strain rate definitions from the orthotropic yield criteria and principle of incremental work per unit volume. In the non proportional channel die experiments, the model was again able to predict the observed material responses under non-proportional loading conditions reasonably well.

Acknowledgements

The first author is grateful for the funding of this project by the Army Research Office under cooperative agreement DAAD19-01-1-0635, under the direction of Dr. Bruce LaMattina (Solid Mechanics Program). The first author is also thankful to Dr. Douglas Templeton, Team Leader of Emerging Technologies at US Army TARDEC for funding of the project and guidance. Various help and comments of Dr. Raj Rajendran at the Army Research Office are also gratefully acknowledged.

Table 1
Chemical composition of the Ti-6Al-4V alloy used

Material	Al	V	Fe	Y	H	N	O	C	Ti
Ti-6Al-4V Titanium alloy	5.97	4.09	0.15	<0.0003	0.0041	0.008	0.174	0.043	REM

Table 2
Material constants for the titanium alloy using the orthotropic yield criteria of Cazacu et al., (2005)

a	k	C_{11}	C_{12}	C_{13}	C_{22}	C_{23}	C_{33}	C_{66}
2	-0.0513	1.5717	2.7749	1.118	1.6907	1.2405	0.5651	1.2133

Table 3
Experimental and Predicted values of the yield stresses and R-ratios under different loading conditions

Yield Stress	σ^T_0	σ^T_{90}	σ^C_0	σ^C_{90}	σ^C_{45}	σ_{xy}	r^C_0	r^C_{90}
Experimental Values (ksi)	138.61	130.9	157.67	135.44	144.01	74.76	0.685	0.507
Normalized Exp. Values	1.02	0.97	1.16	1	1.06	0.55	0.685	0.507
Predicted Values	1.04	0.94	1.14	1.03	1.04	0.58	0.69	0.501

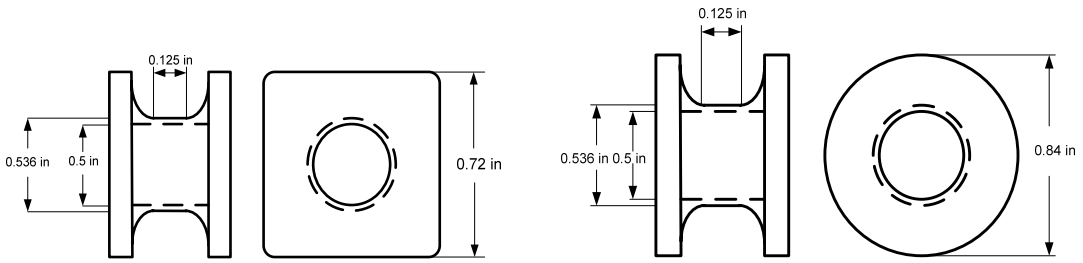

(a) (b)

Figure 1. (a) Specimen geometry for the quasi-static experiments, (b) specimen geometry for the experiments using the Torsional Kolsky bar set up.

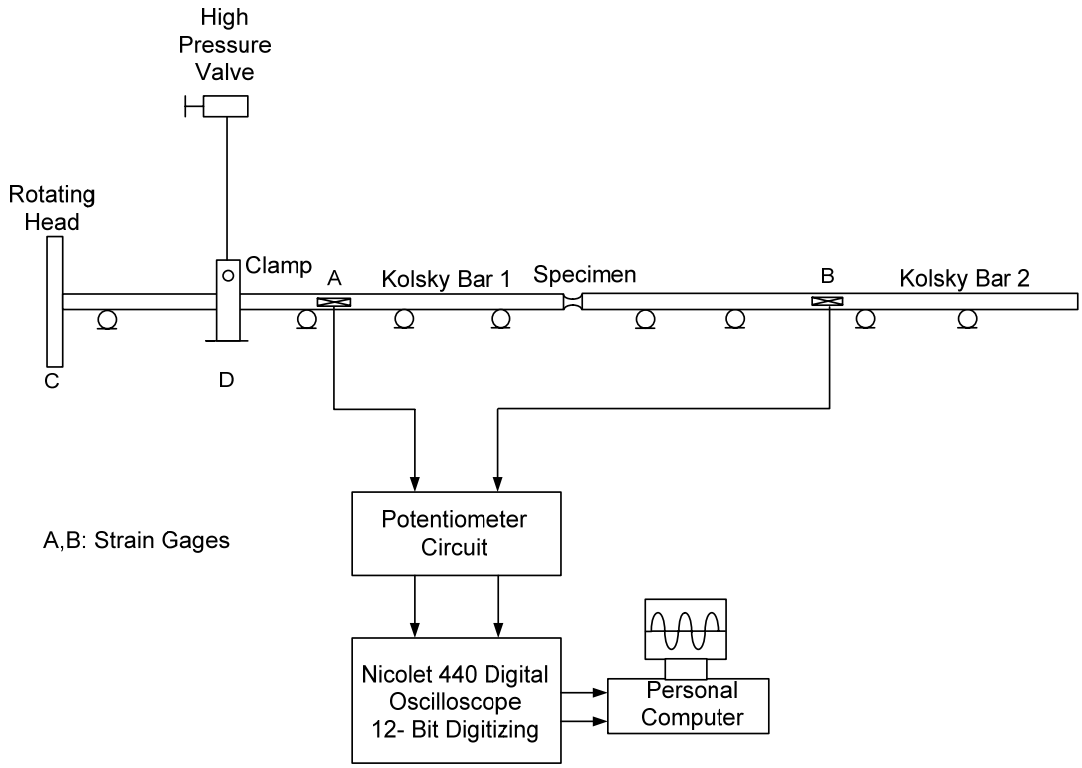

Figure 2. Schematic diagram of the experimental set up for the torsional Kolsky bar experiments.

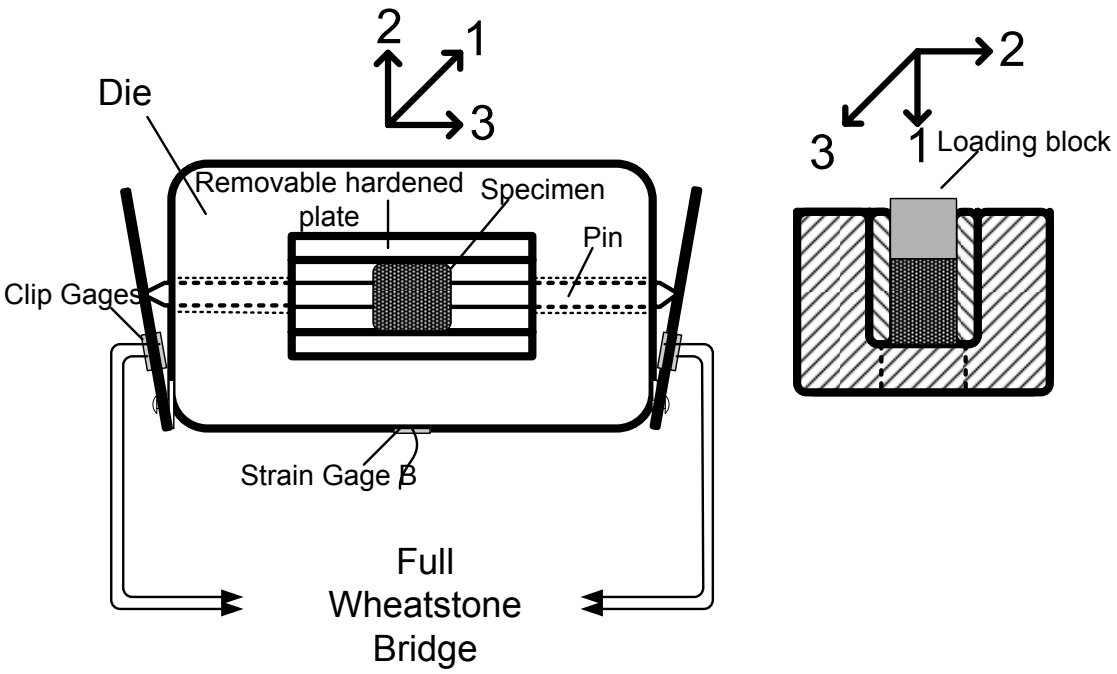

Figure 3. Schematic diagram of the channel die used for non-proportional loading experiments

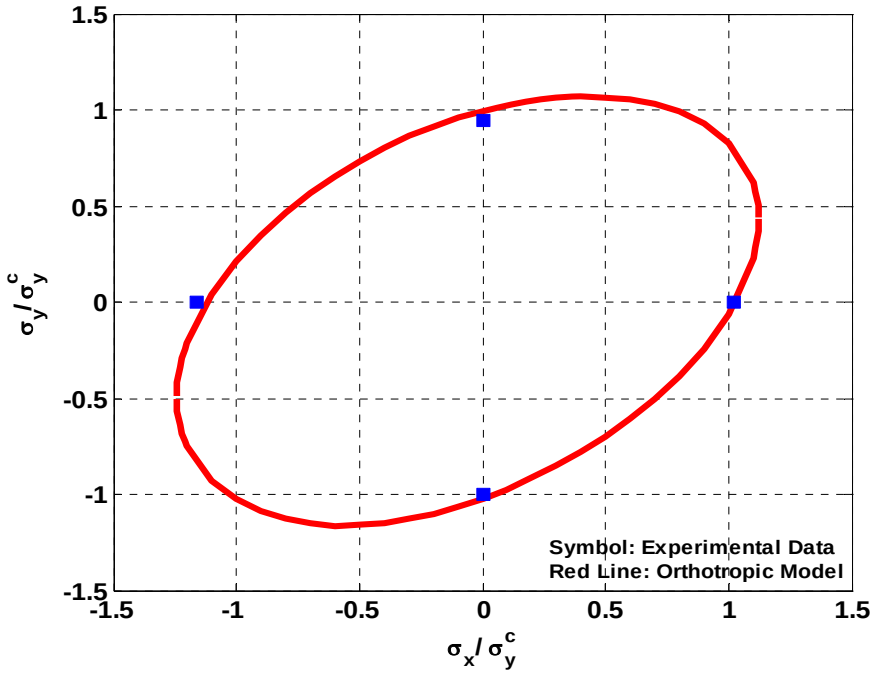

Figure 4. Yield surface generated using the orthotropic yield criteria from Cazacu et al. (2005) for Ti-6Al-4V titanium alloy

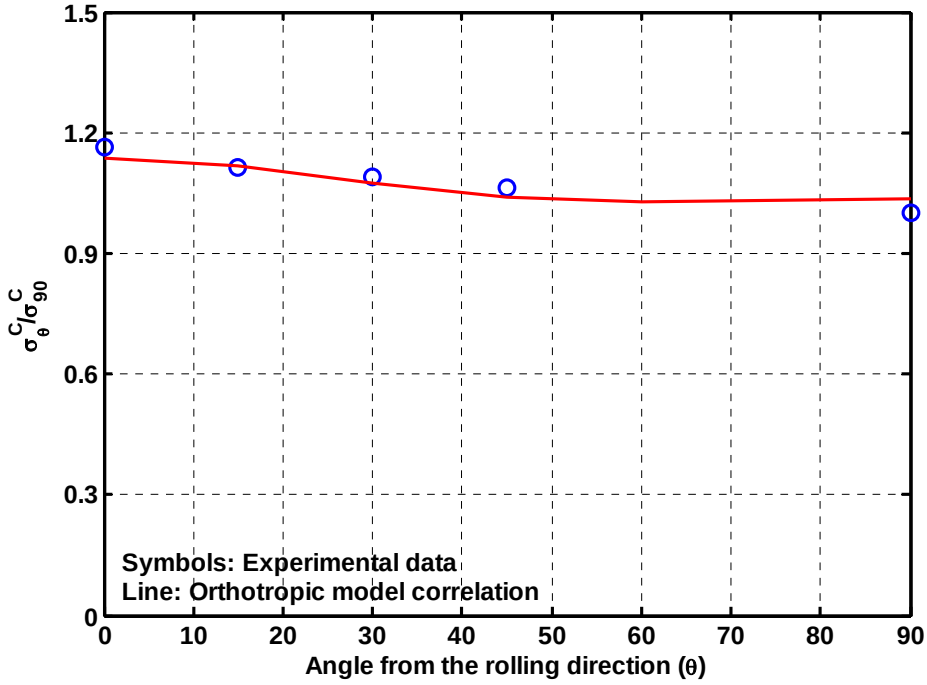

Figure 5. Correlations using the anisotropic yield criterion along with the normalized experimental yield stresses in different directions in the plane of the titanium alloy plate

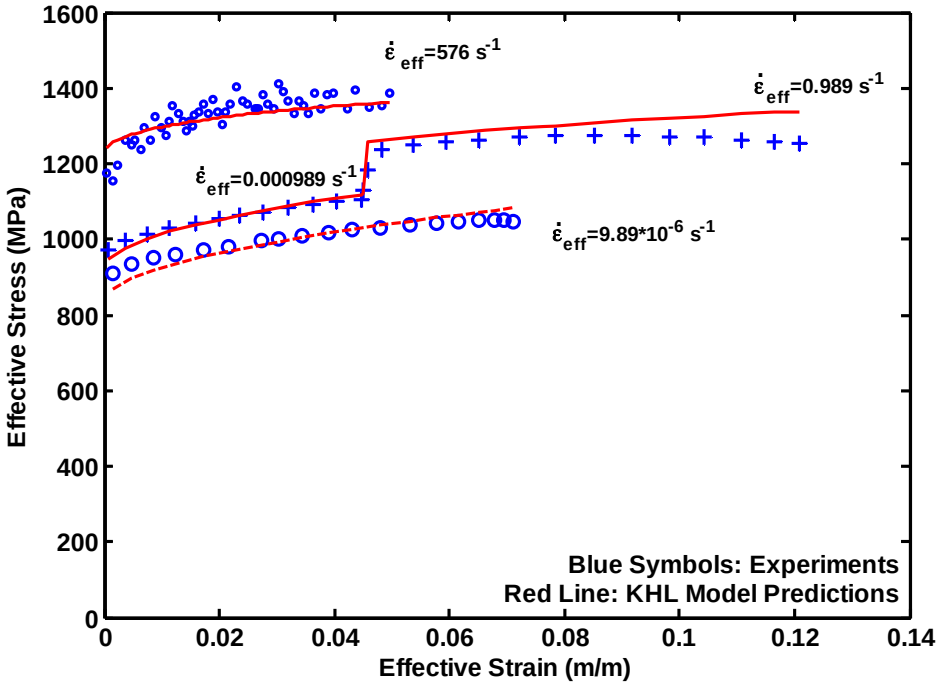

Figure 6. Model predictions with the observed shear response of the titanium alloy converted to effective stress and strain during monotonic, strain-rate jump and dynamic torsion experiments at room temperature (296K). Dynamic and 0.989 s^{-1} effective strain rate predictions are adiabatic.

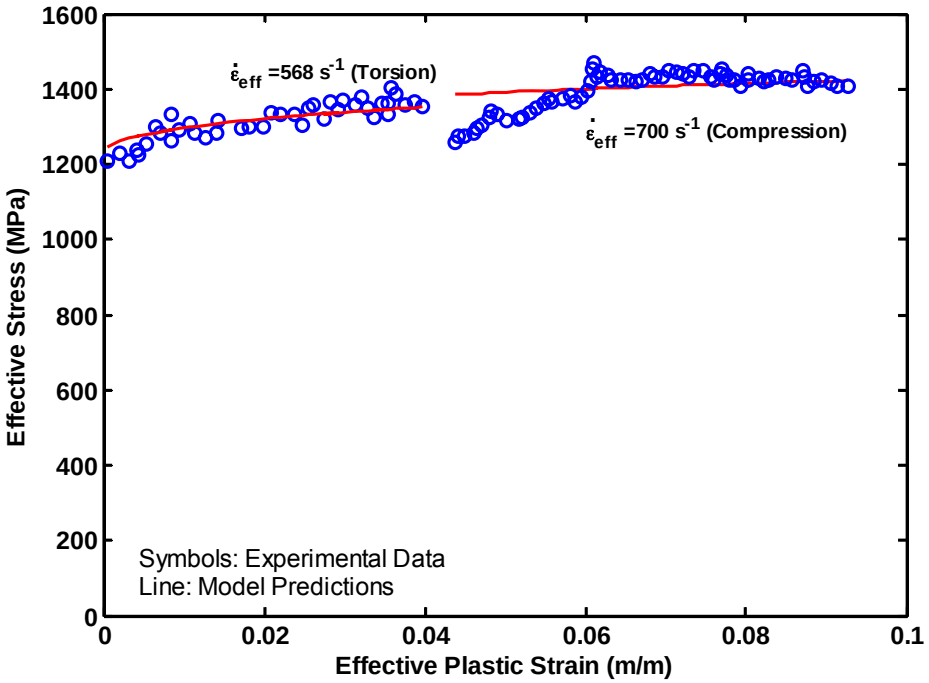

Figure 7. Dynamic shear response at room temperature, followed by dynamic compression response at room temperature of the titanium alloy, and predictions using KHL model with the material constants determined from uniaxial compression experimental data.

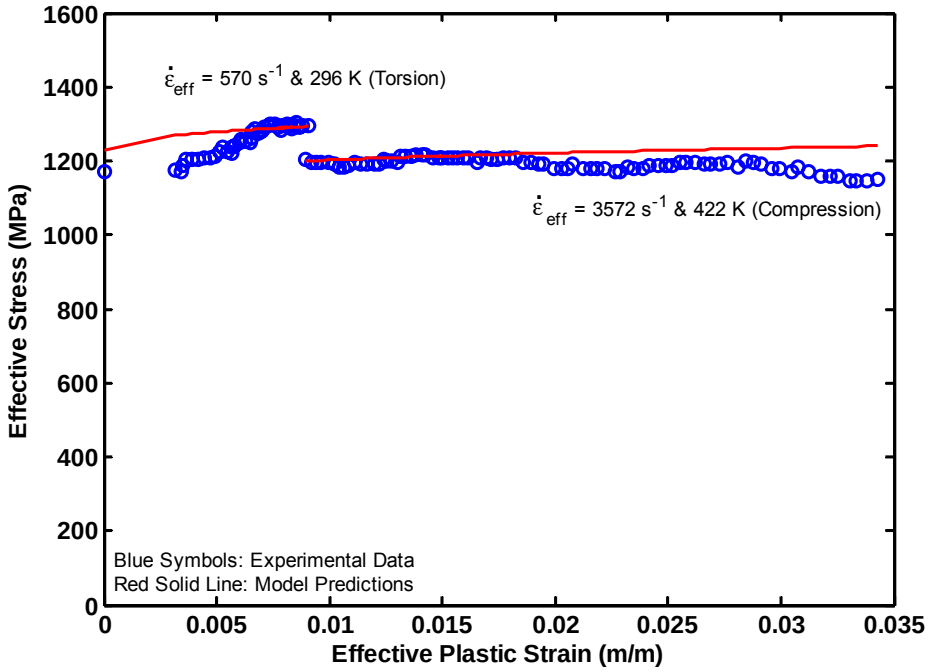

Figure 8. Dynamic shear response at room temperature, followed by dynamic compression response at 422^{o}K of the titanium alloy, and predictions using KHL model with the material constants determined from uniaxial compression experimental data.

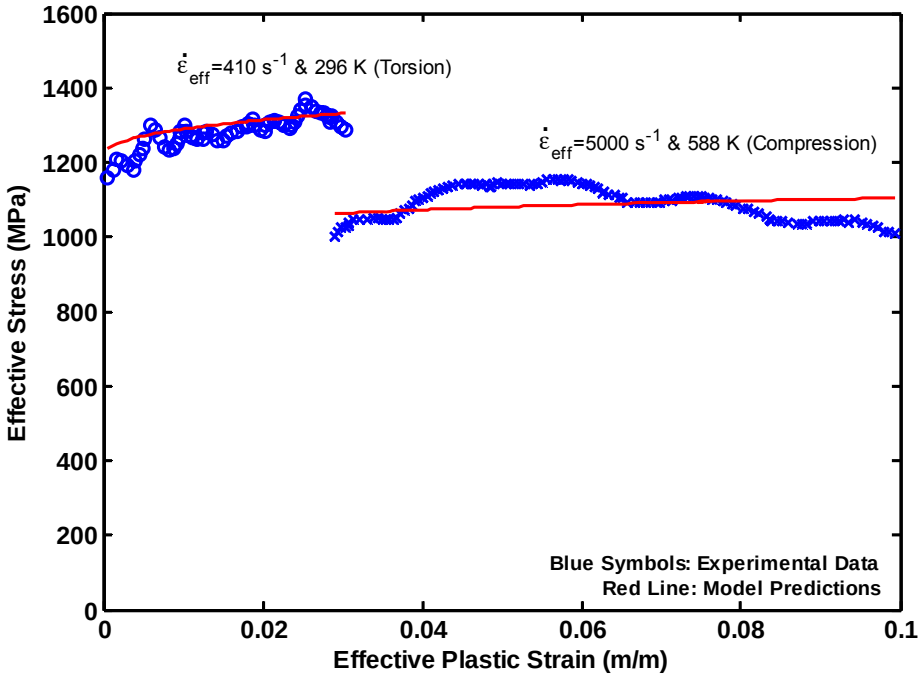

Figure 9. Dynamic shear response at room temperature, followed by dynamic compression response at 588°K of the titanium alloy, and predictions using KHL model with the material constants determined from uniaxial compression experimental data.

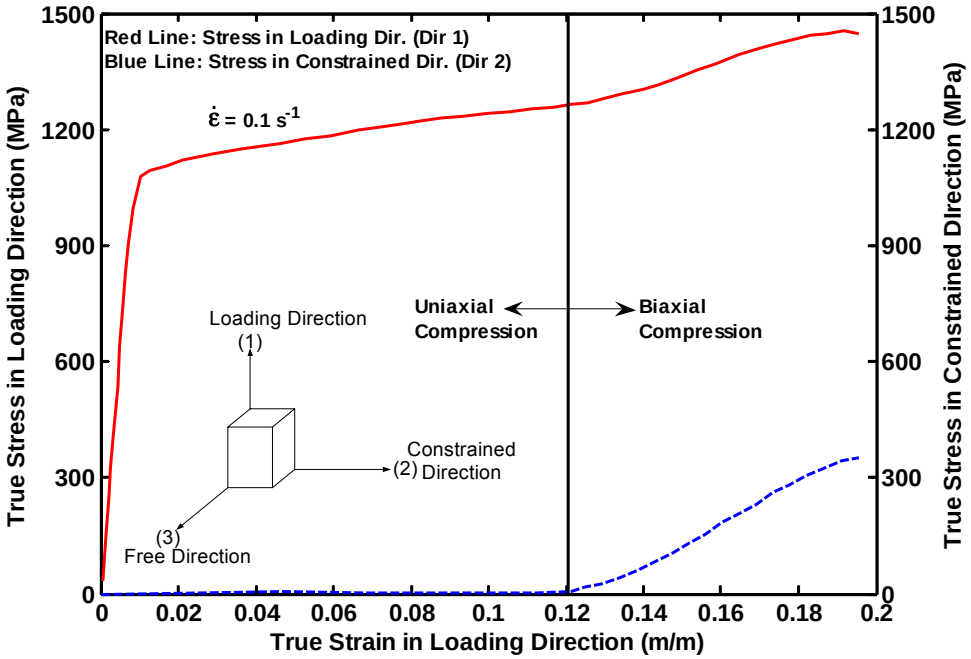

Figure 10. True stress-strains for the non-proportional loading channel die experiment at 10^{-1} s^{-1} strain rate in the loading direction. Note the stress starts to increase in the direction 2 (constrained direction) from zero once the specimen comes in contact with the die walls at approximately 12% strain in the loading direction.

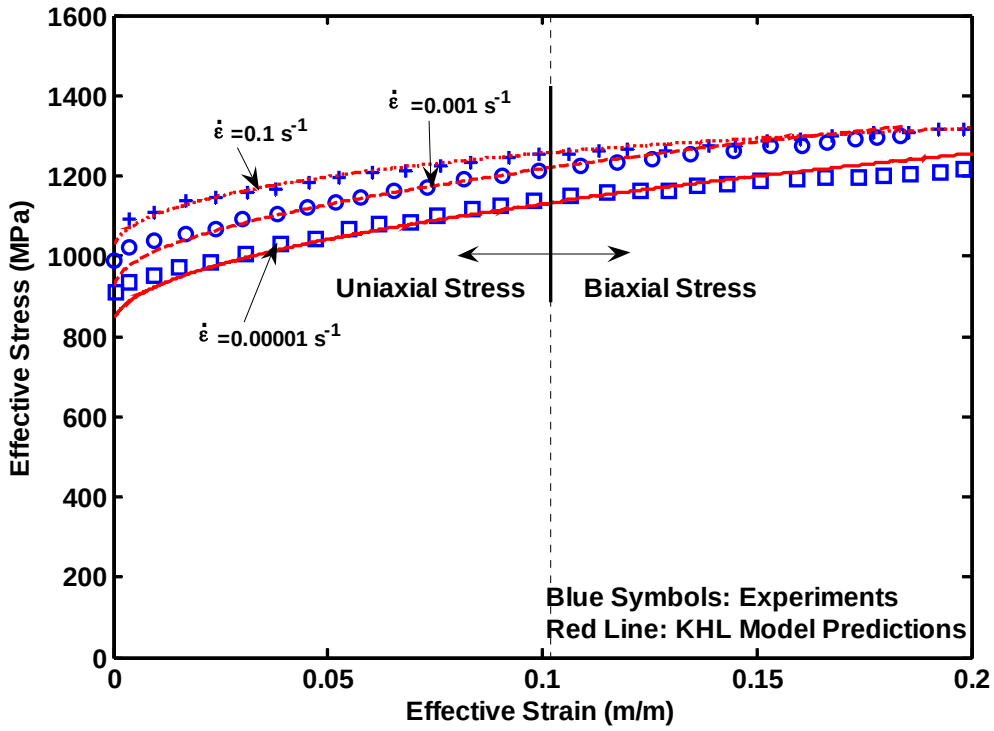

Figure 11. Quasi static response of the titanium alloy under non proportional biaxial loading at room temperature converted to effective stress and strain based on the orthotropic criteria and predictions using KHL model with the material constants determined from uniaxial compression experimental data.

References

Abed, F. H., Voyiadjis, G. Z., 2005. Plastic deformation modeling of AL-6XN stainless steel at low and high strain rates and temperatures using a combination of bcc and fcc mechanisms of metals. International Journal of Plasticity, 21(8), 1618-1639.

Abedrabbo, N., Pourboghrat, F., Carlsey, J., 2006. Forming of aluminum alloy at elevated temperatures- Part 1: Material characterization. Int. J. Plas. 22, 314-341.

Barlat, F., Lege, D.J., Brem, J.C., 1991. A six-component yield function for anisotropic materials. Int. J. Plas. 7, 693-712.

Barlat, F., Becker, R.C., Hayashida, Y., Maeda, Y., Yanagawa, M., Chung, K., Brem, J.C., Lege, D.J., Matsui, K., Murtha, S.J., Hattori, S.,1997. Yielding description of solution strengthened aluminum alloys. Int. J. Plas. 13, 185-401.

Barlat, F., Brem, J.C., Yoon, J.W., Chung, K., Dick, R.E., Lege, D.J., Pourboghrat, F., Choi, S.-H., Chu, E., 2003. Plane stress yield function for aluminum alloy sheet- Part 1: theory. Int. J. Plas. 19, 1297-1319.

Bell, J., 1988. Plane stress, plane strain, and pure shear at large finite strain. International Journal of Plasticity 4, 127-148.

Bridgman, P.W., 1946. Studies of plastic flow of steel, especially in two-dimensional compression. Journal of Applied Physics 17, 225.

Cazacu, O., Plunkett, B., Barlat, F., 2005. Orthotropic yield criterion for hexagonal closed packed metals. International Journal of Plasticity, Article in press.

Chichili, D. R., Ramesh, K. T., Hemker, K. J., 2004. Adibatic shear localization in α-titanium. J. Mech. Phy. of Solids 52 (8), 1889-1909.

De Meester, B., Doner, M., Conrad, H., 1975. Deformation kinetics of the Ti-6Al-4V alloy at low temperatures. Metallurgical Transactions A. Vol. 6A, 1975-65.

Florenz, M., 1969. Two-Dimensional Plastic Compression of Polycrystalline Aluminum. Masters Thesis, The Johns Hopkins University, Baltimore, MD.

Follansbee, P. S., Gray, G. T. III, 1989. An analysis of the low temperature, low and high strain-rate deformation of Ti-6Al-4V. Metallurgical Transactions A, 20A (5), 863-874.

Hartley, K. A., Duffy, J. and Hawley, R. H. (1985). The Torsional Kolsky (split-Hopkinson) Bar. Metals Handbook 8, ASM, 218-228.

Hill, R., 1948. A theory of the yielding and plastic flow of anisotropic metals. Proceedings of the Royal society of London A193, 281-297.

Hosford, W., 1979. On the yield loci of anisotropic cubic metals. In: 7th North American Metalworking conf., SME, Dearborn, MI, 191-197.

Hosford, W., 1998. Reflections on the dependence of plastic anisotropy on texture. Material Science and Eng., A257, 1-8.

Hosford, W., 2005. Mechanical behavior of materials. Cambridge University Press.

Karafillis, A.P., Boyce, M.C., 1993. A general anisotropic yield criteria using bounds and a transformation weighting tensor. J. Mech. Phys. Solids 41, 1859-1886.

Khan, A.S., Wang, X., 1990. An experimental study of large finite plastic deformation in annealed aluminum during proportional and non-proportional biaxial compression. International Journal of Plasticity 6, 484-504.

Khan, A. S., Huang, S., 1995. Continuum Theory of Plasticity. John Wiley & Sons, New York.

Khan, A. S., Suh, Y. S., Kazmi, R., 2004. Quasi-static and dynamic loading responses and constitutive modeling of titanium alloys. International Journal of Plasticity, 20, 2233-2248.

Khan, A. S., Liang, R., 1999. Behaviors of three BCC metal over a wide range of strain rates and temperatures: Experiments and modeling. International Journal of Plasticity, 15 (9), 1089-1109.

Khan, A. S., Liang, R., 2000. Behaviors of three BCC metals during non-proportional multi-axial loadings: experiments and modeling. International Journal of Plasticity, 16 (12), 1443-1458.

Lademo, O.-G., Hopperstad, O.S., Langseth, M., 1999. An evaluation of yield criteria and flow rules for aluminum alloys. Int. J. Plasticity 15, 191-208.

Lademo, O.-G., Hopperstad, O.S., Malo, K.A., Pedersen, K. O., 2002. Modelling of plastic anisotropy in heat-treated aluminium extrusions. J. Mat. Processing Tech. 125-126, 84-88.

Lee, W.S., Lin, M. T., 1997. The effects of strain rate and temperature on the compressive deformation behavior of Ti-6Al-4V alloy. J. Met. Processing Tech., 71 (1997) 235-246.

Lesuer, D. R.. 2000. Experimental investigations of material models for Ti-6Al-4V Titanium and 2024-T3 Aluminum. In: Final Report, DOT/FAA/AR-00/25, U. S. Department of Transportation, Federal Aviation Administration.

Liao, S.-C., Duffy, J., 1998. Adiabatic shear bands in a TI-6Al-4V titanium alloy. Journal of the Mechanics and Physics of Solids, 46 (11), 2201-2231.

Macdougall, D. A. S., Harding, J., 1999. A constitutive relation and failure criterion for Ti-6Al-4V alloy at impact rates of strain. Journal of the Mechanics and Physics of Solids 47 (5), 1157-1185.

Marchand, A., Duffy, J., 1988. An experimental study of the formation process of adiabatic shear bands in a structural steel. J. Mech. Phys. Solids 36, 251-283.

Materials Properties Handbook: Titanium Alloys, R. Boyer, G. Welsch, and E. W. Collings, eds. ASM International, Materials Park, OH, 1994.

Military Handbook, Metallic Materials and Elements for Aerospace Vehicle Structures, MIL-HDBK-5H, DOD and FAA, 1998.

Nemat-Nasser, S., Guo, Wei-Guo, Nesterenko, Vitali F., Indrakanti, S. S., Gu, Ya-Bei, 2001. Dynamic response of conventional and hot isostatically pressed Ti-6Al-4V alloys: Experiments and modeling. Mechanics of Materials, 33 (8), 425-439.

Picu, R. C., Majorell, A., 2002. Mechanical behavior of Ti-6Al-4V at high and moderate temperatures - Part II: constitutive modeling. Materials Science and Engineering A326 (2002), 306-316.

Staroselsky, A., Anand, L., 2003. A constitutive model for hcp metals deforming by slip and twinning: application to magnesium alloy AZ31B. Int J. Plas. 19, 1843-1864.

Tomé, C.N., Agnew, S. R., Blumenthal, W.R., Bourke, M.A.M., Brown, D.W., Kaschner, G.C., Rangaswamy, P., 2002. The relation between texture, twinning and mechanical properties in low symmetry aggregates. Mater. Sci. Forum, 408-412.

Yoon, J.W., Barlat, F., Dick, R.E., Karabin, M.E., 2006. Prediction of six or eight ears in a drawn cup based on a new anisotropic yield function. Int. J. Plas, 22(1), 174-193.